GEOTHERMAL RESERVOIR ASSESSMENT CASE STUDY, NORTHERN BASIN AND RANGE PROVINCE, NORTHERN DIXIE VALLEY, NEVADA

Volume III: Soil Geochemistry and Petrochemistry

Conducted for:

U. S. Department of Energy
Contract number DE-AC08-79ET27006

Work Performed under Subcontract to:

Southland Royalty Company
Fort Worth, Texas

Conducted by:

Mackay Minerals Research Institute
University of Nevada, Reno, Nevada

Submitted:

July 31, 1980

LIST OF AUTHORS

Chapter 1. INTRODUCTION
Elaine J. Bell and Lawrence T. Larson

Chapter 2. GEOGRAPHIC AND GEOLOGIC SETTING
Russell W. Juncal and Elaine J. Bell

Chapter 3. MERCURY AND ARSENIC SOIL GEOCHEMISTRY
Russell W. Juncal

Chapter 4. PETROCHEMISTRY
Elaine J. Bell

Chapter 5. DIXIE VALLEY GEOTHERMAL SYSTEM
Elaine J. Bell

TABLE OF CONTENTS

Table of Contents (cont'd)

Table of Contents (cont'd)

LIST OF TABLES

List of Tables (cont'd)

LIST OF FIGURES

List of Figures (cont'd)

List of Figures (cont'd)

LIST OF PLATES

Chapter 1. INTRODUCTION

By: Elaine J. Bell and Lawrence T. Larson

1.0 INTRODUCTION

1.1 Foreward

This report was prepared for the U. S. Department of Energy (DOE) in compliance with conditions of the statement of work as part of Contract number DE-AC08-79ET27006 for Geothermal Reservoir Assessment in the northern Basin and Range Province. Work was performed by the Mackay Minerals Research Institute (MMRI) under subcontract to Southland Royalty Company (SRC), Fort Worth, Texas.

The MMRI, with the Mackay School of Mines as lead agency, is charged with performing research in the general field of non-renewable resources. Optimal use of the staff and facilities of the University results from the various components of the University cooperating in interdisciplinary research. Table 1-1 lists specific individuals involved in this aspect of the project, their respective affiliation, title, investigation areas, and level of effort. The specific personnel and their individual responsibilities in completing the various investigations are indicated in the following chapters of this report.

The overall reservoir assessment dealt with the northern Dixie Valley area, Nevada (Figure 1-1), and included specific investigations conducted within the study area: 1) Structural-Tectonic Analysis; 2) Petrologic Alteration Studies; 3) Hydrology and Hydrogeochemistry; and 4) Shallow Temperature Survey. The results of these studies were presented in the report submitted January 31, 1980 (Mackay Minerals Research Institute, 1980). Follow-on studies specifically involving 1) Mercury-Arsenic Soil Geochemistry and 2) Petrochemistry are presented in the following technical report in written format supplemented by appropriate graphic data and appended information. This technical report should be viewed as part of the necessary and on-going process of investigation leading to an understanding of the Dixie Valley Geothermal System.

1.2 Purpose

The purpose of this phase of the MMRI program was to provide a large-scale surface geochemical survey for mercury (Hg) and arsenic (As) within and peripheral to an area of exploration for high temperature geothermal resources and to conduct petrochemical analysis of subsurface drill chip samples from two deep exploratory wells (DF 45-14

Table 1-1. MMRI Personnel

Name	Affiliation*	Title (Area of Investigation)**	Level of Effort
Bell, Elaine J.	MSM	PI/Project Administrator	4 man-months
Juncal, Russell W.	MSM	GRF (SG)	4 man-months
Larson, Lawrence T.	MSM	Principal Investigator	1 man-month
Bard, Thomas R.	MSM	GRF (P)	1 man-month
Nosker, Richard E.	MSM	GRF (P)	½ man-month
Nosker, Sue A.	MSM	GRF (P)	½ man-month

* MSM -- Mackay School of Mines

** GRF -- Graduate Research Fellow; P -- Petrochemistry; SG -- Soil Geochemistry;
PI -- Principal Investigator

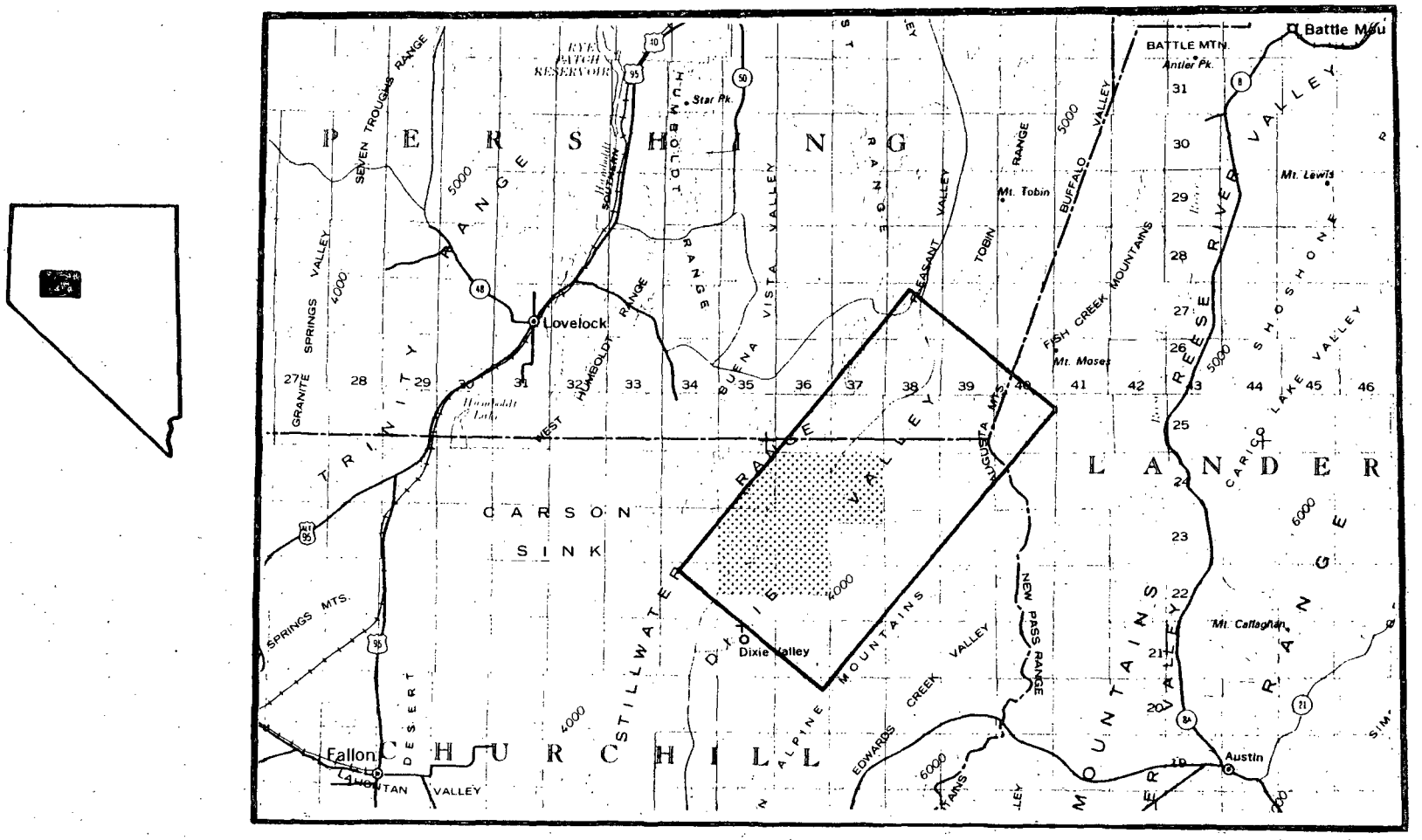

Figure 1-1. Index map of Dixie Valley study region. Shaded area of State shown enlarged. Area encompassing soil geochemistry and petrochemistry studies is shown (in pattern) within the Dixie Valley prospect area; refer to Plate I for detail.

and DF 66-21) to identify steam or hot water entries and to delineate the associated geochemical zonations.

1.3 Scope

The scope of the study as outlined in Appendix A, Scope of Work, of the Prime Contract and Subcontract (Contract number DE-AC08-79ET27006, contract modification A001) included the following major tasks for each investigation:

Soil Geochemistry

(1) Establish broad scale and detailed grid networks and traverse lines within the approximately 30 square mile study area designated along the front of the Stillwater Range.

(2) Collect and analyze an estimated 400 soil samples for mercury and arsenic content.

(3) Evaluate the data.

Petrochemistry

(1) Prepare whole rock and heavy mineral fraction samples for representative intervals within each of the wells: DF 45-14 and DF 66-21.

(2) Analyze the samples, optimally 100-foot composite samples, for the following elements: lead, zinc, arsenic, antimony and mercury.

(3) Evaluate the data.

1.4 Study Approach and Methods

The specific approach and methods of each investigation are presented in the respective chapters of this report.

1.5 Report Organization

This technical report is presented in chapter format with each chapter authored by the person primarily responsible for data development and accomplishing the tasks outlined in the statement of work. Chapter 2 presents a general geologic and geographic setting within which to evaluate the results of the specific soil geochemistry (Chapter 3) and petrochemistry (Chapter 4) investigations. Chapter 5 provides a brief re-evaluation of the integrated model of the Dixie Valley Geothermal System developed during the first phase of the Case Study in terms of the data contained in this report. Where necessary, graphic display of data in the form of tables, charts, photographs,

figures or maps is included to supplement and enhance the text presentation.

Preparation of this technical report involved the following process:

(1) Authorship of the respective chapters on each investigation.

(2) Collation of Chapters 1 through 4 to form the Draft Final Report (DFR).

(3) Review of the DFR by MMRI project personnel and by key SRC personnel.

(4) Preparation of the Final Technical Report.

1.6 Acknowledgements

On behalf of the Graduate Research Fellows and ourselves, we express our sincere appreciation to the following representatives of Southland Royalty Comapny: Mr. Jere Denton, District Manager of Natural Resources, for his continuing support, cooperation and guidance since the inception of this project as a joint venture between the MMRI and SRC; and Mr. Dennis S. McMurdie, Geothermal Geologist, for his patience and invaluable assistance during the course of our investigations.

We wish to express our appreciation to the U. S. Department of Energy for their willingness to support the MMRI and its research in Dixie Valley. We would particularly like to thank Mr. Joe Fiore for his cooperation and encouragement.

We also wish to extend our thanks to the numerous support personnel of the Mackay School of Mines and the University of Nevada who assisted our efforts toward completion of this project. Purchasing agreements and bookkeeping were ably handled by Mrs. Betsy Peck and Mrs. Louise Gibbs. Superb secretarial services provided by Ms. Mollie Stewart made the preparation of this report possible. Ms. Alice Kellames is thanked for her patience and capable assistance in handling personnel contracts and the various unforeseen problems that arose during the course of the study. Contract expenditure records were maintained in timely and efficient manner by Mr. James Murphy and Mr. Barry Myers of the UNR Controllers Office.

And finally, a special thanks to those persons who have patiently and continually supported our efforts and investigations throughout the

entire Dixie Valley project and who we may have inadvertently forgotten to acknowledge.

1.7 References

Mackay Minerals Research Institute, 1980, Geothermal reservoir assessment case study, northern Basin and Range Province, northern Dixie Valley, Nevada: Rept. prepared for U. S. Dept. of Energy, contract no. DE-AC08-79ET27006, v. 1, 223 p. plus appendices, v. II, map plates; also Univ. Utah Res. Inst. Rept. NV/DV/SR-13.

Chapter 2. GEOGRAPHIC AND GEOLOGIC SETTING

By: Russell W. Juncal and Elaine J. Bell

2.0 GEOGRAPHIC AND GEOLOGIC SETTING

2.1 Introduction

The following discussion provides a framework within which to evaluate the soil geochemistry and petrochemistry investigations. General geographic and geologic settings are presented along with specific discussions of pertinent aspects of the study area, such as the mineralized zones. A brief summary is presented here, and the reader is referred to the Case Study (MMRI, 1980) for greater detail.

2.2 Geographic Setting

2.2.1 General

This study focusses on the southwestern portion of the Dixie Valley prospect area (Figure 1-1). Bounded by the Stillwater Range and the Humboldt Salt Marsh on the west and east, respectively, and extending from Dixie Meadows on the south to the Boyer Ranch on the north (Plates I through III), the study area encompasses the two deep exploratory wells (DF 45-14 and DF 66-21; Plate III).

Large alluvial fans slope from the mountain canyons and coalesce to form continuous alluvial plains. The valley floor is dominated by the nearly level playa, with the Humboldt Salt Marsh located within the southern portion of the playa. The Marsh is the sink for waters from Dixie, Jersey and Buffalo Valleys, as well as the Eastgate drainage from the south.

During late Wisconsinan time (approximately 12,000 years before present) a lake contemporaneous with but separated from Pleistocene Lake Lahonton reached an estimated depth of 73 meters (m) (220 feet) in the valley. Geomorphic remnants of the lake remain as old shorelines, bars and delta deposits on some of the fan surfaces.

2.2.2 Climate

The study area is arid to semi-arid with high evapotranspiration and abundant sunshine. Daytime temperatures are hot in summer and mild in winter; nights are cool or cold. Topographic position is an important factor in the local climate. The valley floor at an elevation of approximately 1037m (3400 feet) receives less than 20 centimeters (cm) (8 inches) of precipitation annually, while the upper portions of the

ranges with median elevations of 1830 to 2135 m (6000 to 7000 ft) average 30 cm (12 inches) or more. The elevation moderates the daytime temperatures in the mountains, although at night temperature inversions commonly occur. Recorded temperature extremes on the valley floor range from -24° C to 43° C (-11° F to 109° F).

2.2.3 Soils

The moderately to poorly developed arid soils of the area largely reflect their geographic position. Soils within and adjacent to the playa are poorly drained with groundwater within 1 m (39 inches) of the surface. Composed mainly of clay and silt they show little or no horizon differentiation (entisols). A surface salt crust or a salt horizon is sometimes present; vegetation is lacking.

Further from the playa are poorly and somewhat poorly drained soils of the basin-fill plains. The water table is commonly less than 1 m (40 inches) below the surface. The soils are clays, silty clay loams or silty loams underlain by silt and clay basin-fill deposits. These soils show little horizon development, although they may have a salic horizon. All are saline. Greasewood (Sarcobatus vermiculitis), saltbush (Atriplex lintiformus), iodine bush (Allenrophea accidentalis) and salt grass (Distichlis apicata stricts) are the most common plants.

The third important soil environment is on the alluvial fans. Two important soil groups within the study area are found in this environment. The toes of the fans (2-4% slope) are covered largely by loamy, well drained soils showing a moderately fine textured subsurface horizon where clay has accumulated (argillic or cambic horizon). Shadscale (Atriplex confertifolia), and greasewood are the predominant shrubs. Rabbit brush (Chrysothamus, species unsure) inhabits the drainage courses and localized areas where the water table may be close to the surface. Further up the fan slopes (4-15% slope) are well drained loamy skeletal (35% gravel, cobble or stone) soils which generally show a weak argillic or cambic horizon. Typical vegetation is similar to the lower fans with the addition of bud sagebrush (Artemesia spinecens) and halogeton (Halogeton glomeratus); several species of grass are sparsely distributed. For a more detailed discussion of the soils, the reader is referred to Alexander and Peterson (1974).

2.3 Geologic Setting

2.3.1 General

The recent geologic history of the area is most important to this study and includes considerable seismic and geothermal activity. Large earthquakes accompanied by displacement and rupture of the ground surface occurred in 1903, 1915 and 1954. The waxing and waning of surface thermal activity may be related to the seismic activity in the area. Surface evidence of far greater thermal manifestations in the past is shown by areas of highly altered rock along the range front and large tufa mounds such as those at Sou Hot Springs in the north end of the valley. Numerous hot springs and fumaroles are still active, including a group of approximately ten fumaroles along the range front within the study area (Plate III).

The schematic model of northern Dixie Valley shown in Figure 2-1 depicts the valley structure as a complex asymmetric graben. The innermost portion of this stepped graben structure may contain as much as 3000 m (10,000 feet) of alluvial fill (Thompson and others, 1967). It can be seen that the general trends are northeasterly. However, cross-cutting structures such as the White Rock Canyon fault may be of particular significance to the geothermal system. Generalized structural trends within the specific study area are shown on Plate III.

The mountain ranges are largely composed of folded and faulted Triassic and Jurassic metasiltstone and limestone overlain by upper Jurassic to Tertiary rhyolitic to dacitic tuffs, welded tuffs and flows, andesite and basalt flows and tuffaceous sediments (Figure 2-2). Intrusions of gabbroic and dioritic rocks of probable Mesozoic age are also volumetrically significant.

2.3.2 Dixie Valley Geothermal System

The complex structural setting of Dixie Valley has made the geothermal system difficult to characterize. Many of the structures serve or have served as preferential conduits for fluid migration as evidenced by the alignments of springs, seeps and fumaroles and the subsurface and surface concentration of intense hydrothermal alteration along these features. This is best seen along the front of the Stillwater Range where very intense localized alteration is observed, along with fumaroles

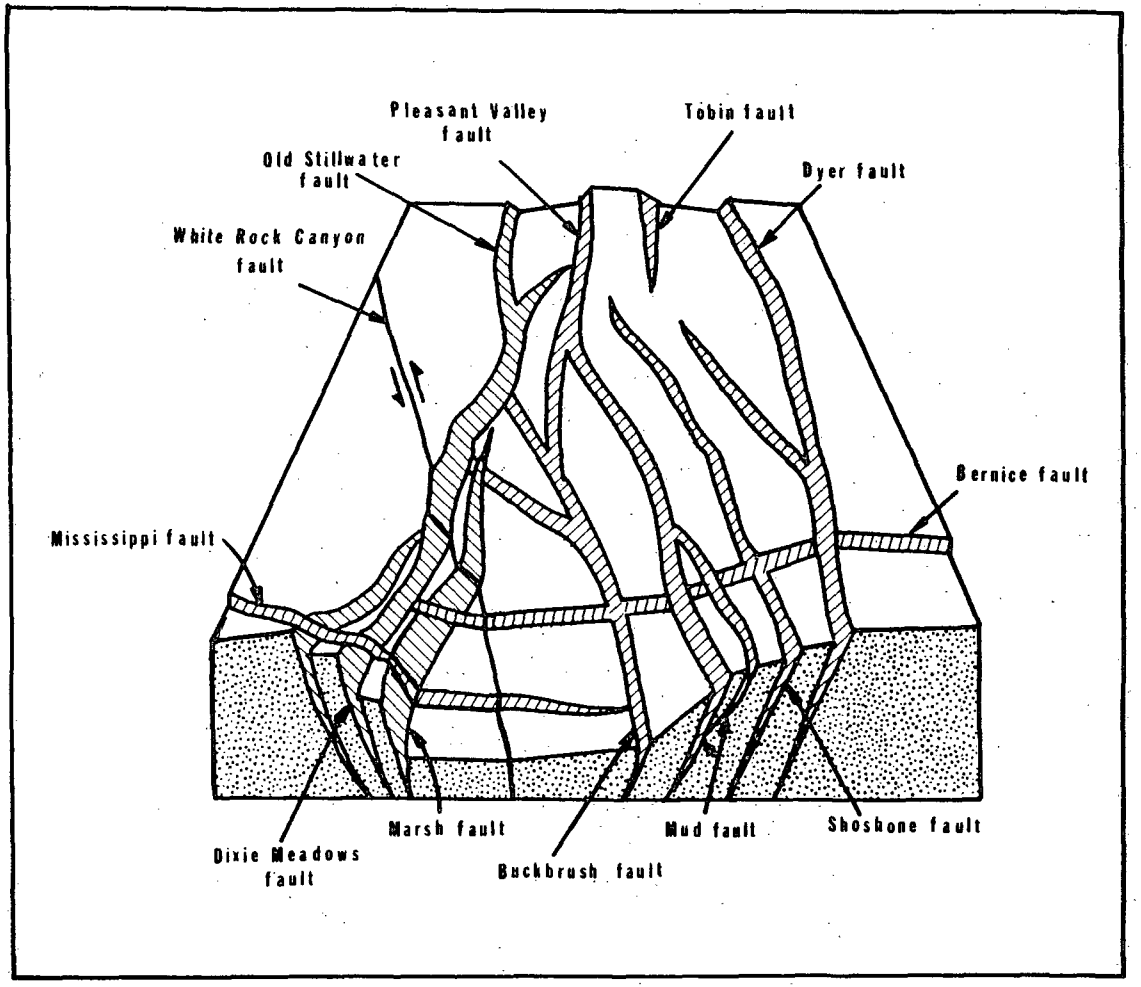

Figure 2-1. Structural model of northern Dixie Valley. Alluvium is removed and bedrock surfaces restored. Modified from Whitney (1980).

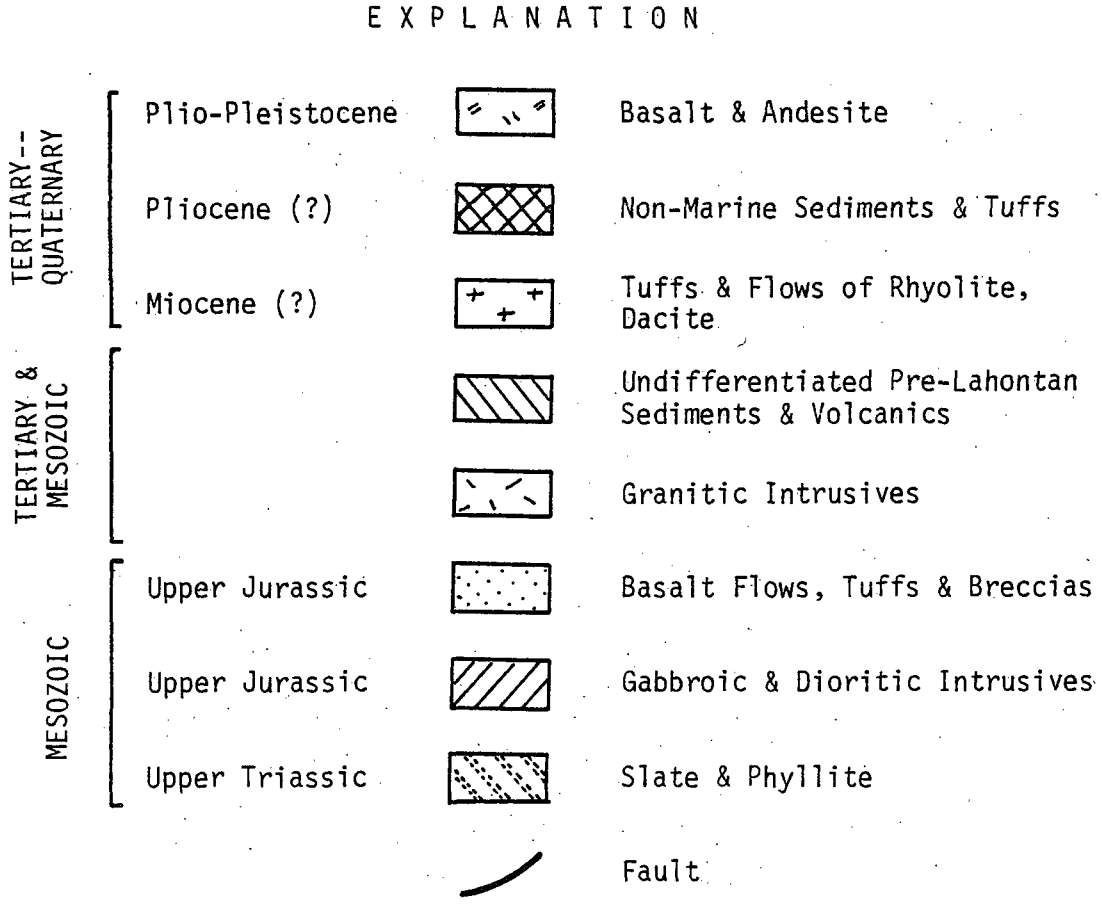

Figure 2-2. Generalized geologic map of the Dixie Valley area. Modified from Meister (1967); map on following page.

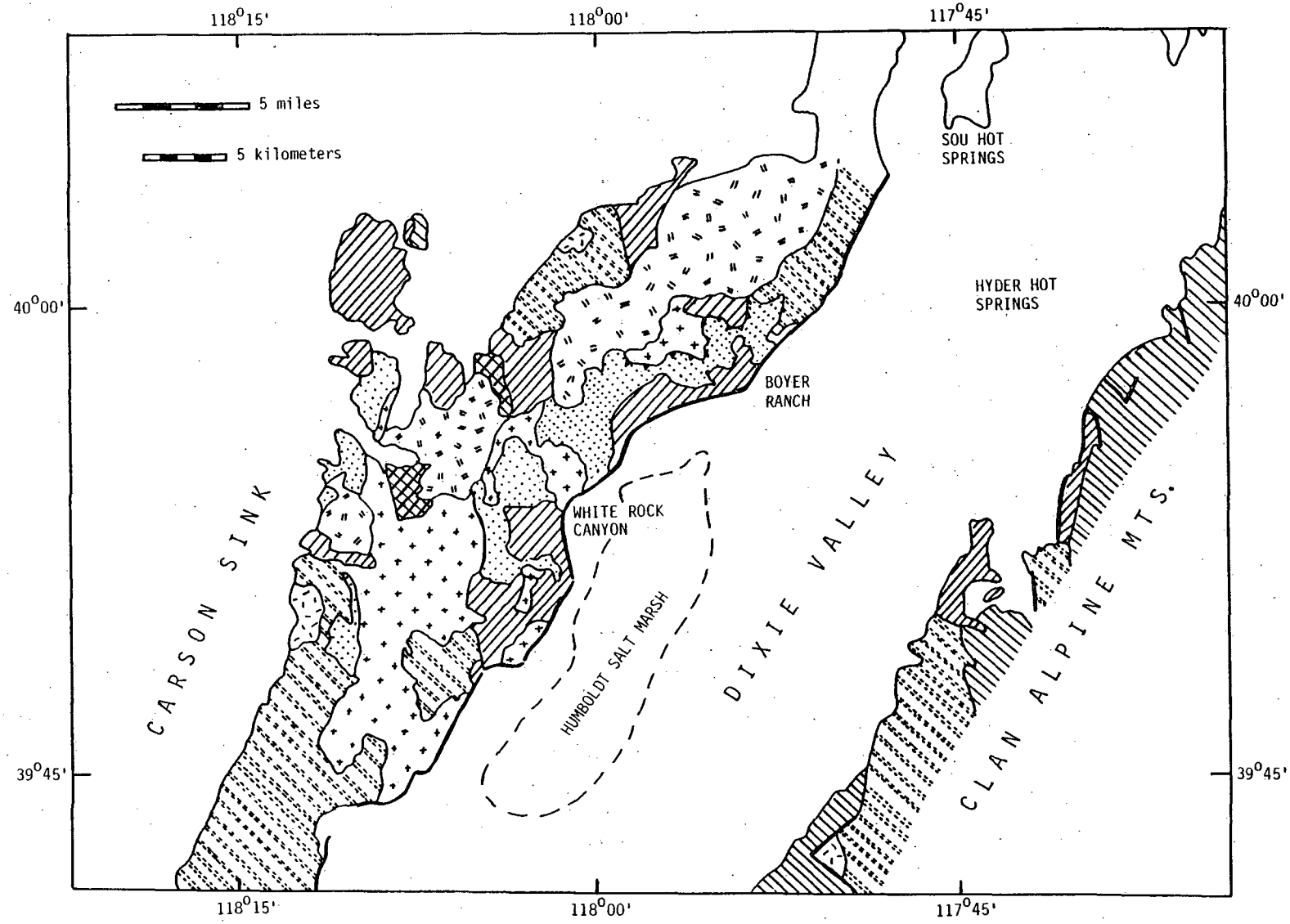
118°15'
118°00'
117°45'
5 miles
5 kilometers
SOU HOT SPRINGS
HYDER HOT SPRINGS
40°00'
BOYER RANCH
WHITE ROCK CANYON
CARSON SINK
HUMBOLDT SALT MARSH
DIXIE VALLEY
CLAN ALPINE MTS.
39°45'

and the presence of hot water within 30 m (100 feet) of the surface.

Water chemistry data have shown major differences between hot spring systems at Sou, Hyder and Dixie Meadows, implying a general lack of communication between the springs. As yet however, the heat source and the precise structural or stratigraphic factors which may control the system have not been defined.

Exploratory drilling has confirmed the existence of a hot water-steam(?) system at depth. This conclusion is based on very limited information available for a group of wells (SW Lamb #1, #3 and #4) drilled by Sun Oil Company in the vicinity of the Boyer Ranch. Wells DF 45-14 and DF 66-21 have shown high temperature fluids in certain intervals, but flow rates have generally been low. The locations of the various deep exploratory wells are shown on Plate III.

2.3.3 Mineral Deposits

Numerous mineral deposits occur in or near the study area and, although production has been limited, they are significant to the present work. In the Corral Canyon area (Plate III) on the east front of the Stillwater Range, small gold deposits were worked in the 1920's and 1930's with minimal production and, more recently, some prospecting for titanium minerals was done along albite-calcite dikes which cut the gabbroic country rock (Willden and Speed, 1974). The Dixie Comstock Mine (Plate III) also lies along the eastern front of the Stillwater Range. Recently reopened, it was last worked for gold and silver prior to World War II. The ore body is a quartz vein in altered rhyolite. An amalgamation mill was erected in 1935 but is no longer standing. Production figures show $293,304 from 17,880 tons of ore with a 2 to 3 gold/silver ratio (Willden and Speed, 1974). The mining was hampered by large quantities of hot water encountered less than 75 feet from the surface.

The upper reaches of both White Rock Canyon and, to a lesser extent, Cottonwood Canyon (Plate III) contain numerous mineral workings within the Table Mountain district. These include a nickel mine, a cobalt-nickel-copper mine, several copper prospects and several small iron deposits. The nickel-cobalt mines may be particularly significant to the study as the ore reportedly occurs as arsenides and sulfarsenides (Willden and Speed, 1974).

Just outside the study area on the west side of the Clan Alpine Range are deposits of mercury, silver and antimony in the Bernice Canyon district. Most important is the Red Bird Mine and associated prospects in Shoshone Canyon. Shoshone Creek which drains the area flows ~~east~~ west and south into the Humboldt Salt Marsh. A portion of the study area is within the Shoshone Creek flood plain and the creek may be a source of anomalous concentrations of both mercury and arsenic. The Red Bird cinnabar deposit produced approximately 40 flasks of mercury prior to 1943 (Willden and Speed, 1974).

Numerous prospect pits are found throughout the entire Dixie Valley area and much small-scale mineralization is evident.

2.4 References

Alexander, E. and Peterson, F., 1974, Reconnaissance soil survey, Dixie Valley, Nevada: Nevada Agri. Expt. Station, Water Planning Report, 92 p.

Meister, L.J., 1967, Seismic refraction study of Dixie Valley, Nevada, in U.S. Air Force Cambridge Research Labs., Spec. Rept. 66-848, 72 p.

Mackay Minerals Research Institute, 1980, Geothermal reservoir assessment case study, northern Basin and Range Province, northern Dixie Valley, Nevada: Rept. prepared for U.S. Dept. of Energy, Contract no. DE-AC08-79ET27006, v. I, 223 p. plus appendices, v. II, map plates; also Univ. Utah Res. Inst. Rept. NV/DV/SR-13.

Thompson, G.A., Meister, L.J., Herring, A.T., Smith, R.E., Burke, D.B., Kovach, R.L., Burford, R.O., Salehi, A., and Wood, M.D., 1967, Geophysical study of the Basin-Range structure, Dixie Valley region, Nevada: U.S. Air Force Cambridge Research Labs., Spec. Rept. 66-848.

Whitney, R.A., 1980, Structural-tectonic analysis, in Mackay Minerals Research Institute, Geothermal reservoir assessment case study, northern Basin and Range Province, northern Dixie Valley, Nevada: Rept. prepared for U.S. Dept. of Energy, Contract no. DE-AC08-79ET27006, v. I, p. 61-87.

Willden, R., and Speed, R., 1974, Geology and mineral deposits of Churchill County, Nevada: Nevada Bur. Mines and Geol., Bull. 83, 95 p.

Chapter 3. MERCURY AND ARSENIC SOIL GEOCHEMISTRY

By: Russell W. Juncal

3.0 MERCURY AND ARSENIC SOIL GEOCHEMISTRY

3.1 Introduction

3.1.1 Purpose and Scope

The purpose of the present study was to map and interpret the soil geochemical distribution of mercury (Hg) and arsenic (As) in Dixie Valley, Nevada and to relate the observed distribution patterns, where possible, to the presence of a geothermal influence. The location and approximate extent of the study area are shown on Plates I through III.

The study utilized a broad sampling network to identify and delineate specific areas for more detailed study. Additionally, high density sampling was performed in the vicinity of the two exploratory wells and across specific structural features as outlined by earlier work (Whitney, 1980).

Dixie Valley is presently undergoing exploration for geothermal resources and much geologic, geophysical and hydrologic data, as well as shallow temperature gradient and deep exploratory drilling information is available and can be related to the geochemical results (Mackay Minerals Research Institute, 1980). The data have been correlated to known structures, producing wells, geophysical anomalies and sites of near surface thermal activity to evaluate the cost-effectiveness of the technique for delineating permeable structures which may serve as drilling targets.

3.1.2 Methods and Analytical Techniques

3.1.2.1 Sampling

The initial sampling grid of approximately 400 points is shown on Plate I. The majority of the grid consists of parallel profile lines approximately 730 meters (2400 feet) apart bearing N60^{o}W, essentially normal to the average valley trend. Sample points along these lines are approximately 305 m (1000 ft) apart. The data from the grid were evaluated and used as the basis for selection of follow-up profiles sampled at 30 m (100 ft) intervals which are indicated on Plate III. Certain known structures and the areas around two geothermal wells (DF 45-14, DF 66-21) were sampled at 30 to 180 m (100-600 ft) intervals (Plate III).

Points on the sampling grid were located by bearing and traverse

using a surveyor's wheel. Field notes at each sample point included a description of the soil, the surrounding vegetation, soil moisture condition and additional comments including local morphology and proximity to roads or streams.

Soil samples were collected from a depth of 25-30 cm (10-12 in). The depth was chosen on the basis of three randomly selected vertical profiles from the three major soil environments in the area: upper alluvial fan slopes, fan piedmont and playa. The results of the profiles show the Hg and As values generally increasing with depth, with a zone from 15-25 cm (6-10 in) where values tended to increase substantially and then level off. These results were taken as representative of the study area as a whole and indicated much higher As and Hg values roughly corresponding to the B horizon. This is not unexpected as it is commonly the site of accumulation of clays and iron/manganese oxides both of which are important scavengers of mercury and arsenic (Fang, 1978; Horsnail and others, 1969; Boyle and Jonasson, 1973). Organic material has been shown to be even more effective in scavenging mercury (Trost and Bisque, 1971; Fang, 1978), but this effect should not be important in Dixie Valley as the soils are generally only moderately to poorly developed with very little organic matter. Because identification of specific soil horizons is difficult in many places and considering the study of Klusman and Landress (1979) which showed that variation of secondary soil parameters did not mask significant geothermal mercury anomalies, a standard sampling depth was chosen.

Dry samples were sieved in a stainless steel sieve at the site and the minus 80 mesh (.177 mm) fraction sealed immediately in airtight glass vials. Wet samples were dried at ambient temperature before sieving.

3.1.2.2 Quantitative Analysis

A Jerome 301 Gold Film Mercury Detector was used for determining mercury concentrations in the soil samples. This analytical method is based on the change in electrical resistance undergone by gold film when mercury is adsorbed. Weighed samples are heated to 600^{o} C for approximately one minute. The mercury which is vaporized by this process is collected on a gold plated coil. The coil is then heated to 600^{o} C on a 13 second timed cycle and the sample mercury is carried by

filtered air to the meter which consists of two gold films comprising opposite arms of a wheatstone bridge circuit. Before tha air stream reaches the meter it is split and the mercury removed from one side by passing over steel wool impregnated with Palladium Black ($PdCl_2$). This stream serves as the reference for the other fraction from which the mercury is collected by the sensor film. The resultant difference in resistance between the bridge leg exposed to filtered air and that exposed to air containing mercury vapor reflects the amount of mercury in the sample and is displayed on a digital readout. The accuracy of the gold film analyzer used in this study was not determined, however, the mercury values of replicated samples which were reanalyzed by two cold vapor atomic absorption techniques including borohydride generation methods generally ran 60-80% of the AAS values.

The precision of the instrument under field conditions is reported as greater than 1 ppb (Matlick and Buseck, 1976; J. McNerney, Jerome Instrument Corporation, pers. commun., 1980), although a precision of 1 to 4 ppb is representative of the instrument used in this study. The reproducibility of the results is affected by several factors. The small sample size (approximately 0.1 gram) from within such an inhomogeneous medium as soil may not make a given sample representative, particularly in an area such as Dixie Valley where mercury mineralization is known. Other sources of variation include temporal changes in the soil mercury content and experimental errors. The former possibility was investigated by reoccupying five sample sites at two week intervals for eight weeks. The results, shown in Table 3-1, show some variability with time, although no consistent pattern is evident. The variance is similar to that observed in replicate samples used to determine the analytical variability. Matlick and Buseck (1976) showed very little variation in mercury content of four sites resampled periodically over a two month period. Capauno and Bamford (1978) report significant variations upon resampling a traverse two weeks later but note that the anomalous area remained the same.

Seventy percent of the samples were analyzed for mercury within 72 hours using the Gold Film Mercury Detector. Due to mechanical malfunction of the instrument, delays of up to 20 days occurred prior to analysis of some samples. However this delay was found to be insignificant.

Table 3-1

Sample Stations Reoccupied at Two-Week Intervals

	Mercury Values (in ppb)			
Sample number	1	2	3	4
1	104	117	101	79
39	180	139	131	249
45	8	0	0	6
92	80	110	122	48
152	68	65	80	68

Upon rerunning 13 samples ranging from 28 to 272 ppb at one week intervals for four weeks to determine if mercury was escaping, no consistent pattern of declining mercury was observed (Table 3-2). Moreover, samples showed variations upon remeasurement similar to those of replicate samples rerun consecutively. Sample numbers, which correspond with sites indicated on Plate I, and their respective mercury concentrations are listed in Appendix A.

The arsenic analyses were performed by Rocky Mountain Geochemical Corporation of Salt Lake City using a colorimetric technique after Vasak and Sedivic (1952). In this method As is reduced to the trivalent state with potassium iodide and tin (II) chloride. The arsenic is then converted to its hydride by the action of nascent hydrogen, generated by adding zinc metal to the acid solution. The evolved arsenic hydride (arsine) is bubbled through a solution of silver diethyldithiocarbamate in a basic brucine-chloroform (or pyridine) solution. A brownish-red color is produced by the absorbing solution, the intensity of which is measured by a colorimeter and the arsenic concentration calculated. Results of the analysis indicating sample number and arsenic content are listed in Appendix A, with geographic distribution and values plotted on Plate II.

The arsenic content in many samples was not measured for up to two months from the time of sampling. Due to its lower volatility relative to mercury this was not expected to pose a problem. To verify this assumption, eight samples were rerun after more than four months in sealed storage. These samples showed no significant loss of arsenic as indicated by Table 3-3.

3.1.2.3 Data Presentation

Much of the data reduction and presentation has been performed by computer. The subroutines SRFACE and EZMXY from the National Center for Atmospheric Research graphics package (Wright, 1977) were used to make the chemical surface plots and profile line graphs, respectively. Subroutine CONRCSM from the same package generated the contours of the mercury and arsenic values for the broad grid and well site sampling. The programs were run from time share and output to a Hewlett Packard 7202A plotter.

Table 3-2

Successive Mercury Analyses at One-Week Intervals

	Mercury Values (in ppb)			
Sample Number	1	2	3	4
15	88	82	50	63
36	232	170	305	280
65	28	10	21	15
85	116	109	124	125
98	376	308	366	343
125	52	87	48	85
160	272	240	350	248
193	156	135	130	120
242	40	25	50	20
287	156	165	120	115
310	28	55	38	35
362	84	70	62	75
401	16	10	10	12

Table 3-3

Successive Arsenic Analyses at Four-Month Interval

Sample Number	Arsenic in ppm (9-6-1979)	Arsenic in ppm (3-4-1980)
1-10	11	10
1-35	14	15
2-5	15	15
2-15	12	10
2-35	16	10
3-15	46	50
3-35	25	30
3-45	24	20

Statistical analysis of the data utilized portions of the Statistical Package for the Social Scientist (Nie and others, 1975). Subprogram CONDESCRIPTIVE was used to compute descriptive statistics which included mean, standard error, standard deviation, kurtosis and skewness. Subprogram FREQUENCIES provided histograms of the data, and computed absolute and relative frequencies as well as cumulative frequency (%). The cumulative frequency data were used in the preparation of log probability plots.

The relationship between the arsenic and mercury values was evaluated using the subprogram SCATTERGRAM. This routine draws an x-y plot and computes the correlation coefficient (Pearson's r), significance of r, standard error of the estimate and the equation of the regression line.

Analysis of replicate samples for temporal and analytical variance was performed by subprogram ONEWAY. Output from this routine is a standard analysis of variance table which includes degrees of freedom, sum of squares, mean square, F ratio and F probability.

The computer methods were supplemented with the use of probability graph paper with a logarithmic ordinate scale and an abscissa scale of cumulative frequency (%) or probability. The probability axis is arranged such that a population that is lognormally distributed will plot as a straight line. An important consequence of this property is that a bimodal distribution, such as background plus anomaly, which is frequently encountered in geochemical sampling will show a sigmoid probability curve with two fairly linear segments joined through an inflexion point. Both the arsenic and mercury values from the broad grid sampling were plotted on log probability paper prior to the computer analyses which greatly aided their interpretation. For a more detailed discussion of probability plots including their use in partitioning mixed populations and selecting threshold values the reader is referred to Sinclair (1974).

3.1.3 Previous Work

A general association of arsenic and mercury with geothermal activity has been demonstrated by many workers. Weissberg and others (1979) reviewed a number of active geothermal systems where Hg and As precipitates occur and/or where thermal fluids contain high concentrations of

these elements. White (1967) showed the occurrence of Hg and As mineralization in numerous active or fossil hot spring systems. Robertson and others (1978) gave evidence of elevated Hg and As levels in the noncondensible gas, steam condensate and flashed brine phases of effluent from nine geothermal fields. Tonani (1970) showed high mercury levels in stream sediments around two Italian geothermal areas. Koga and Noda (1976) found anomalous Hg and As concentrations in both fumarole condensates and altered rocks in several Japanese thermal systems. Matlick and Buseck (1976), Phelps and Buseck (1978) and Klusman and Landress (1978, 1979) have shown broad Hg anomalies in the soils of several known geothermal areas. Klusman and others (1977) also showed broad arsenic soil anomalies in six Colorado thermal areas. More detailed soil surveys in known geothermal areas have shown mercury anomalies associated with faults and/or geophysical anomalies (Klusman and Landress, 1978; Souto, 1978; Capauno and Bamford, 1978). Surveys of this type may prove useful in selecting drilling targets.

Some mercury sampling of a reconnaissance nature was done in Dixie Valley by the Southland Royalty Company. This amounted to analysis of samples obtained during the installation of a one meter temperature survey net. The data will probably not be published but are mentioned briefly in this report.

3.1.4 Geochemistry of Mercury and Arsenic

Evaluation and interpretation of the field and laboratory data require consideration of certain aspects of the geochemistry of As and Hg. The elemental soil distribution patterns associated with geothermal activity in Dixie Valley are complicated by the presence of sulfide mineralization. Mercury and arsenic geochemical haloes associated with a variety of mineral deposits are well known. Numerous mineral exploration efforts using Hg and As content in soils have been conducted in the past and many of the geochemical principles developed in this work are applicable to geothermal exploration.

3.1.4.1 Mercury

Mercury can exist in three principal oxidation states, +2, +1 and the native metal (0). The relatively high vapor pressure of the native

element and, to lesser degrees, certain Hg compounds is unique among the metals. Mercury volatility is enhanced by the elevated temperatures within a geothermal system and its mobility in the vapor phase allows it to migrate to the surface through permeable zones. Robertson and others (1978) noted that elemental mercury was the dominant gaseous form of mercury in a study of effluent from eight geothermal areas.

While native mercury is known to occur in certain mineral deposits, including several within the Bernice Canyon district on the east side of Dixie Valley, generally it is found as the sulfide (cinnabar HgS) or as a trace within the lattice of other minerals. Various mechanisms have been proposed whereby mercury bound in this manner may be converted to the native element.

Figure 3-1 shows the relative stability fields of the important inorganic mercury compounds. The sulfide which has a restricted field of stability will yield native mercury in the zone of oxidation. Mercury contained within the lattice of other sulfides such as pyrite (FeS_2) or sphalerite (ZnS) may also be released as the native element upon oxidation. This involves the coupled oxidation of sulfur with the reduction of mercuric (+2) ion. The oxidation may occur in steps initially producing mercurous (+1) ions. The mercurous ions may then disproportionate by the following reaction (Jonasson and Boyle, 1972):

$$2Hg^{+} \rightleftharpoons Hg^{++} + Hg^{0}$$

Natural reducing agents such as iron may account for Hg(0) release below the zone of oxidation. McNerney and Buseck (1973) proposed stoichiometric adjustments within sulfide lattices as a possible source of electrons which could reduce mercuric ion and release vaporous mercury. Khayretdinov (1971), citing the inert behavior of mercury at higher temperatures, indicates elemental mercury may be electrochemically bound to the surface of mineral grains at depth and migrate in response to electrochemical gradients. Dickson (1968) proposed a source of native mercury from thermal decomposition of existent cinnabar combined with the reaction of sulfur with certain other ionic species. The release of Hg(0) by the thermal dissociation of various inorganic mercury compounds has been shown by Koksoy and others (1967). They indicated complete decomposition of mercurous and mercuric chloride below 250^{o} C, and HgS below 340^{o} C. Detectable quantities of native mercury and the

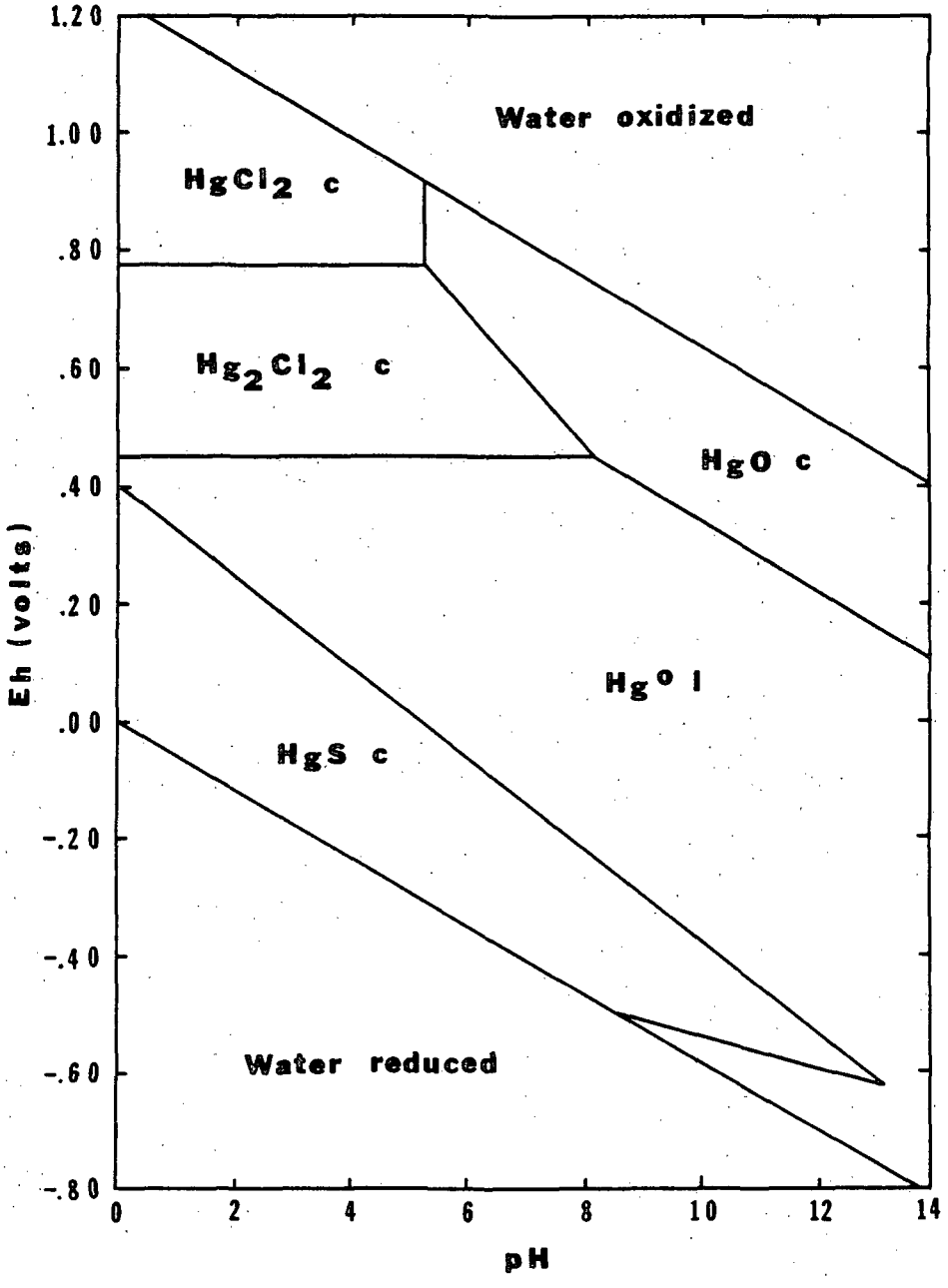

Figure 3-1. Stability fields of important inorganic mercury compounds at STP; total chloride = 36 ppm; total sulfur (as sulfate) = 96 ppm (from Hem, 1970a).

chlorides were liberated within 30 seconds at less than 80° C, detectable amounts of the sulfide were released at 210° C. Note that the samples for this experiment were crushed to pass a .074 mm (200 mesh) screen and that the amount of mercury released in 30 seconds is generally less for larger grain sizes.

Regardless of the mechanism of formation, elemental mercury will migrate in the vapor state through permeable zones toward the surface. Mercury in soil gas as an exploration technique has been demonstrated by McCarthy (1972), McNerney and Buseck (1973), and others. However, the soil-air mercury gradient is not fixed and may fluctuate temporally due to changes in temperature, barometric pressure, or moisture conditions. Because mercury tends to adsorb on clay and organic matter and to coprecipitate with hydrous oxides of iron and manganese it can accumulate in soils. A mercury anomaly in soil may be more consistent and pronounced than a corresponding soil gas anomaly.

Soil vapor anomalies are known over ore deposits as well as geothermal areas and the two can be difficult to distinguish from each other and from hydromorphic or mechanical dispersion haloes associated with mineralization. Anomalies related to both of the latter processes may occur in Dixie Valley.

Generally mechanical dispersion haloes are restricted in extent, occurring directly above or downslope from a mineralized area. The elements in this type of halo are held tightly by metallic bonds. Hydromorphic anomalies may be of greater extent and commonly occur as seepage anomalies at a break in slope. The elements in this type of anomaly are commonly adsorbed on clays or chelated by organic matter and not as tightly bound as mechanically dispersed haloes.

Figure 3-2 shows the stability fields and relative solubilities of the important inorganic aqueous species of mercury at STP in solution, with 36 ppm Cl^- and 96 ppm SO_4^{-2}. It can be seen that mercury is relatively insoluble under most circumstances. Additionally, the disproportionation reaction mentioned earlier can produce native mercury in water which may then volatize and escape, effectively lowering its solubilities even further.

Oxygenated high chloride waters can carry a considerable amount of mercury if the waters are relatively acidic. This effect has been

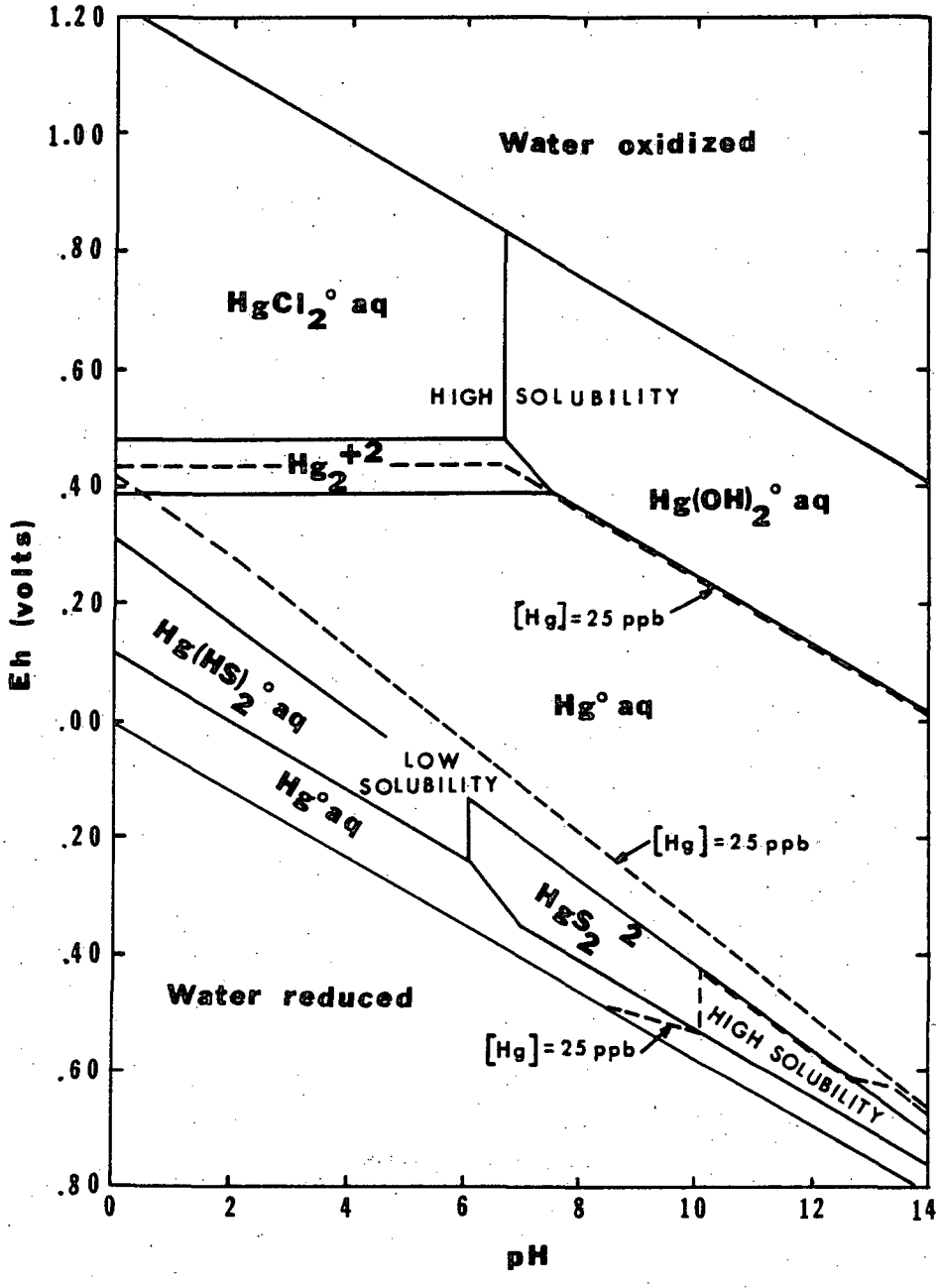

Figure 3-2. Stability fields of important inorganic aqueous mercury species at STP; total chloride = 36 ppm; total sulfur = 96 ppm (from Hem, 1970a).

observed in various geothermal areas where much higher mercury values are found in certain hot springs of high chloride and sulfate contents (Davy, 1974; Nakagawa, 1974). These types of springs probably represent supergene conditions and have been affected by surface oxidation and possibly evaporation. While relatively high chloride water is common in Dixie Valley, the deeper thermal waters exhibit low Eh values and the oxygenated surface waters are generally alkaline.

Most hot springs closely associated with the active hypogene transport and deposition of cinnabar carry only a few parts per billion mercury. The overall transporting capability of the springs is probably greater since the samples are representative of mercury concentration after deposition. Where total sulfur is high (approximately 3200 ppm) very large amounts of mercury can be held in solution as sulfide complexes. Mercury ore is typically deposited at temperatures of 100^{o} to 200^{o} C and pressures of 1 to 30 atmospheres from neutral to weakly alkaline waters of moderate to low salinity (Barnes, 1979). Above 200^{o} C mercury is mobile in steam even in the presence of excess sulfide (Ellis and Mahon, 1977). This effect has been observed at the Senator fumaroles in northern Dixie Valley where cinnabar and native sulfur are being actively deposited by H_2S bearing vapors with no liquid phase present (Lawrence, 1971).

Once in the surface environment in aqueous or vaporous form, the tendency of mercury to be adsorbed onto sediments will greatly restrict its mobility. In Dixie Valley where soils and waters are mostly alkaline, aqueous dispersion haloes should not persist for any great distance from the source of the mercury. However, sediments which have adsorbed mercury are susceptible to mechanical dispersion processes which may increase the size of a halo to some extent.

The adsorption behavior of mercury is central to the formation of soil anomalies. Numerous authors have demonstrated its ability to adsorb on clays and organic matter (Fang, 1978; Trost and Bisque, 1971; 1972; Rogers and McFarlane, 1978; Landa, 1978). High mercury values associated with the iron/manganese oxide fractions of some sediments suggest a coprecipitation or scavenging effect which has been demonstrated for other metals by Horsnail and others (1969). The possibility of secondary soil parameters masking mercury soil anomalies was

investigated by Klusman and others (1977) and Klusman and Landress (1978). This work indicated positive correlation between mercury content and soil pH, organic content, Fe/Mn oxides and aspect. Total carbon was found to be the most significant factor statistically. The authors concluded that, while significant, the controlling effects of these secondary parameters are overwhelmed in an area of prominent geothermal activity.

3.1.4.2 Arsenic

Arsenic exists naturally in three principal oxidation states, +3, +5 and 0. It may also occur in a -3 oxidation state in the very unstable hydride arsine (AsH_3) under extreme reducing conditions in natural waters (Sergeyeva and Khodakovskiy, 1969). The geochemistry of arsenic is complex and many factors bear on the mobility and fixation of the element in the geologic environment. Although the chemical states in which arsenic may migrate in a thermal system have not been characterized, several volatile phases are known. The native metal, $AsCl_3$, AsO_3 and AsS, among others are known to be relatively volatile below 300°C. The chloride is highly volatile but hydrolyzes readily in the presence of water. It may be important in acid chloride vapors or thermal waters (Boyle and Jonasson, 1973). Despite its potential to migrate in the vapor phase, Robertson and others (1978) report low As levels (.003 to .016 mg/l) in the noncondensible gas fraction of effluent from eight geothermal areas. Steam condensates from that study showed somewhat higher As levels (.001 to .09 mg/l), but the majority (.028 mg/l to 10 mg/l) remained in the flashed brine.

Arsenic forms ions of high charge (+3, +5) which are rapidly hydrolyzed in aqueous solutions and rarely exist as cationic complexes. In natural processes, it commonly forms anionic complexes and polymers, primarily with oxygen and sulfur. Where oxidation potential is low, arsenite $(AsO_2)^{-1}$ or thioarsenite $(AsS_2)^{-1}$ species would predominate. In more oxidizing environments, arsenate $(AsO_4)^{-3}$ and thioarsenate $(AsS_4)^{-3}$ species would be stable.

Depending on its complexed form arsenic may be mobile in both alkaline and acidic waters and, like mercury, arsenic can form sulfide complexes of high solubility. Orpiment (As_2S_3) and realgar (AsS) are common hot spring precipitates, frequently associated with mercury

minerals. The hypogene transport of arsenic is not completely characterized but is probably similar to mercury (Barnes, 1979). High arsenic concentrations in thermal waters in general have been reported from many geothermal areas (Weissberg and others, 1979; Hem, 1970b).

In the weathering cycle arsenic enters surface and ground water mainly as soluble arsenates. Thermodynamic data indicates the species $(H_2AsO_4)^-$ and $(HAsO_4)^{-2}$ are the equilibrium forms over the pH range of most natural waters, with the former dominant below pH 7.2 and the latter above (Hem, 1970b). In reducing conditions $HAsO_2$ may be present.

Arsenic concentrations in surface water depend on cation concentrations as well as the solubility of individual arsenate species which could exist as precipitates. While magnesium and calcium form relatively soluble arsenates, certain trace metals such as copper can greatly limit its solubility. The solubility products of various metal arsenates indicate very low solubility in terms of the anion AsO_4^{-3} (Sillen and Martell, 1964); however, this form is dominant only above pH 11.4 which is much higher than most natural waters. This effect could have some bearing in part of Dixie Valley particularly in or near the playa, where extremely alkaline conditions prevail.

Arsenic also may be taken from solution by coprecipitation/adsorbtion by hydrous iron oxides or adsorbtion on clays or organic matter. The tendency of hydrous iron oxides as well as certain iron bearing colloids to concentrate As explains why many mineral exploration soil surveys have found B horizons, the site of hydrous oxide accumulation, to be the most effective for sampling.

Klusman and others (1977) in a study of six Colorado geothermal areas found anomalous arsenic values generally outlined the same area as the mercury anomalies though not as strongly. They concluded that arsenic was not as effective as mercury in delineating areas of geothermal influence due to its closer affinity for the liquid phase.

3.1.5 Acknowledgements

This work was sponsored by the U.S. Department of Energy whose support is gratefully acknowledged. Many thanks are due to Dr. Pat L. Beaulieu, Dr. Larry T. Larson, Mr. Dennis S. McMurdie, Ms. Elaine J. Bell and Ms. Mollie A. Stewart for scientific advice, desperately needed editorial assistance, and positive encouragement throughout this project.

3.2 ANALYTICAL RESULTS

3.2.1 Mercury

3.2.1.1 Geochemical Surface

The results of the broad grid sampling of mercury are shown by three dimensional plots in Figures 3-3 and 3-4. The z axis represents the soil mercury concentration in parts per billion. This geochemical surface reveals some of the important aspects of the distribution of mercury in Dixie Valley. Most notable is the isolated high at the Dixie Comstock Mine and the prominent spike and cluster of somewhat lesser peaks between the fumaroles and Cottonwood Canyon. Both areas exhibit mineralization along the range front. Also apparent is the trend toward lower values away from the range front, closer to the playa. The geochemical surface for mercury is contoured on Plate I with sample locations and values shown.

3.2.1.2 Frequency Distribution

The frequency distribution for mercury is shown in Table 3-4 along with certain descriptive statistics. The distribution is highly skewed with most of the values smaller than the mean, but with a few extreme values being much greater indicating a more log-normally distributed population. A log-normal distribution is common for trace elements in geochemistry (Ahrens, 1954).

Deviations of the data set from log normality may be explained by the presence of a polymodal distribution. The polymodal or mixed frequency distribution can arise in various ways. In geochemistry it is common for a trace element to have a regional distribution pattern of values that may then be mingled with another population associated with mineralization which will have a markedly different frequency distribution. This would produce a bimodal distribution indicated by two peaks (modes) on the histogram of values. Where several sources or dispersion mechanisms contribute to the abundance of a given element a polymodal distribution will occur.

The possibility of a mixed frequency distribution can be examined by graphing the data on log probability paper as shown in Figure 3-5. The graph suggests the presence of three log-normally distributed populations. These consist of a set of values ranging from 0 to 20 ppb comprising approximately 15% of the samples, an intermediate group of

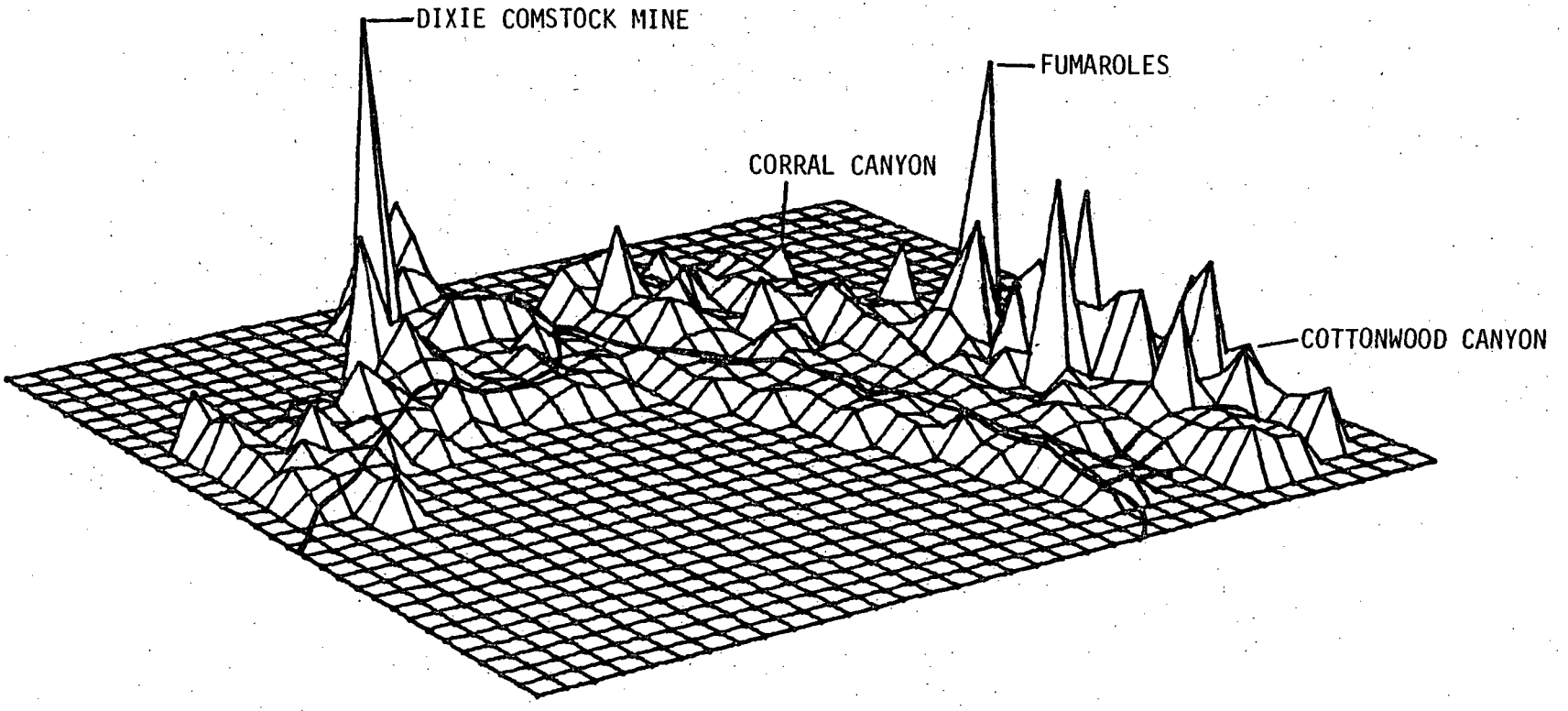

Figure 3-3. Mercury geochemical surface looking N15W.

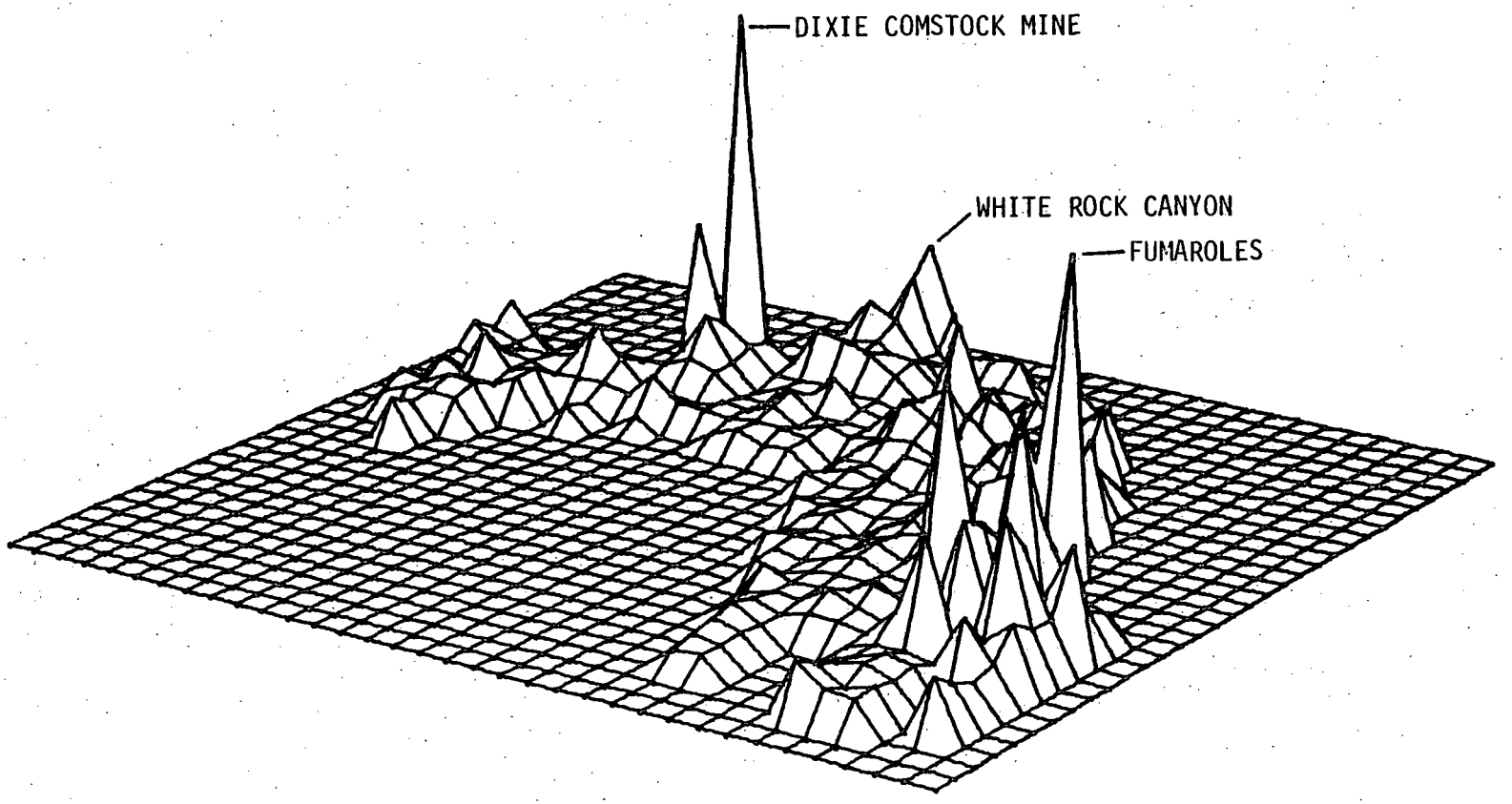

Figure 3-4. Mercury geochemical surface looking S75W.

Table 3-4

Frequency Distribution for Mercury

ppb Value	Freq.	Adj. Freq.%	Cum. Freq.%	Value	Freq.	Adj. Freq.%	Cum. Freq.%
0	2	0	0.5	144	2	0	87.4
4	6	1	1.0	148	1	0	88.2
8	13	4	4.7	152	2	0	88.7
12	14	3	8.6	156	5	1	89.8
16	16	4	12.6	160	5	1	91.0
20	6	1	14.1	164	2	0	91.5
24	18	4	18.6	168	3	1	92.3
28	22	5	24.0	176	3	1	93.0
32	20	5	29.0	180	1	0	93.3
36	16	4	32.9	188	2	0	93.8
40	28	7	39.8	204	1	0	94.1
44	10	2	42.3	212	1	0	94.3
48	19	5	47.7	220	1	0	94.6
52	6	1	48.2	232	2	0	95.1
56	24	6	54.2	248	1	0	95.3
60	10	2	56.6	256	2	0	95.8
64	13	3	59.9	272	2	0	96.3
68	13	3	63.1	284	1	0	96.6
72	11	3	65.8	288	1	0	96.8
76	8	2	67.8	296	1	0	97.0
80	7	2	69.5	364	1	0	97.3
84	7	2	71.2	376	1	0	97.5
88	9	2	73.5	388	1	0	97.8
92	4	1	74.5	392	1	0	98.0
96	8	2	76.7	400	1	0	98.3
100	3	1	77.4	480	1	0	98.5
104	7	2	79.2	488	1	0	98.7
108	8	2	81.2	560	1	0	99.0
112	2	0	81.7	976	1	0	99.3
116	6	1	83.1	1240	1	0	99.5
120	9	2	85.4	1400	1	0	99.8
124	1	0	85.7	2120	1	0	100.0
128	1	0	85.9				
132	3	1	86.6				
136	1	0	86.9				
140	2	0	87.4				

Mean	87.901	Variance	25432.764
Mode	40.000	Standard Deviation	159.477
Median	55.000	Standard Error	7.934
Minimum	0	Skewness	8.158
Maximum	2120.000	Kurtosis	84.794

values ranging from roughly 20 to 300 ppb making up about 83% of the samples and a small group of values above 300 ppm. The degree of overlap between groups is indicated by the steepness of the bend joining linear segments on the graph. A steep break between linear segments indicates a sharp demarcation, whereas a gentle break indicates considerable overlap between populations. The break between the lowest and intermediate populations is gentle and occurs over a small range of values indicating a large degree of overlap.

The group of lowest values probably represents a background population. It is comparable to background values for soil mercury in other geothermal areas as reported by Matlick and Buseck (1976) and Capauno and Bamford (1978). Four widely separated samples taken in the southern portion of the valley where there are no thermal manifestations and no nearby mineralization all had mercury values in this range. The majority of the points within the background group are in or near the playa, which is not unexpected for several reasons. First, the playa area is away from the mineralized bedrock and mercury is not easily transported in neutral to alkaline surface waters such as those commonly found in Dixie Valley. Also the potential vaporous mobility of mercury in the playa is inhibited by the near-surface water table, by the plastic weakly permeable nature of the sediments which will tend to close potential migration conduits such as faults, and by the ability of clays below the surface to effectively adsorb large amounts of mercury.

The population of highest values on the probability plot is almost exclusively associated with areas of mineralization along the range front. This segment of the graph is not as well defined as the central region due to far fewer points and because values in this range tend to tax the capabilities of the gold film detector making the results less reproducible, however a distinct break from the middle segment is clear.

The well-defined central segment of mercury values on the graph is being tentatively attributed to the geothermal influence where no mineralization occurs, though other sources are possible. Motor vehicle traffic is known to account for anomalous concentrations of mercury, although anomalies would then be expected to trend along the main roads; this was not observed. Pesticides and seed are possible sources but considering the limited cultivation within the study area this too seems

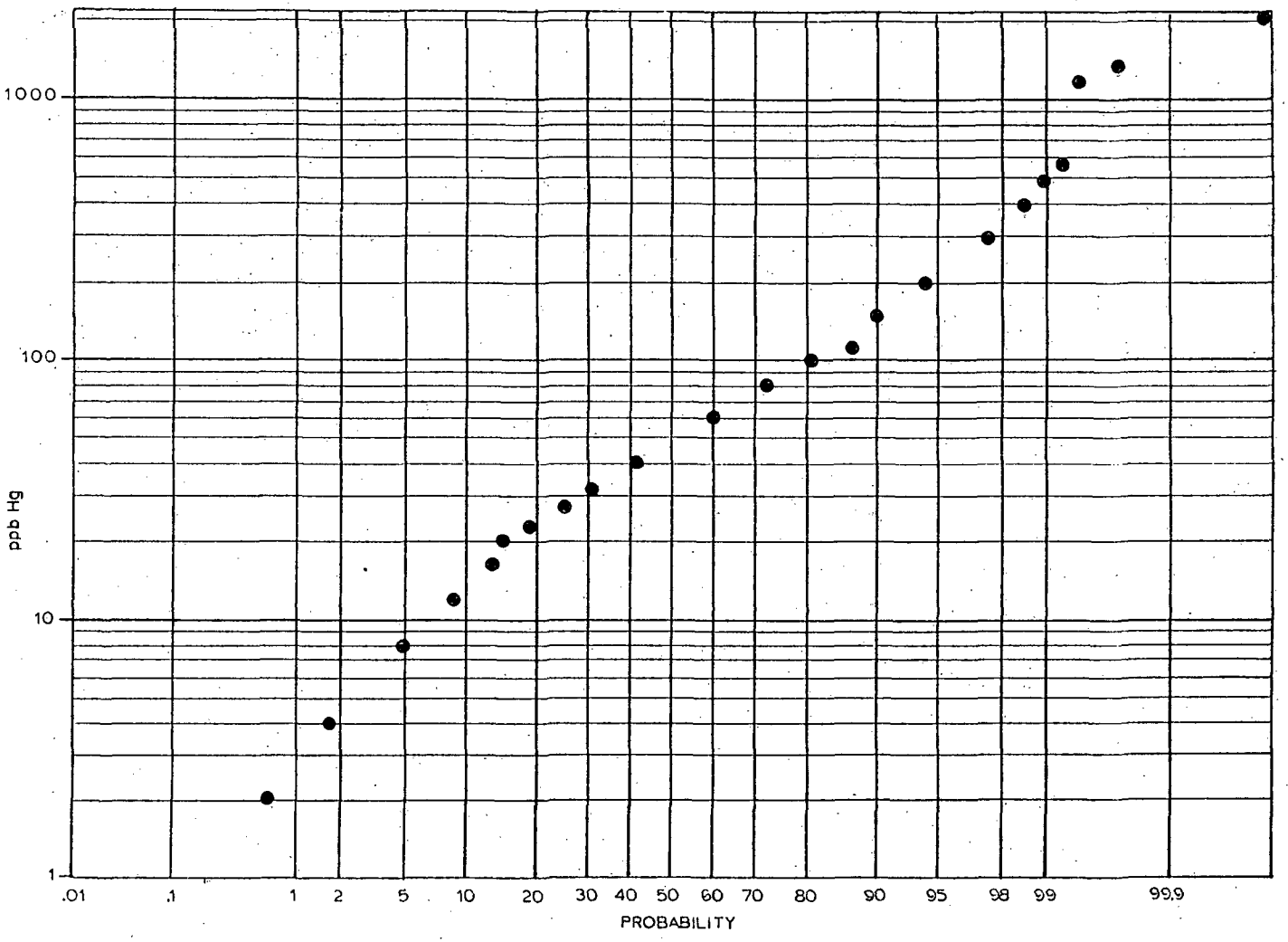

Figure 3-5. Log probability plot of broad grid mercury data.

unlikely. The nature of the break between the intermediate and high populations on the probability plot indicates somewhat less overlapping than observed for the low and intermediate populations. Some of the overlapping portion may represent areas where mercury previously concentrated by mineralizing processes has been remobilized by a thermal mechanism.

3.2.2 Arsenic

3.2.2.1 Geochemical Surface

The arsenic geochemical surface is depicted in Figures 3-6 and 3-7. There are some marked differences when compared to the mercury surface. The arsenic peak in the fumarole area is only moderate and the high near the Dixie Comstock is not nearly as anomalous as it is for mercury. Moreover, in contrast to the mercury values, high arsenic seems more prevalent towards the playa, particularly right at the playa margin. The N60^{o}W trending zone of low mercury values in the area of the most mountainward advance of the playa is the site of highly anomalous arsenic values (Section 14). The geochemical surface for arsenic is contoured on Plate II with sample locations and values shown.

3.2.2.2 Frequency Distribution

Descriptive statistics for the arsenic distribution are listed in Table 3-5. Like the mercury it is roughly log-normally distributed. Figure 3-8 depicts the arsenic data using a log probability plot. The graph shows an apparent bimodal distribution with a large population ranging from 5 to approximately 35 ppm and a smaller group of values above 35 ppm. Unlike the mercury data the highest population of arsenic is not as clearly associated with mineralization. However many of the high values are associated with the drainage from mineralized areas and may be hydromorphic dispersion halos. This is consistent with the affinity of arsenic for the liquid phase, particularly in comparison to mercury. At least four relatively high arsenic values are associated with springs, and another possibly with drillhole discharge during testing. Thermal fluids from drillholes DF 45-14 and DF 66-21 showed rather high As contents (0.59 ppm and 2.1 ppm, respectively; Bohm and others, 1980) making source implications for these latter anomalies clear.

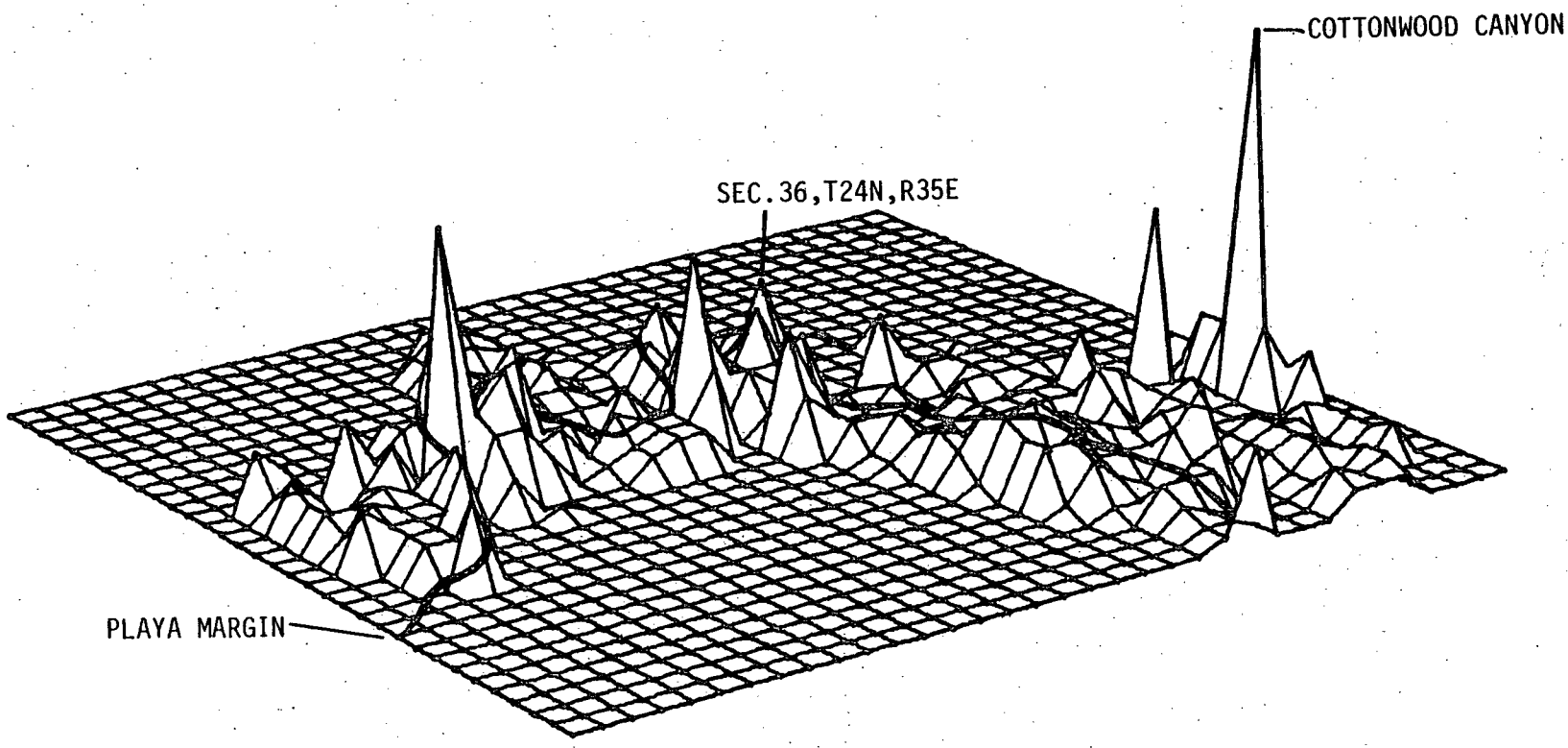

Figure 3-6. Arsenic geochemical surface looking N15W.

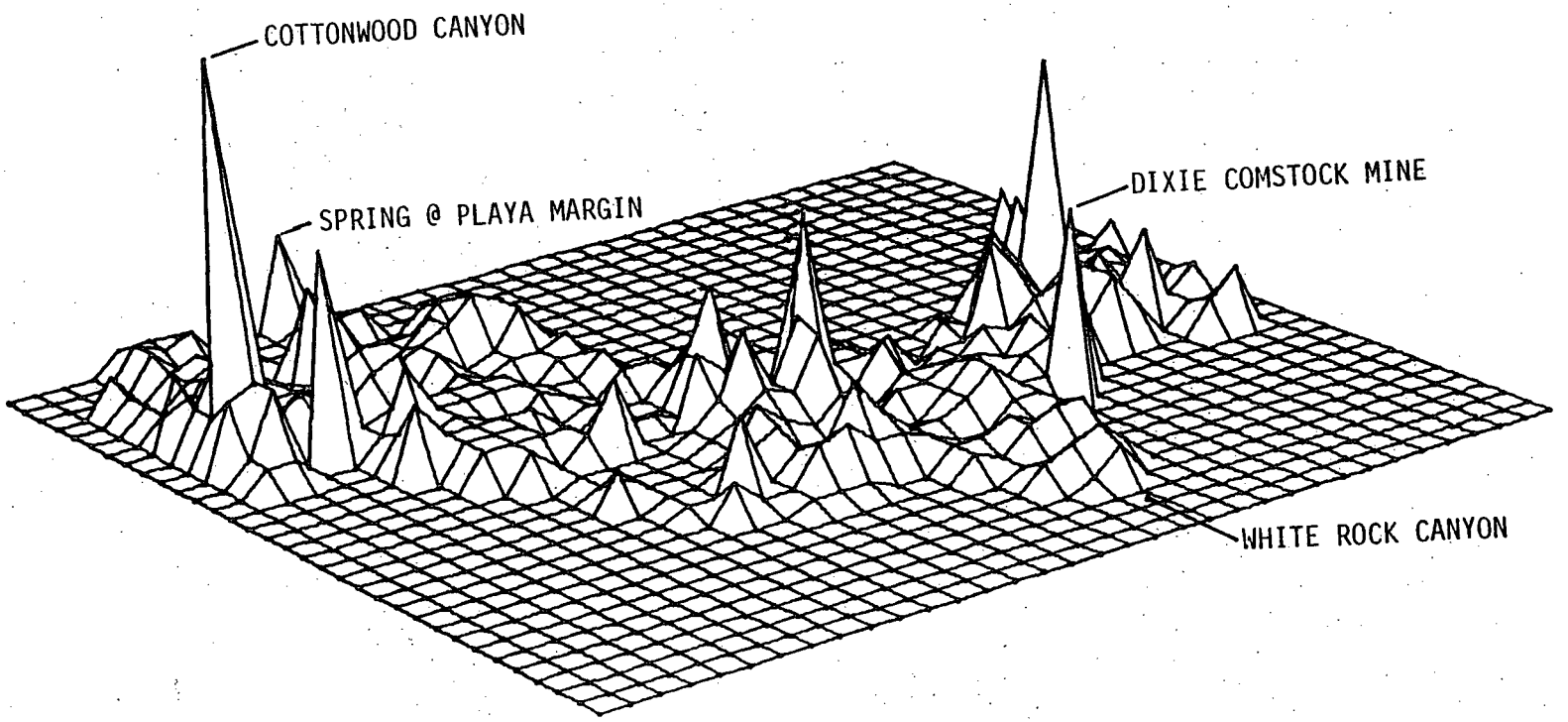

Figure 3-7. Arsenic geochemical surface looking S15E.

Table 3-5

Frequency Distribution of Arsenic

ppm Value	Freq.	Adj. Freq.%	Cum. Freq.%
1	4	.9	.9
5	46	9.8	10.7
10	139	29.7	40.4
15	137	29.3	69.7
20	34	7.3	76.9
25	45	9.6	86.5
30	16	3.4	90.0
35	21	4.5	94.4
40	9	1.9	96.4
45	5	1.1	97.4
50	3	.6	98.1
55	1	.2	98.3
60	1	.2	98.5
65	1	.2	98.7
80	2	.4	99.1
85	2	.4	99.6
115	1	.2	99.8
270	1	.2	100.0

Mean	18.010	Variance	272.794
Mode	15.000	Standard Deviation	16.516
Median	14.440	Standard Error	.822
Minimum	1.000	Skewness	6.270
Maximum	225.000	Kurtosis	65.184

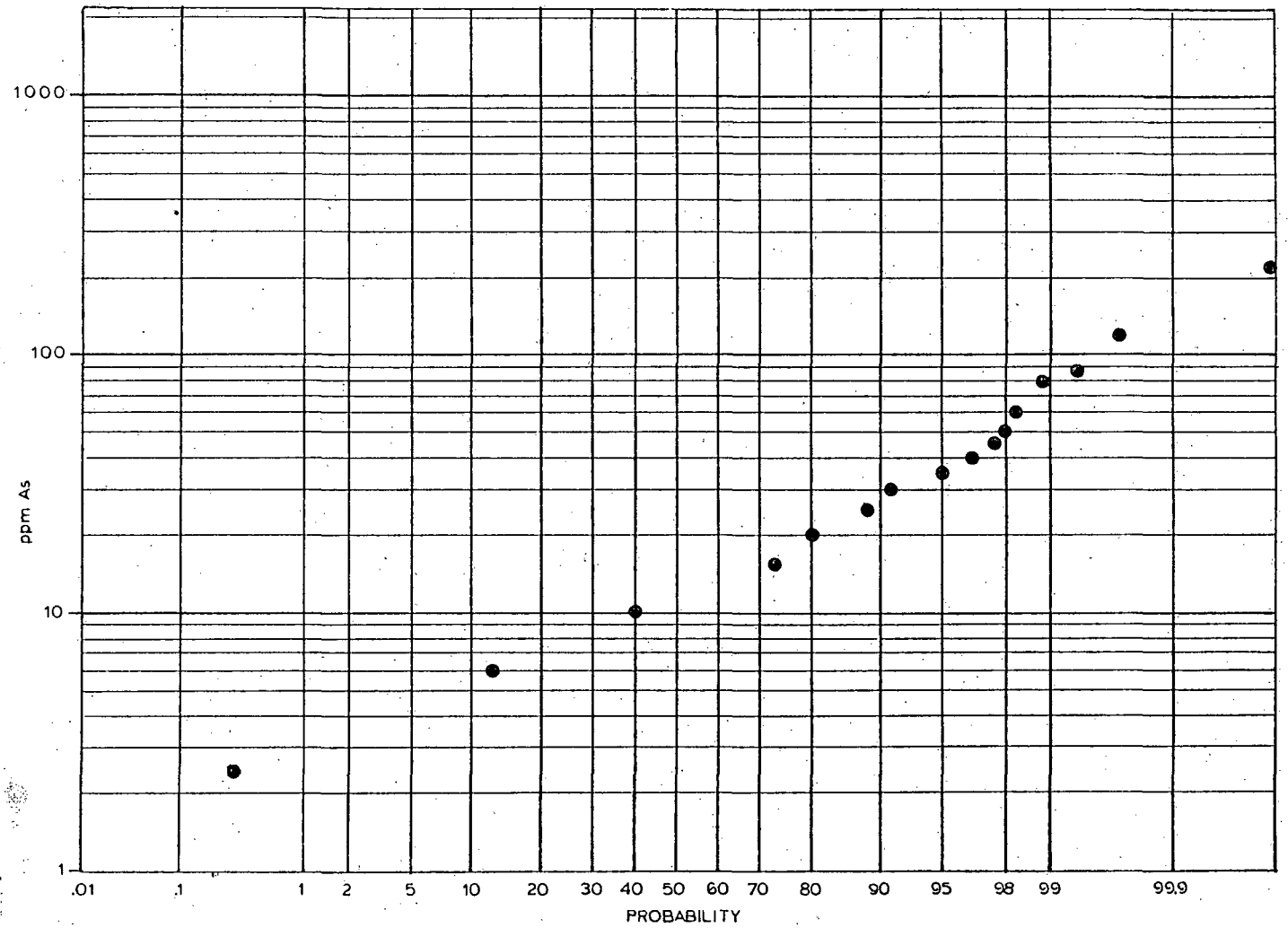

Figure 3-8. Log probability plot of broad grid arsenic data.

Plate II shows the approximate line where vegetation ends. This line also coincides closely with the site of several arsenic highs, most notably in the area south of the Dixie Comstock Mine. This may be due to a fairly abrupt chemical change in the near-surface environment. A rapid rise in alkalinity at the edge of the playa is indicated by crusts and salic horizons in the soil. This rapid pH change as surface water or near-surface ground water enters the area may cause deposition of arsenic. Perhaps a more likely source of these observed anomalies is the leakage of high arsenic waters from depth along faults at the margin of the playa. The active playa appears to be structurally controlled (Whitney, 1980), with numerous indicative geomorphic features found at its edge, including slumps, grabens and conspicuous springs, many of which show high arsenic values in the adjacent soil. This potential source of high arsenic values is discussed in more detail later.

The possibility exists that arsenic like mercury may be trimodally distributed. The sensitivity of the colorimetric method is limited to 5 ppm and it may be that a lognormally distributed background population exists in the 0 to 5 ppm range. Average arsenic values for "normal" soils from several data sources are given by Boyle and Jonasson (1973) as ranging from 3 to 12 ppm. Of four samples taken in the southern portion of the valley two showed less than 5 ppm, one 10 ppm and one 15 ppm. These results tend to support the above hypothesis. The thermal water and at least part of the nonthermal ground water of Dixie Valley is high in arsenic. Thus, the entire area may have a background population which is relatively high with no distinction between a geothermal and nonthermal source of arsenic. This possibility could be examined by reanalyzing with a more sensitive method such as hydride generation using AAS. The following discussion assumes a bimodal distribution of arsenic.

3.2.3 Correlation of Mercury and Arsenic

The correlation between the arsenic and mercury values for the grid sample locations is shown in Figure 3-9. The correlation (r) value indicates that they are very weakly correlated, with only two percent of the variation in mercury accounted for by the presence of arsenic. Generally away from the playa, particularly in areas of mineralization, the correlation is somewhat stronger but the presence of very high arsenic near the playa, probably from hydromorphic sources, obscures the

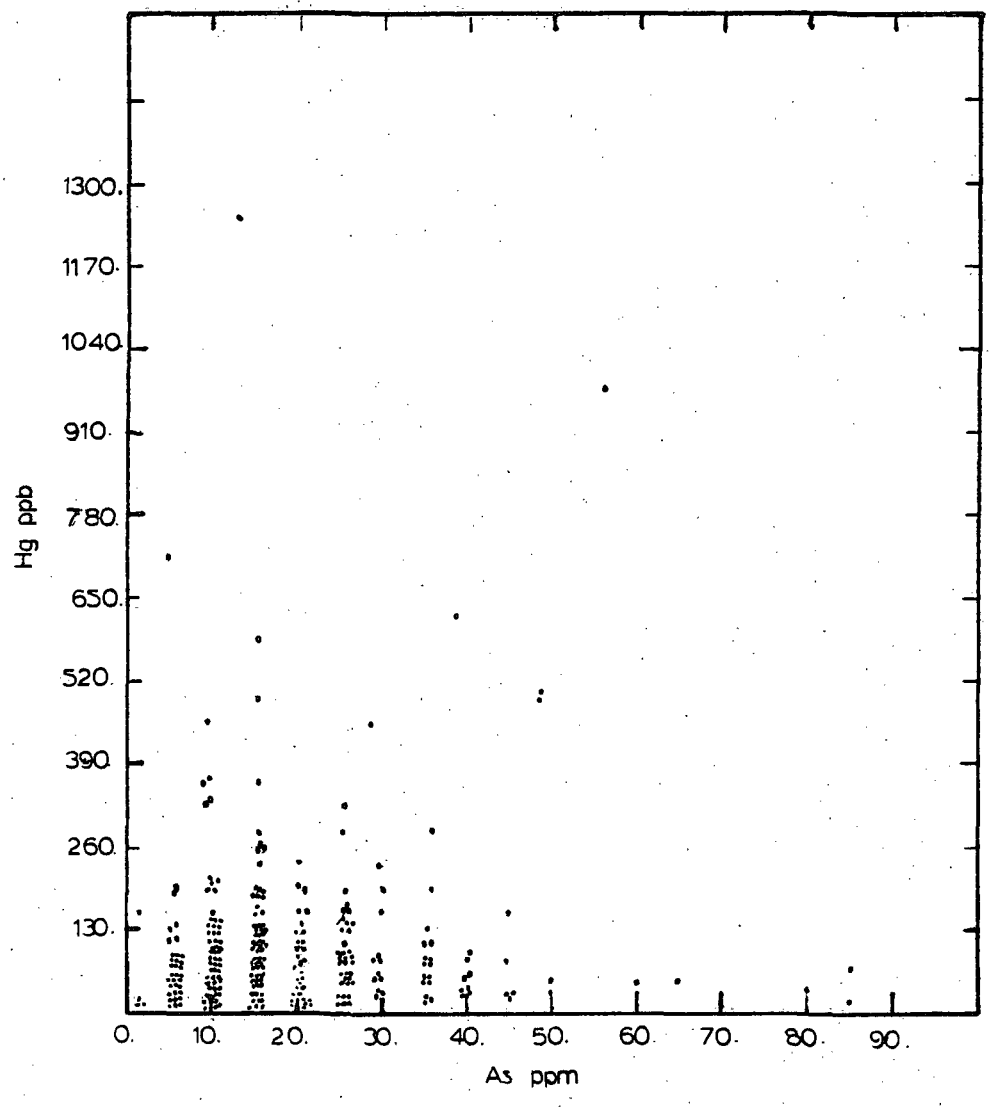

Correlation	(r)	.14	Std. Error Est.	121.87	Sig. r	.001
Intercept	(A)	125.51	Std. Error A	9.79	Sig. A	.0002
Slope	(B)	1.50	Std. Error B	.46	Sig. B	.001
r^2		.02				

Figure 3-9. Correlation of broad grid arsenic and mercury data.

relationship. Mercury anomalies will not tend to coincide with these latter arsenic highs since it does not form strong hydromorphic anomalies, particularly in waters typical of Dixie Valley, and also the presence of vapor anomalies is limited by the nature of the playa sediments.

3.2.4 Anomalous Areas

3.2.4.1 Geochemical Thresholds

Threshold values above which a particular sample is considered anomalous have been calculated by the method of Sinclair (1974) using the 1st and 99th cumulative percentiles of partitioned populations.

The mercury distribution has been partitioned into three separate populations in Figure 3-10. For the present purposes of this study the discrimination of the background and intermediate geothermally influenced populations is most important since the highest population is very small and can also be indicative of geothermal manifestations. Thresholds between the two lower populations are indicated at 10 and 80 ppb. The set of mercury values above 80 ppb, referred to as high anomalous, contain approximately 35% of the anomalous values attributed to geothermal influences and will be almost entirely from the anomalous group.

Values in the range of 10 to 80 ppb, referred to as low anomalous, contain approximately 64% of the anomalous population and will be comprised of about 90% samples from the anomalous population. Values below 10 ppm are considered background.

Figure 3-11 shows the arsenic data partitioned into two separate log-normal populations. Thresholds corresponding to the 99th cumulative percentile of the lower population and the 1st cumulative percentile of the higher population divides the data into three groups. Values above 47 ppm are referred to as high anomalous. Eighty five percent of the anomalous population falls into this group and approximately 64% of the samples in this group are from the anomalous population. Values between 30 and 47 ppm are referred to as low anomalous. Approximately 14% of the anomalous values fall in this range and about 7% of the values in this group are from the anomalous population. Values below 30 ppm are considered background, but may contain 1% of the anomalous population.

Although the definition of threshold as used here is arbitrary it does provide a measure of the likelihood that a value has arisen due to

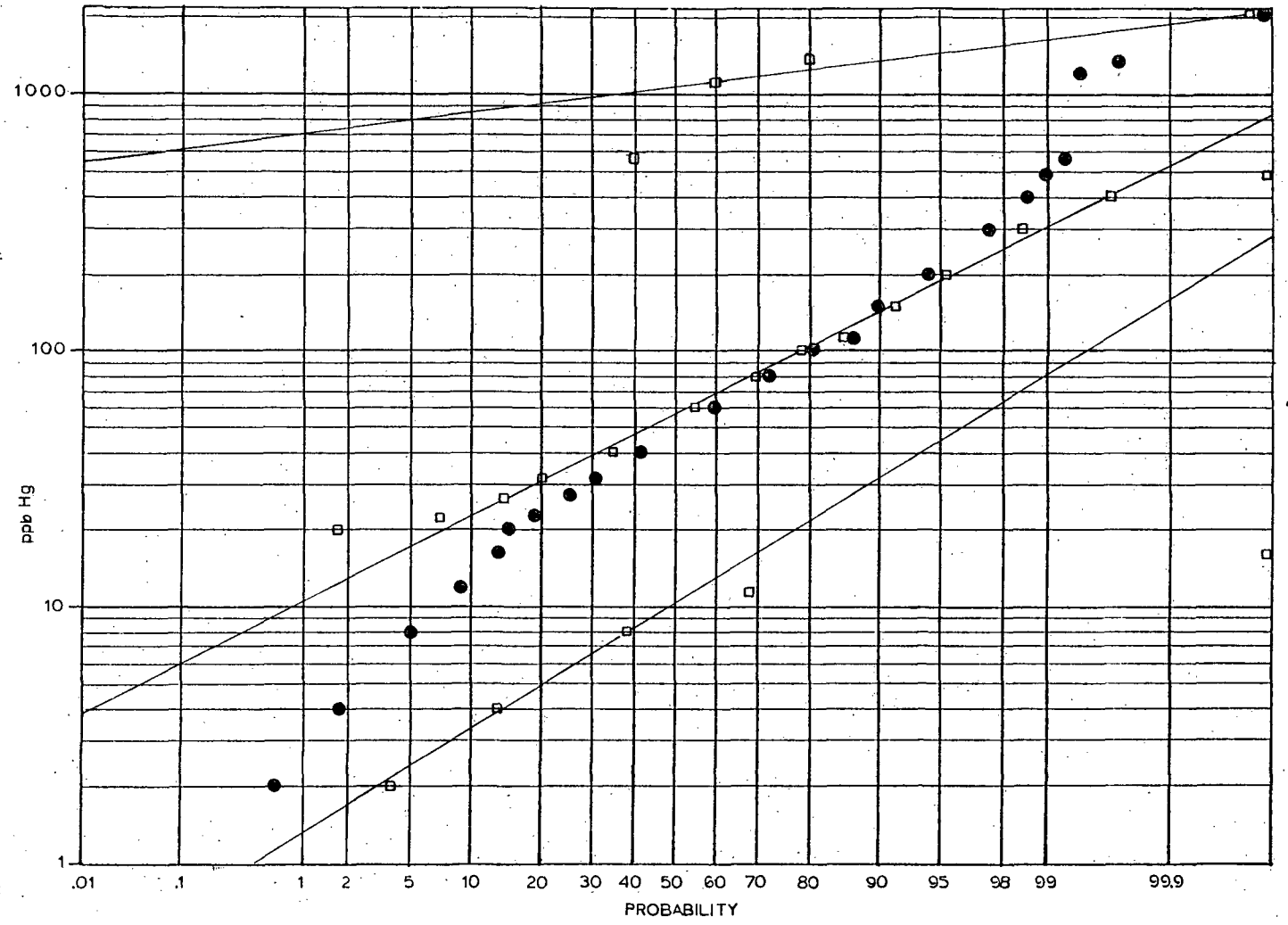

Figure 3-10. Partitioning of broad grid mercury data into three separate log-normal populations.

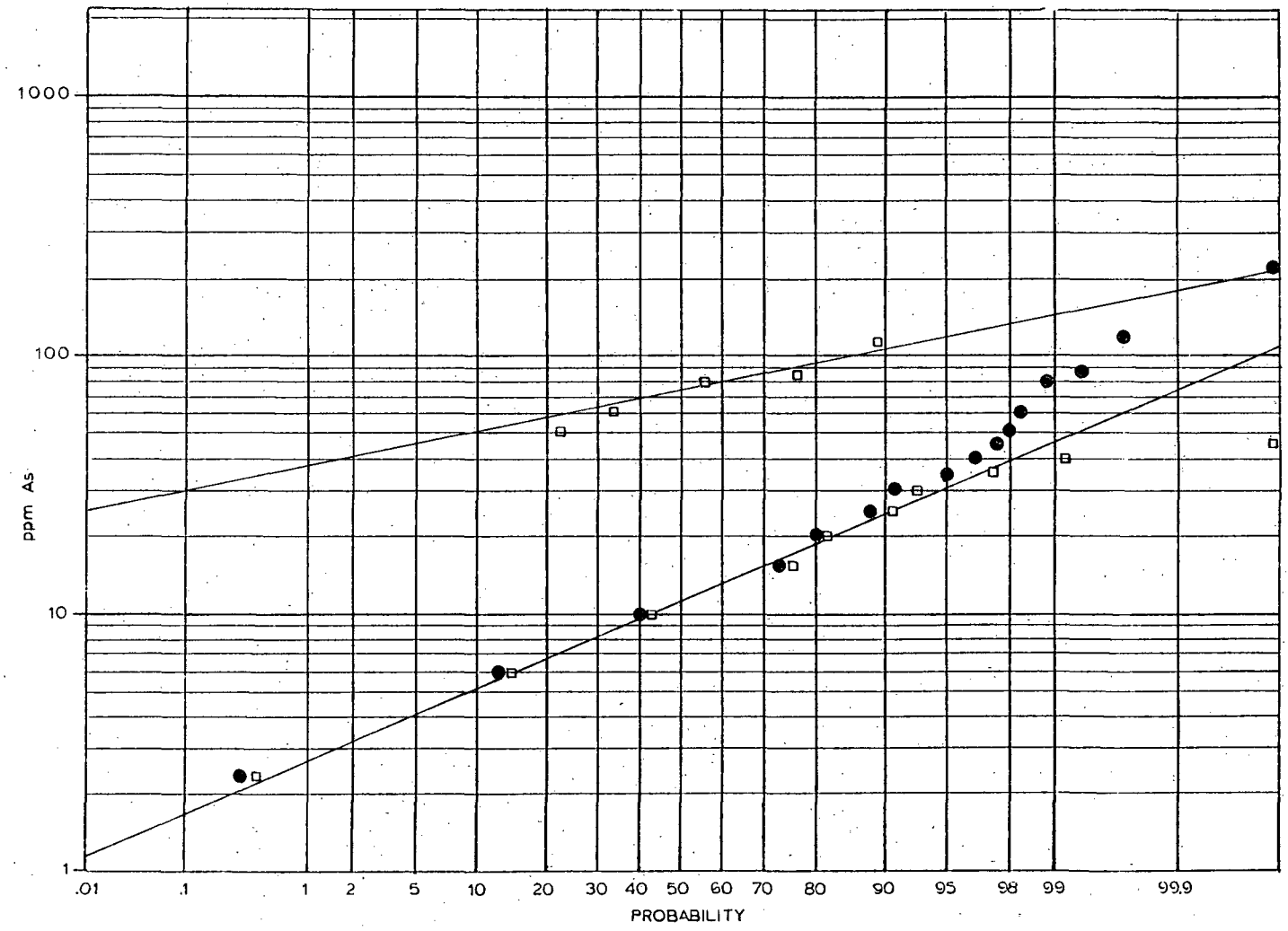

Figure 3-11. Partitioning of broad grid arsenic data into two separate log-normal populations.

a given source or mechanism. Also it serves to divide the data into priority groups for follow-up work. This is particularly important with regard to the mercury data where a majority of the samples fall in the 'geothermally influenced' population which overlaps significantly with the background population.

Much of the following discussion is based on Plates I through III. It must be noted that where isolated high values occur, contours around them may be misleading since the natural variability of the data can account for occasional extreme values.

3.2.4.2 Fumaroles and Corral Canyon

The highest mercury values are generally associated with mineral occurrences along the range front fault. The source of this mercury may be mechanically dispersed material from the deposits themselves with a geothermally related source also present. This seems likely in the area of the fumaroles in Section 15, T24N, R36E. The steam vents occur along the range front at an old mine site where two adits go into the hillside and a tailings dump is evident. Although it is not specifically mentioned in the literature the structural setting is similar to Corral Canyon where gold is found along the contact of albite/calcite dikes within the gabbroic country rock (Willden and Speed, 1974).

Extensive alteration and formation of red ferruginous clay has occurred adjacent to the ten fumaroles in the area and one of the adits is quite warm. Mercury values along the fumarole chain are much higher than those in the vicinity of the tailings dump at Corral Canyon. This suggests that the mercury is primarily related to the geothermal heat source, although the heat source could be mobilizing mercury which has already been preferentially concentrated by mineralizing processes. The size of the mercury halo around the fumaroles compared with Corral Canyon probably reflects the increased mobility of mercury in the vapor phase. Arsenic values at Corral Canyon and the fumaroles are similar, in the range of 25 to 35 ppm. High values of arsenic also exist down the fan slope from both of these areas, which is suggestive of a mechanically dispersed halo. Alternatively the geochemical distribution near the fumaroles, particularly for mercury, may be due to a north to northwest trending structure. While no obvious structure appears to intersect the range front at the fumaroles, it may be significant that

to the north the Senator fumaroles occur near the mapped intersection of the trace of the northern splay of the Buckbrush fault and the range front.

3.2.4.3 Dixie Comstock Mine

Although no fumaroles are present at the Dixie Comstock Mine, high heat flow and hot water very close to the surface are known. Very high anomalous mercury values may be due at least in part to the thermal influence. It should be noted that this mine is a considerably larger operation than the two small adits in the fumarole area, its tailings dump is many times larger, and at one time an amalgamation mill existed on the site. Therefore potential mercury anomalies associated with the mineralization and subsequent mining operation would be expected to be far more obvious here.

3.2.4.4 Cottonwood Canyon

Isolated high As and Hg values occur near the mouth of Cottonwood Canyon which contains known mineral deposits. The highest value near Cottonwood Canyon occurs in the area where drainage has been diverted to the Boyer Ranch reservoir and which was not affected by the flash flooding of July, 1979. Areas that were affected by the flooding generally showed background or low anomalous values of mercury and arsenic. The significance of this is not clear, although it may be that the debris of the flood contains most of its metal values in the larger grain sizes and/or does not possess an horizon of metal accumulation such as the typical soil. Because a standard sampling depth was employed only the flood debris and not the underlying soil was sampled. The thickness of the flood deposited material was too great to allow sampling of the underlying soil to test the above hypothesis. However, samples taken from the area prior to the flooding were analyzed for mercury by Southland Royalty Company and the values ran significantly higher. The arsenic value corresponding to the highest mercury was the largest recorded in the study. This may be due to the previously mentioned arsenide and sulfarsenide ores found three miles up the canyon, although adjacent values in the flood deposits from the canyon were at background levels.

3.2.4.5 White Rock Canyon

Several anomalous geochemical values occur near the mouth of White Rock Canyon. A high of 373 ppb mercury appears to be part of a somewhat linear trend of high anomalous values which is suggestive of a structurally controlled feature. The peak values of arsenic and mercury in the area coincide, although the arsenic values are generally low anomalous or background.

Although mineralization is known in the upper portions of the canyon, it is not extensive. A sample taken approximately 305 m (1000 ft) into the canyon where soil had formed on an older stream terrace, showed values of only 40 ppb mercury and 10 ppm arsenic. Several lineaments mapped in this area from low-sun-angle aerial photography (Whitney, 1980) are mimicked by the mercury contour trend. The White Rock Canyon fault, a major cross cutting structure in the valley intersects the range front Stillwater fault approximately at the mouth of the canyon (Plate III). A temperature gradient hole (H-2 on Plate III) drilled to a depth of 152 m (500 ft) near the mouth of the canyon showed a relatively low thermal gradient. A negative gradient is observed to a depth of 20 m (65 ft) before an approximately $2.5^{o}C/100$ m ($1.4^{o}F/100$ ft) gradient is established to TD. It seems likely that shallow ground water flow is responsible for the negative temperature gradient in the upper 20 m (65 ft) east of the range front fault. The Stillwater fault is indicated on the drill logs by a zone of lost circulation which coincides with the gradient reversal. One meter temperature measurements in the area are inconclusive being neither significantly lower nor higher than adjacent areas. These results seem to indicate that any near-surface thermal effects along and just to the east of the range front are largely overwhelmed by the mountain front ground water recharge.

The possibility of a structure or structures further east of the range front which might conduct or previously conducted thermal fluids was investigated by sampling at 30 m (100 ft) intervals along a $N60^{o}W$ traverse (line B-B'; Plate III) approximately 500 m (1640 ft) south of White Rock Canyon. The results of this profile are shown in Figure 3-12.

A significant zone of high anomalous mercury values exists along the traverse which may be due to upward migration from a splay of one of the faults to the west or perhaps may be related to one of several

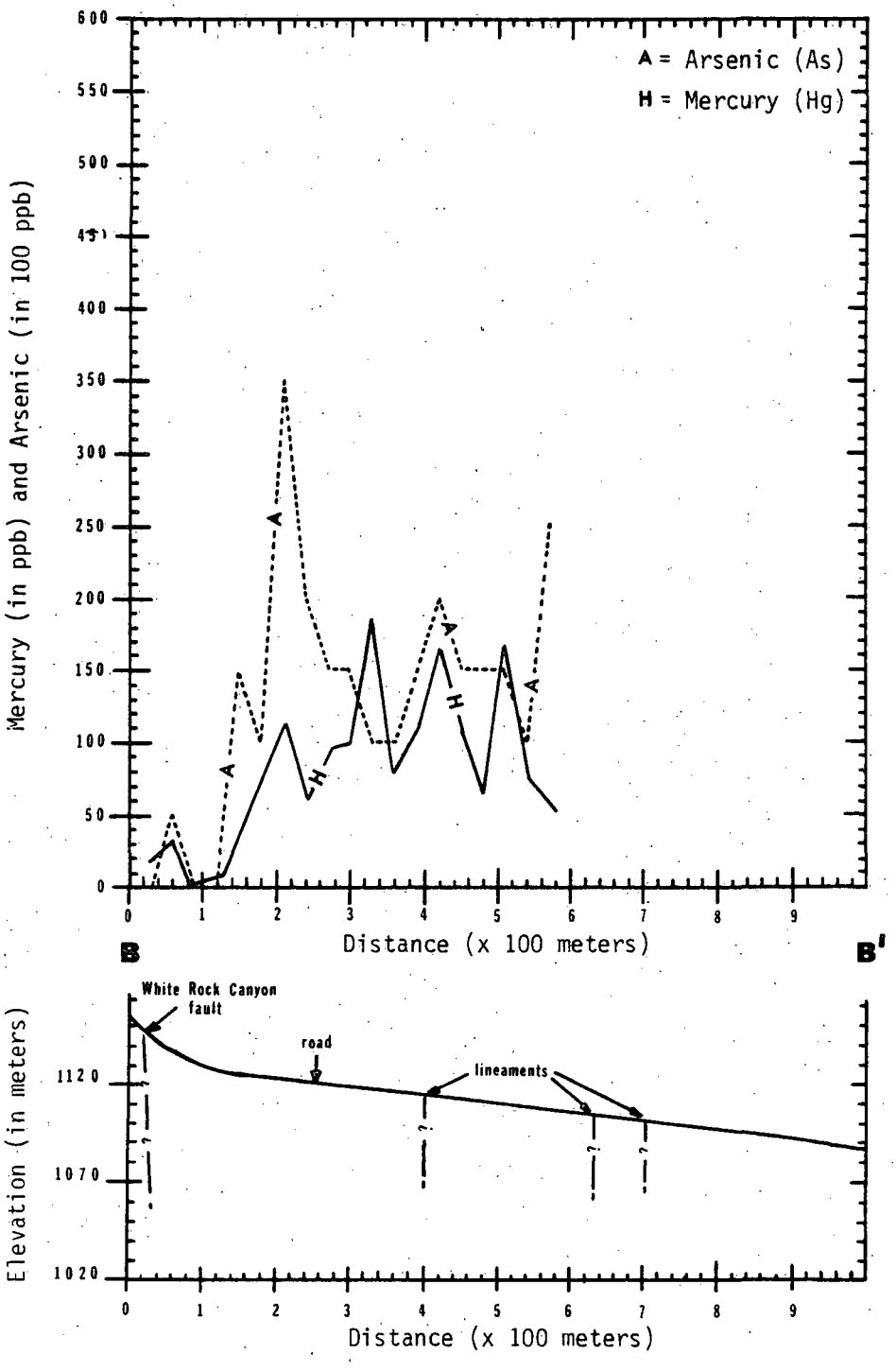

Figure 3-12. Profile of mercury and arsenic along traverse B-B' south of White Rock Canyon (see Plate III).

lineaments in the area representing older structures which are serving as paths for geochemical migration. It is conceivable that at one time the Stillwater fault broke across the fan emerging from White Rock Canyon and that these lineaments represent this older structure.

The correlation coefficient for the mercury and arsenic values along traverse B-B' is -.07 indicating the two are probably unrelated. However, the zone of highest arsenic occurred in an area where a well-developed, finely textured, damp soil existed. To the east this area changes abruptly into the gravelly, poorly developed soil typical of the upper portions of the fans. This transition could bear on the arsenic-mercury observations in several ways. First, a locally high water table, perched by faults, may promote more rapid soil development with the arsenic values associated with the seepage and mercury migration being suppressed by the water. Or second, the confluence of drainage from the several canyons may affect the local heat flow patterns with arsenic deposited at the range front break in slope. The mobility of mercury would be inhibited in areas of ground water influx while arsenic would have a greater tendency to be associated with areas of high water table. The abrupt change from coarse to fine material with a localized water condition is highly suggestive of a structural discontinuity. Possibly the arsenic is associated with the water bearing fault zone at the surface and mercury migrates through splays or more permeable zones just east of the fault. While largely speculative, a structurally controlled source for the high mercury values seems feasible.

3.2.4.6 Section 36, T24N, R35E

Another area where geochemical trends indicate possible structural controls occurs in the central part of the study area (Section 36, T24N, R35E) where the playa most closely approaches the range front, coming within approximately 610 m (2000 ft). A spring occurs at the base of the steep talus slope which joins the mountain front and playa. The valley drainage is also displaced closer to the western range front in this area so that streams flow nearly east-west toward this area before turning south toward the Humboldt Salt Marsh. This topographic low shows rather low mercury values similar to most other areas of fine-grained sediments. The area is, however, the site of a linear trend of high anomalous arsenic values. This arsenic could be related to the

spring issuing from the range front, or it may be due to water migrating up from deeper zones along permeable structures. This latter possibility is supported by the convergence of several of the major fault systems in the area: the Stillwater, Marsh and Dixie Meadows faults (Plate III). Additionally the southernmost, probably southeast trending, margin of the Humboldt gabbroic complex probably occurs very near this point in the valley. An area of abnormal aeromagnetic gradients also terminates at or near this area and may be related to the gabbro.

3.2.4.7 Dixie Meadows Fault (Section 32, T24N, R36E)

The Dixie Meadows fault describes an arcuate path to the northeast from Section 36 (T24N, R36E). In the southeast corner of Section 32 (T24N, R36E) an area of anomalous temperatures measured at one meter depth (Campana and others, 1980) occurs near the fault trace. This area is near the 455 m (1500 ft) gradient hole drilled by Southland Royalty Company in 1978 which showed an average gradient of approximately $7.5^{o}C/100$ m ($4.1^{o}F/100$ ft). Both arsenic and mercury show high anomalous values in this area with fairly linear northwesterly trends (Plates I and II) near the postulated trace of the Dixie Meadows fault. Follow-up sampling was done in this area at 30 m (100 ft) intervals along a traverse (Line A-A'; Plate III) transecting the Dixie Meadows fault; the results are shown in Figure 3-13. A dominant mercury peak appears to be spatially associated with the approximate trace of the Dixie Meadows fault. Arsenic values tend to mimic the mercury particularly west of the fault trace. While indicated by only three points on the traverse mercury values appear to fall off rather rapidly to background levels east of the fault trace. This may be due to the presence of finer-grained sediments to the east. The correlation between arsenic and mercury is very weak for this traverse ($r = -0.02$) and, as at White Rock Canyon (Line B-B'; Plate III), may be due to the effects of hydromorphic processes upon arsenic.

The fault zone in this area may be relatively wide thus accounting for the rather broad band of anomalous mercury. This is supported by a wide area of lineaments and other fault related features identified on low-sun-angle aerial photography (Whitney, 1980). While structural control of the observed geochemical trend across profile A-A' is likely,

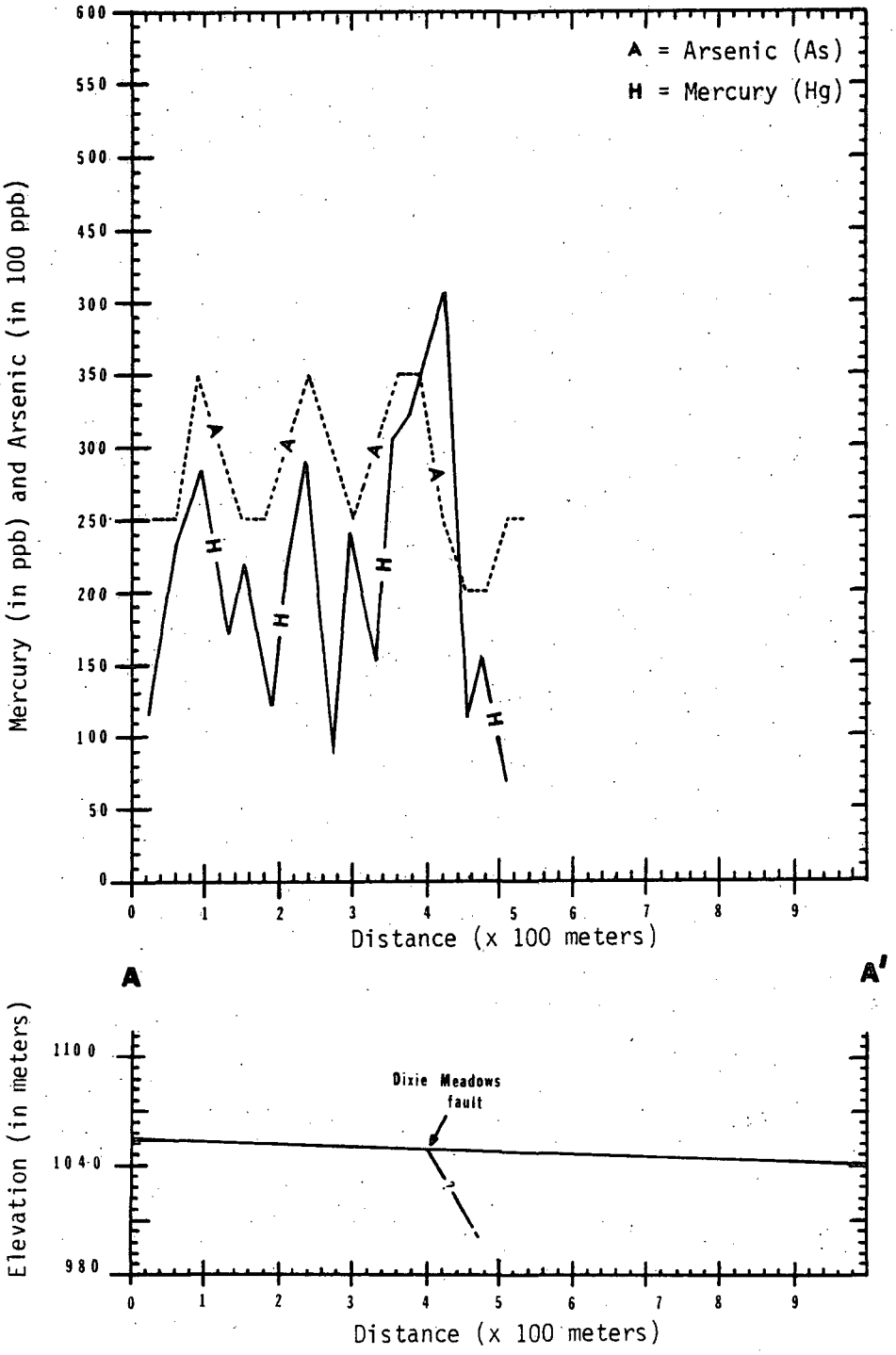

Figure 3-13. Profile of mercury and arsenic along traverse A-A', transecting the Dixie Meadows fault (see Plate III).

the effects of nearby mineralization may be at least partly responsible. The geochemical values, particularly arsenic, may be influenced by drainage from the Stillwater Range. The drainages of several mineralized zones along the range front fault flow through this area. However, considering the apparent structural interactions in this area, it seems more likely arsenic is coming from deeper water migrating upward along faults.

3.2.4.8 Dixie Meadows Fault (Section 14, T24N, R36E)

Further north along the trend of the Dixie Meadows fault (Plate III) are several coincident geochemical trends. Most notable is the linear zone of high mercury in and around Section 14 (T24N, R36E). Arsenic trends in the area are similar but not coincident. At the intersection of the Dixie Meadows fault trace and the range front is an extensively altered area, with high anomalous mercury and arsenic values, which appears to be an old landslide block. This strong correlation between the geochemical and structural trend is significant, although nearby range front mineralization may also contribute to the anomalous values.

Approximately 2 km (1.25 mi) southwest of this intersection in Section 15 is the chain of fumaroles previously discussed. Whether these two zones of high geochemical values indicate a structural relationship is not clear.

3.2.4.9 Buckbrush Fault Trace

As shown on Plate III, the southern splay of the Buckbrush fault appears to intersect the range front in the same area as the Dixie Meadows fault. A very conspicuous line of springs occurs along the fault trace in Section 26 (T24N, R36E) and is accompanied by low anomalous arsenic and mercury trends. The springs have not been sampled for arsenic but the possibility of communication with high arsenic thermal water exists. A similarity between the waters of the Buckbrush Seeps which occur along the Buckbrush fault to the south, and the Hyder Hot Springs to the north has been noted by Bohm and others (1980). Buckbrush Seeps have not been analyzed for arsenic but Hyder showed some of the highest values noted for surface water in the valley, approximately 300 ppb.

Another possible source of the arsenic is streams draining the Bernice District in the Clan Alpine Range. Both Spring and Shoshone

Creeks drain the area of the Red Bird mercury mine and could contribute anomalous amounts of arsenic and/or mercury.

The mercury values associated with the Buckbrush fault trace are generally low but the higher values are among the low anomalous group. Given the nature of the sediments and mercury values associated with the playa elsewhere, the areas above the 40 ppb contour along the Buckbrush fault trace must be considered anomalous. The path of this fault trace becomes less clear to the north due to cultural modifications to the land surface, but several other geochemical highs are associated with the postulated fault trace. While it is not clear on the contour map (Plate I), point 373 which is approaching the fault trace is a high anomalous mercury value. Profile C-C', discussed in more detail below, shows progressively higher values towards the fault trace.

3.2.4.10 Sun Oil Company Wells

Observed coincident geochemical and structural trends discussed above are significant in relation to the deep exploratory wells which have been drilled by Sun Oil Company in this area. At least three of the four wells are producers, with the depth of production from approximately 2200 to 2900 m (7200 to 9500 ft).

No obvious geochemical anomalies were identified near these wells by the 305 m (1000 ft) sampling. One potential reason for the generally low to moderate mercury values is the presence of very fine-grained sediment. Although the wells are considerably north of the furthest extent of the playa at present, the surface is quite likely underlain by older fine-grained playa material.

Since the Sun Oil Company Wells are proven producers and since a splay of the Buckbrush fault lies to the east, it was decided to profile across the zone of drilling at 30 m intervals (line C-C'; Plate III). The results of the traverse are shown in Figure 3-14. The correlation of arsenic and mercury along the traverse is stronger here ($r = .38$) than in other areas but is still rather weak. Similar to other areas in the valley, this may be due to a difference in sources or dispersion mechanisms for these two elements. The arsenic and mercury values become consistently higher to the east near the Buckbrush fault trace. Whether the fault, the geochemical values, and producing wells are related is not clear but comparison to nonproducing wells DF 45-14

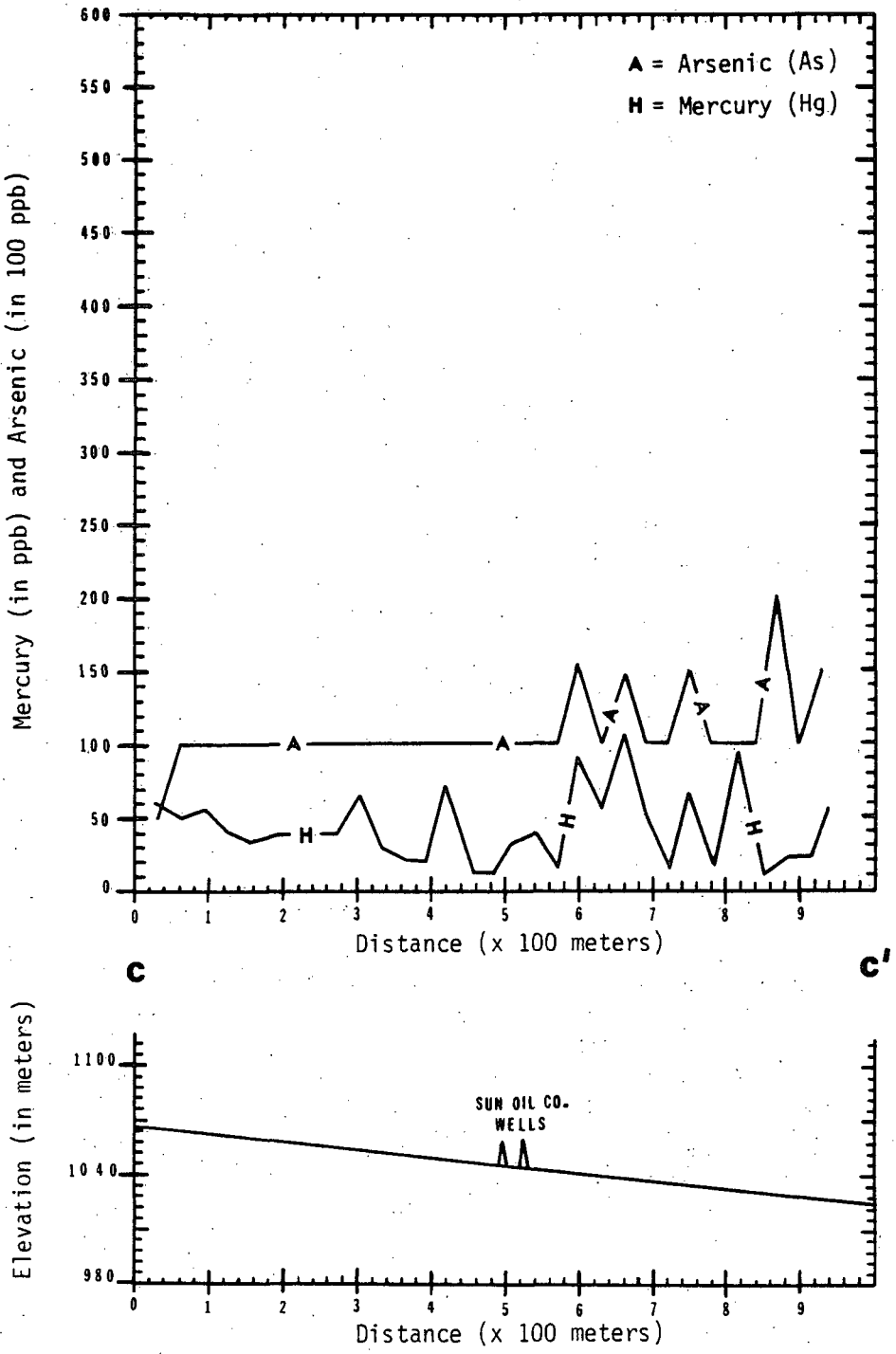

Figure 3-14. Profile of mercury and arsenic along traverse C-C' north of Boyer Ranch (see Plate III).

and DF 66-21 argues favorably for it.

3.2.4.11 DF 66-21

A square grid of points spaced at 183 m (600 ft) has been sampled around well DF 66-21 as shown in Figure 3-15 with geochemical contours imposed upon it. It can be seen that the values around the well site are considerably higher in places than any detected in the area by the broad grid sampling as shown on Plate I. This may be due to disturbance of the area during drilling and testing, an effect which has been inferred for other geothermal areas (Capauno and Bamford, 1978).

No particularly significant trends occur around the well, which is not unexpected since no thermal fluids were encountered near the surface here nor were any structures mapped (Whitney, 1980). The drillhole did penetrate zones of high temperature fluid but flow rates were generally low. Zones of thermal activity encountered in DF 66-21 would be expected to correlate with structures to the west, most notably the Stillwater fault. Where a zone of high pressure hot water found just below 1430 m (4700 ft) may connect to the surface is unclear. If the zone at 1430 m were postulated to be a basin and range type structure of 55^{o} to 60^{o} dip, its trace would coincide with an area of lineaments which have been mapped approximately 1000 m (3300 ft) west of DF 66-21 (Whitney, 1980). Perhaps significantly the trend of these lineaments intersects the range front at the fumaroles. Similarities between downhole mineralogy and mercury content for cuttings from the well (Chapter 4, this report) and samples taken from the fumarole chain to the northwest also suggest some association. No significant geochemical anomalies occur along the Stillwater fault in this part of the valley which may mean it has been sealed to some extent by mineral deposition. This is an area of the fault which has apparently been unaffected by the most recent tectonic events.

It also appears that DF 66-21 has been drilled west of a major structure that may border or communicate more directly with the geothermal reservoir which could account for the low flow rates. This is suggested by the coincident geochemical and geomorphic trends to the east along the Dixie Meadows and Buckbrush faults.

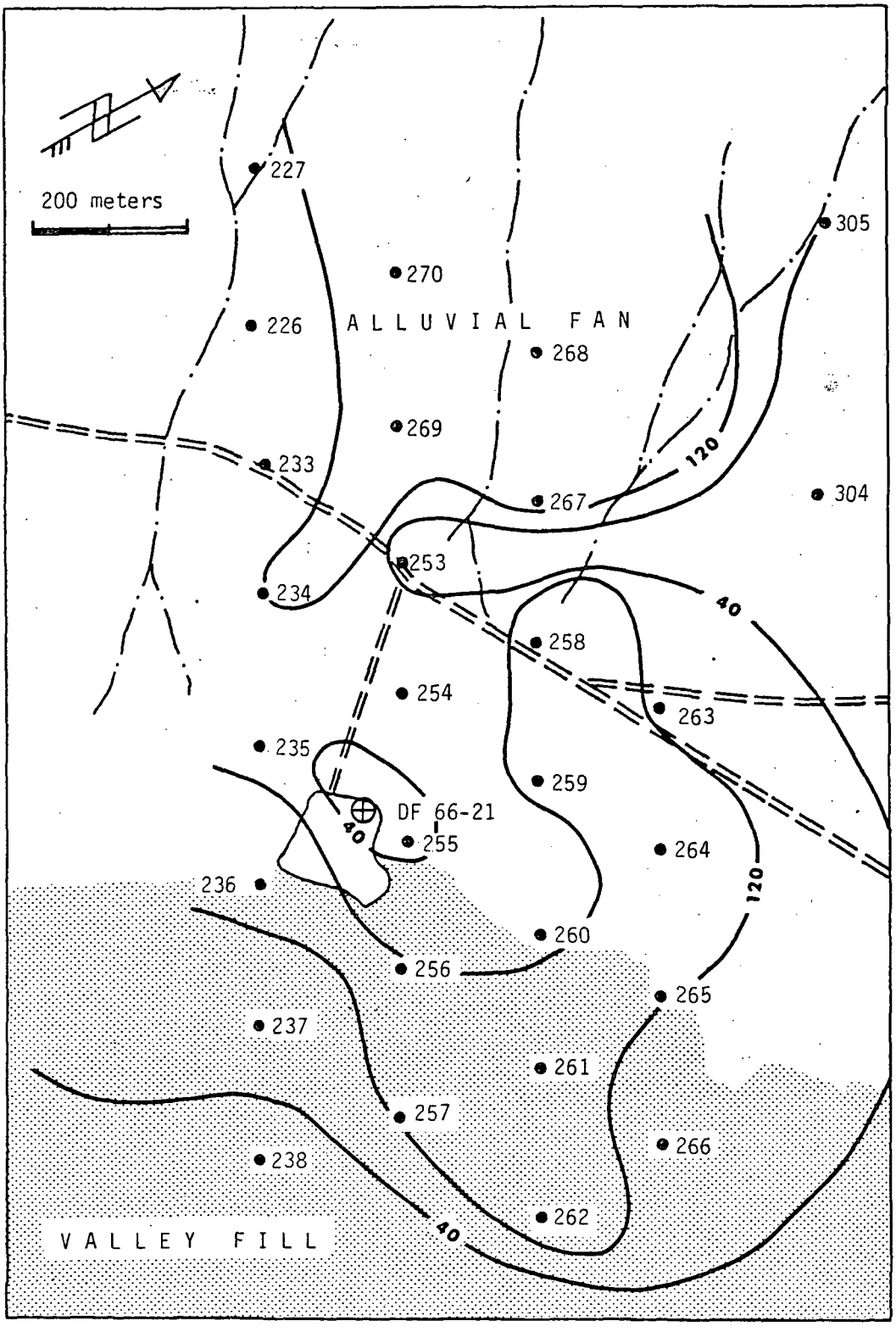

Figure 3-15a. Contoured mercury geochemical surface in vicinity of DF 66-21. Values indicated by contours; sampling sites indicated by solid circles; extent of geomorphic surfaces indicated by shading.

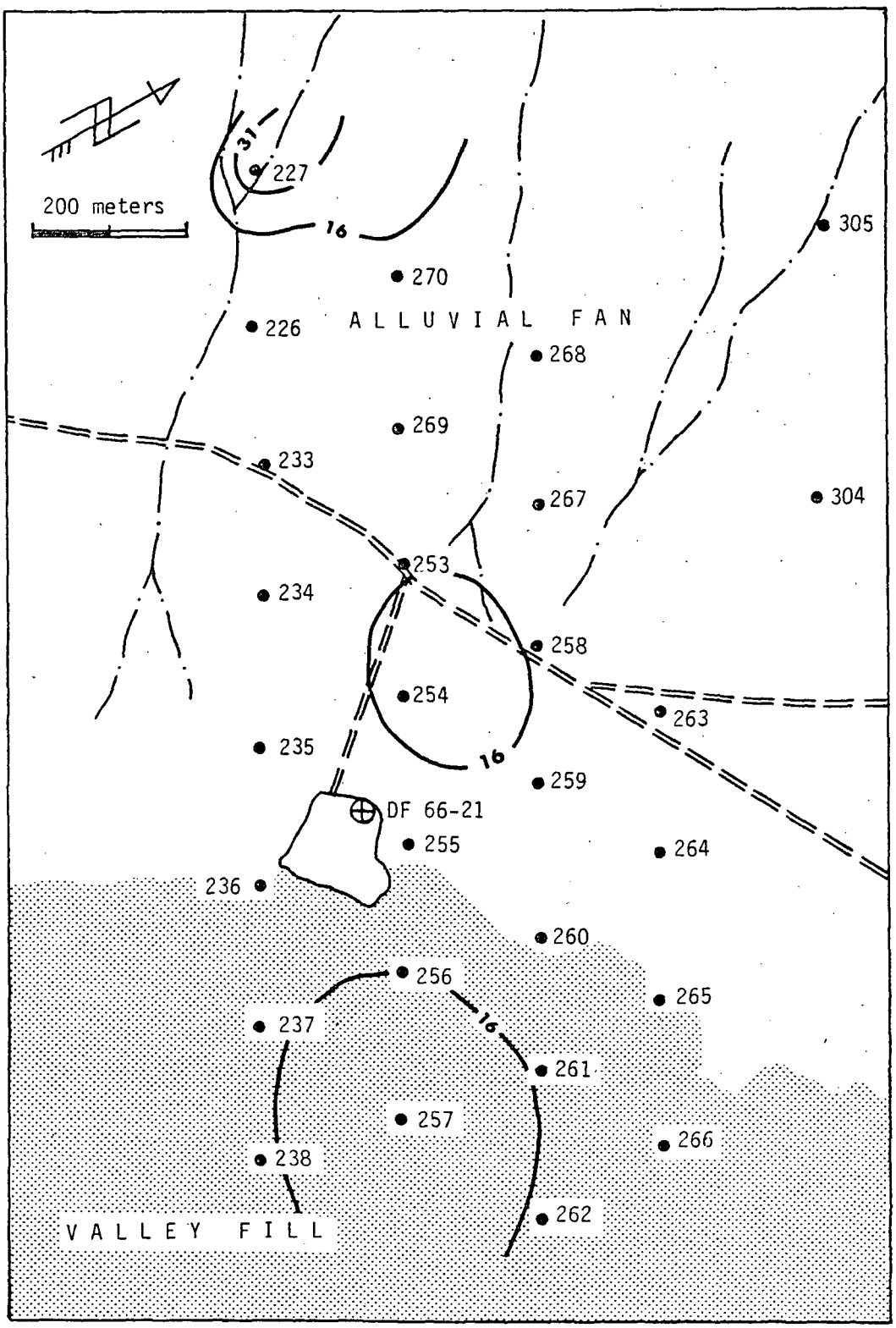

Figure 3-15b. Contoured arsenic geochemical surface in vicinity of DF 66-21. Values indicated by contours; sampling sites indicated by solid sircles; extent of geomorphic surfaces indicated by shading.

LIST OF AUTHORS

Chapter 1. INTRODUCTION
Elaine J. Bell and Lawrence T. Larson

Chapter 2. GEOGRAPHIC AND GEOLOGIC SETTING
Russell W. Juncal and Elaine J. Bell

Chapter 3. MERCURY AND ARSENIC SOIL GEOCHEMISTRY
Russell W. Juncal

Chapter 4. PETROCHEMISTRY
Elaine J. Bell

Chapter 5. DIXIE VALLEY GEOTHERMAL SYSTEM
Elaine J. Bell

TABLE OF CONTENTS

Table of Contents (cont'd)

Table of Contents (cont'd)

LIST OF TABLES

List of Tables (cont'd)

LIST OF FIGURES

List of Figures (cont'd)

List of Figures (cont'd)

LIST OF PLATES

Chapter 1. INTRODUCTION

By: Elaine J. Bell and Lawrence T. Larson

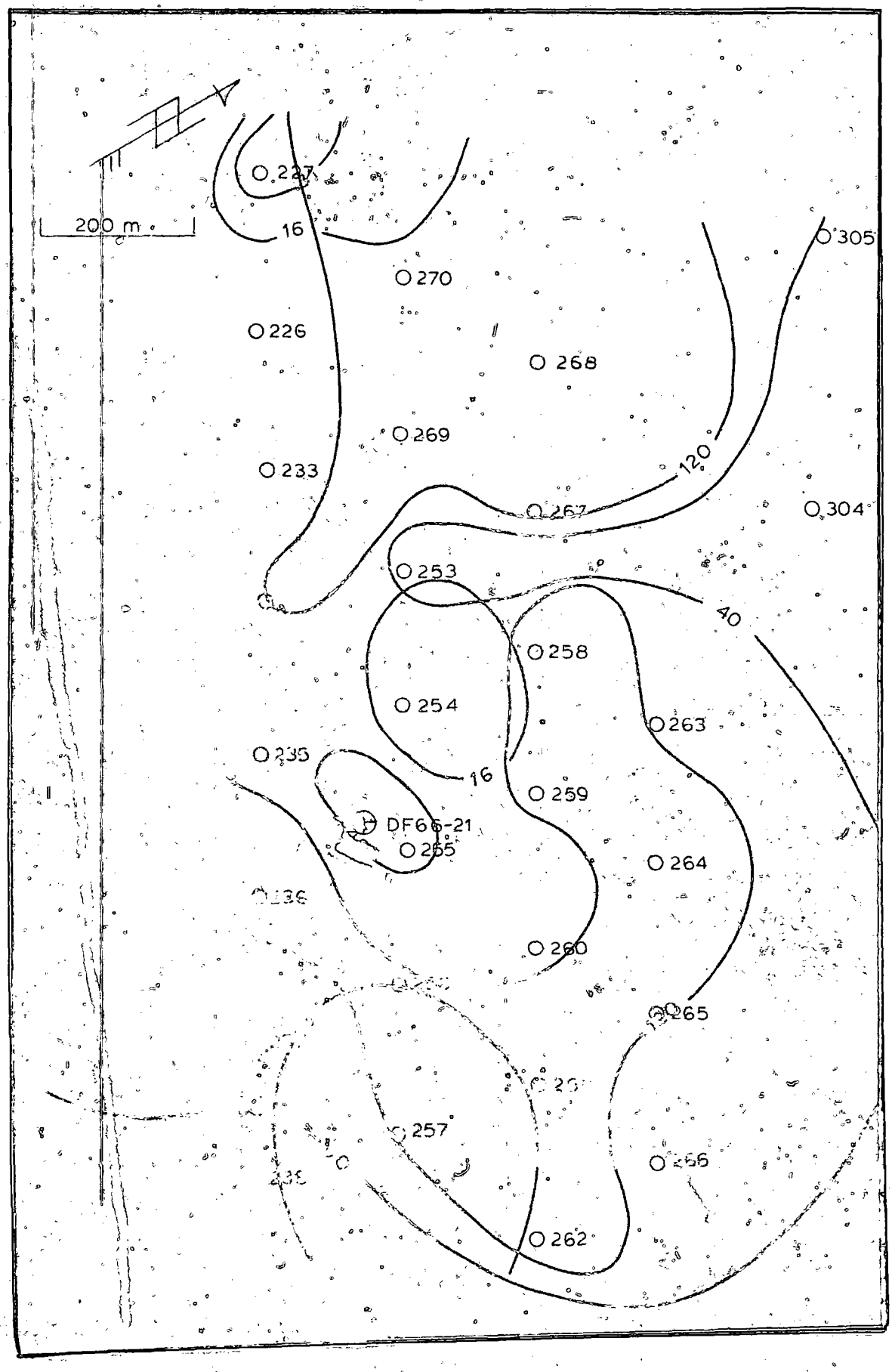
200 m
227
16
270
305
226
268
269
233
120
267
304
253
40
258
254
263
235
16
259
DF66-21
255
264
136
260
265
257
256
262

3.2.4.12 DF 45-14

The results of the closely spaced sampling around DF 45-14 are shown by geochemical contours in Figure 3-16. Interpretation of the data is complicated by the presence of the Dixie Comstock Mine with its large associated mercury and arsenic values.

Away from the range front a rather obvious scarp occurs and is mimicked by the mercury trend. The significance of this structure is unclear but it may be an older splay of the Stillwater fault. Several structures appear to run through and to the east of the well site, and are associated with high anomalous arsenic and mercury values. The mercury values drop off quickly to the east, coincident with the occurrence of fine-grained sediments.

Similar to Section 36 (T24N, R35E) the playa comes quite near the range front in the vicinity of DF 45-14. High arsenic values at this site may be due to the convergence of structures with arsenic migrating upward. The graben, scarp and slump features east of the well are along the trace of the Dixie Meadows fault and are typically associated with profuse growth of rabbit brush, indicative of a higher than normal water table.

Any zones of fluid migration within DF 45-14 would be expected to show geochemical manifestations to the west since, like DF 66-21 to the north, it is west of the inner graben bounding faults that may be more directly connected to the geothermal reservoir. Like DF 66-21, well DF 45-14 hit high temperature fluids but flow rates have been low. This may indicate some sealing effects creating lower permeabilities (see Chapter 4; this report).

Some contamination may have occurred during flow tests of DF 45-14. The site of the highest arsenic values occurs directly downwind of the well where it may have been affected by wind carried effluent. However, the area around DF 66-21 does not exhibit high arsenic values even though its fluids contained significantly higher concentrations of the element.

3.3 SUMMARY AND CONCLUSIONS

While the soil geochemical values for arsenic and mercury have several sources of variation in Dixie Valley, it appears these sources may be identified. The Dixie Meadows fault shows numerous zones of high

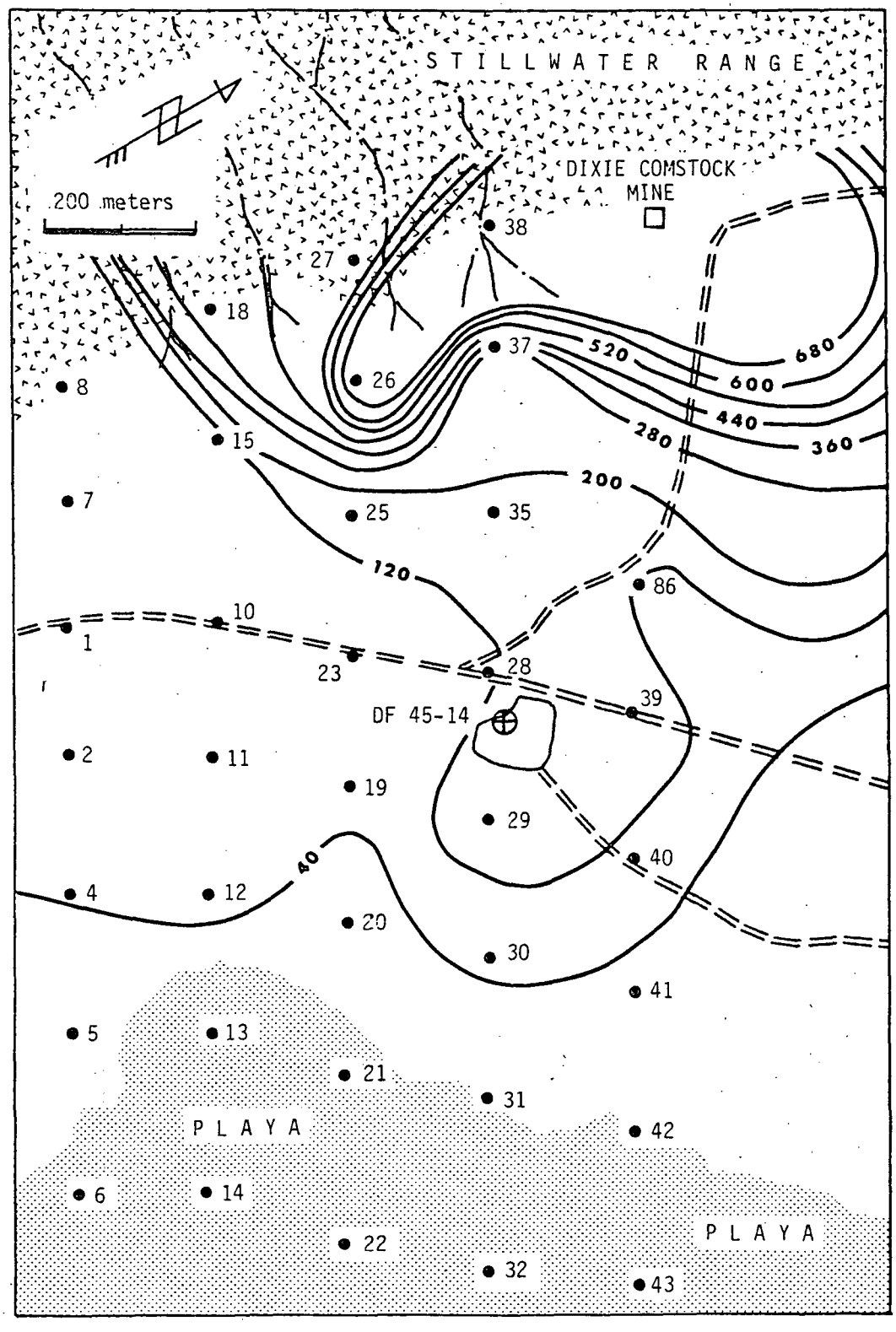

Figure 3-16a. Contoured mercury geochemical surface in vicinity of DF 45-14. Values indicated by contours; sampling sites indicated by solid circles; extent of geomorphic surfaces indicated by shading.

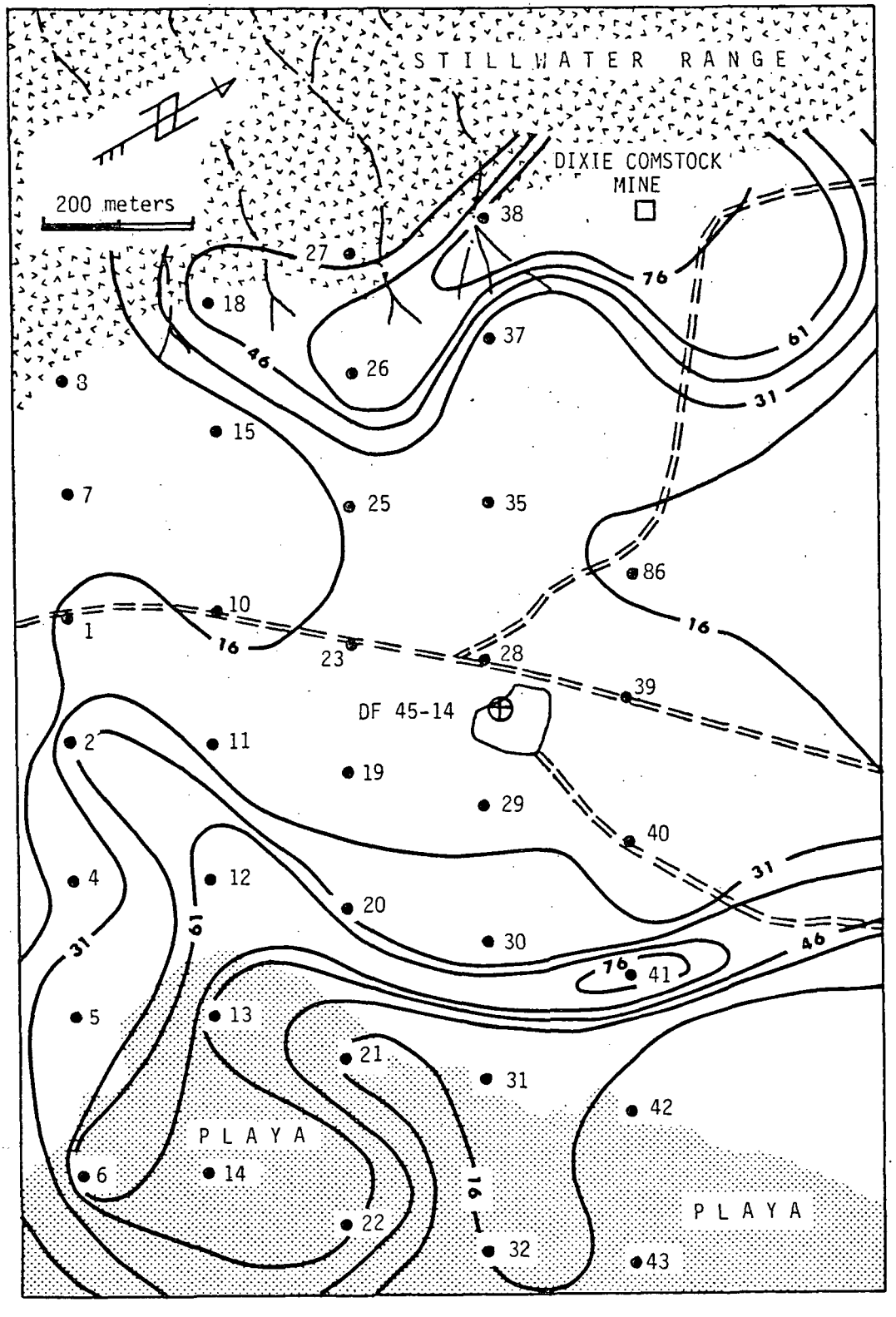

Figure 3-16b. Contoured arsenic geochemical surface in vicinity of DF 45-14. Values indicated by contours; sampling sites indicated by solid circles; extent of geomorphic surfaces indicated by shading.

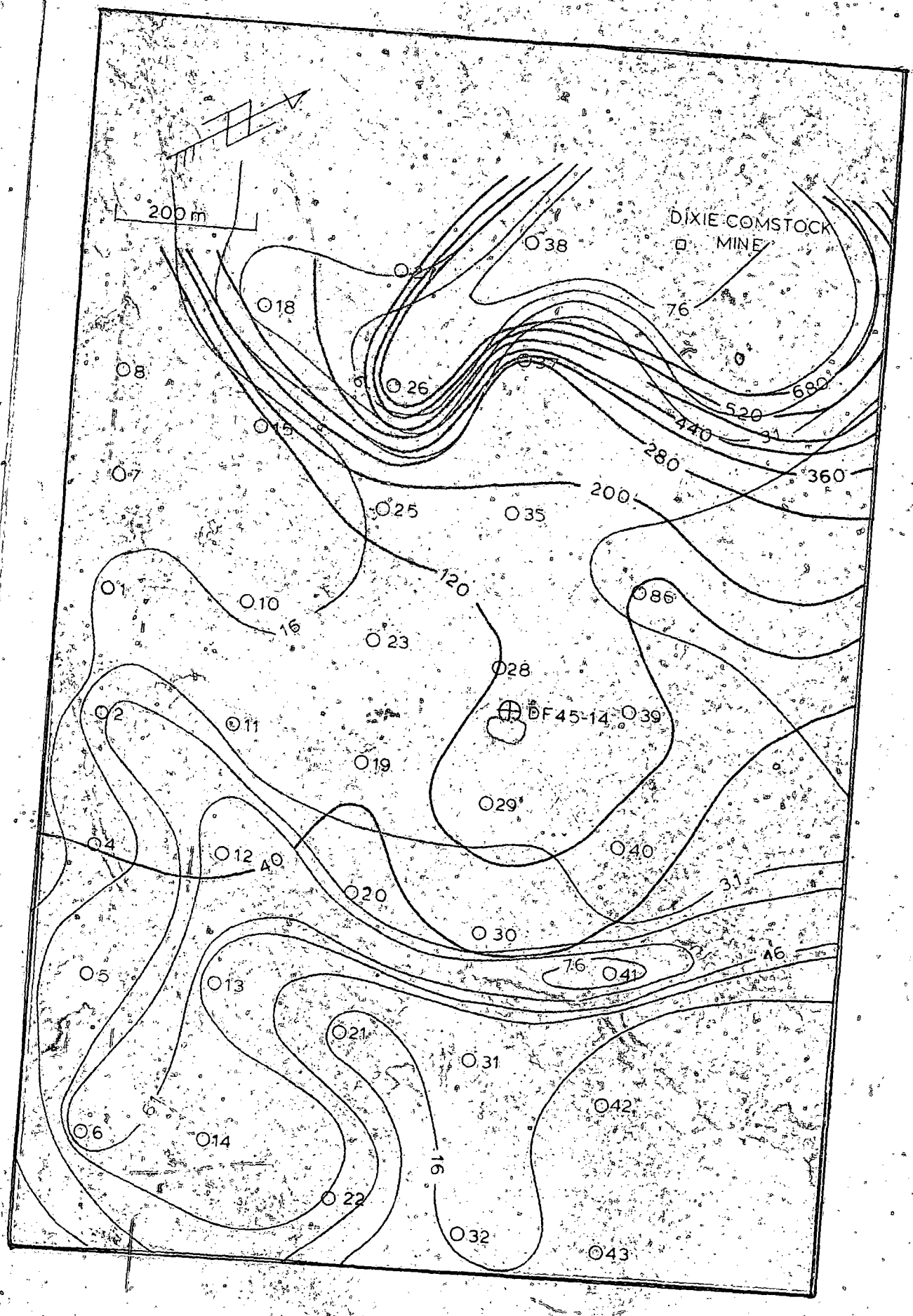
200 m
DIXIE COMSTOCK MINE
DF 45-14
1
2
3
4
5
6
7
8
10
11
12
13
14
15
16
18
19
20
21
22
23
25
26
28
29
30
31
32
35
38
39
40
41
42
43
86
120
200
280
360
440
520
680
760
46
31
16
40
61

anomalous arsenic and mercury along its trend. High anomalous arsenic values along the apparently structurally controlled playa margin, including several associated with springs, suggests some communication with arsenic rich thermal waters at depth. The anomalous arsenic values near the playa are seldom accompanied by high mercury concentrations but this may be due to the nature of the sediments and the affinity of arsenic for the liquid phase. Low anomalous values of mercury and arsenic also occur near and along the Buckbrush fault trace in the northern portion of the study area. Geochemical trends west of the Dixie Meadows fault also suggest some structural control. The association of geochemical anomalies with the more easterly fault traces is significant. Two low-production wells have been drilled to the west of these 'inner' faults whereas at least three productive wells have been drilled east of them.

Although contamination from mine tailings complicates the interpretations around DF 45-14 it appears that it has been drilled west of the two inner graben faults which may communicate with a reservoir at depth. Very high heat flow in this area is probably due to some fluid movement along the range front fault or a structure between the range front and the well.

DF 66-21 is also west of the inner graben structures as outlined by geochemical anomalies and geomorphic features. A zone of high pressure hot water occurs at 1430 m in this well and may represent a zone which communicates with reservoir conduits to the east. This zone is associated with a layer of red clay which is similar in mineralogy to that of the extensively altered, high mercury area at the fumarole chain northwest of the drill site. A possible structural link between the high heat flow zone and the fumaroles is suggested by a zone of lineaments which would correspond to the surface trace of a basin and range structure intersecting the drillhole at 1430 m. These lineaments if extended along trend intersect the range front at the fumaroles. Some anomalous surface geochemical values near the lineaments lend support to this possibility. Based on the available data it appears that the geothermal reservoir in Dixie Valley lies east of the Dixie Meadows fault and that communication with the Stillwater fault and other structures to the west is generally poor, perhaps due to sealing by mineral deposition.

Where follow-up sampling at 30 m (100 ft) intervals has been performed

a correlation with structures has been observed. More sampling at this interval should be conducted, particularly to the north in the area around Section 14 (T24N, R36E). An extension of profile C-C' further across the valley could be quite useful.

Because the nature of the Dixie Valley Geothermal System is still not completely understood, it is difficult to evaluate the effectiveness of mercury and arsenic soil geochemistry as an exploration tool. Tentatively it appears that the soil sampling together with previous structural interpretations has provided a plausible explanation for much of the observed drilling data, including the one meter and shallow gradient holes. It would also appear as though the broad grid sampling with follow-up work on close center could be useful in selecting drilling targets. Clearly, it rests with further deep drilling to confirm, modify or contradict the conclusions of this work.

The results of the survey are not clear cut and considerable interpretation has been necessary, particularly with regard to the geochemical behavior of the indicator elements. In many ways, As and Hg have complemented each other in this work. Their correlation is strongest in mineralized areas and this is a useful way of interpreting the origin of those type of anomalies.

Several other methods of determining the source of geochemical anomalies in surveys of this type might be a useful refinement. A selective leach method of analysis as proposed by Bradshaw and others (1974) would allow for the discrimination of different chemical forms of arsenic and mercury. The different chemical forms such as sulphide, chloride or adsorbed complex have clear source implications so that by selectively leaching, for instance the sulphide, a mechanically dispersed mineral origin for an anomaly could be detected.

Another method for discriminating chemical species and hence origins has been proposed for mercury by Koksoy and others (1967). The essence of the method is differentiation by the temperature of decomposition for different species.

Another useful refinement to the present work may be the inclusion of other elements in the analysis. Possibly suitable for this work would be boron which is found in elevated concentrations (approximately 10 ppm) in the thermal waters of DF 66-21 and DF 45-14. Boron is a volatile element commonly associated with geothermal fluids (Hem, 1970b; Koga and

Noda, 1976). Being generally unassociated with sulphide mineral deposits it might be a more reliable indicator in regions such as Dixie Valley.

3.4 References

Ahrens, L.H., 1954, The log-normal distribution of the elements: Geochim. Cosmochim., Acta 6, p. 121-131.

Barnes, H.L., 1979, Solubilities of ore minerals, in Barnes, H.L., ed., Geochemistry of hydrothermal ore deposits: J. Wiley and Sons, New York, p. 404-460.

Bohm, B.W., Jacobson, R.L., Campana, M.E., and Ingraham, N.L., 1980, Hydrology and hydrogeochemistry, in Mackay Minerals Research Intitute, Geothermal reservoir assessment case study, northern Basin and Range Province, northern Dixie Valley, Nevada: Rept. prepared for U. S. Dept. of Energy, Contract no. DE-AC08-79ET 27006, v. I, ch. 5, p. 159-186.

Boyle, R., and Jonasson, I., 1973, Geochemistry of arsenic and its use as an indicator element in geochemical prospecting: Jour. Geochem. Expl., v. 2, no. 3, p. 251-296.

Bradshaw, P.M.D., Thompson, I., Smee, B.W., and Larson, J.O., 1974, The application of different analytical extractions and soil profile sampling in exploration geochemistry: Jour. Geochem. Expl., v. 3, p. 209-226.

Campana, M.E., Jacobson, R.L., and Ingraham, N.L., 1980, Shallow temperature survey, in Mackay Minerals Research Institute, Geothermal reservoir assessment case study, northern Basin and Range Province, northern Dixie Valley, Nevada: Rept. prepared for U. S. Dept. of Energy, Contract no. DE-AC08-79ET27006, v. I, ch. 6, p. 187-205.

Capauno, R., and Bamford, R., 1978, Initial investigation of soil mercury geochemistry as an aid to drill site selection in geothermal systems: Univ. Utah Research Inst., Rept. 13, 32 p.

Davy, H.A., 1974, Mechanisms for mercury deposition at Ngawha Springs, New Zealand: Papers Proc. Royal Soc. Tasmania, 108, p. 157-158.

Dickson, F.W., 1968 The origin of mercury haloes: Proc. 23rd Internat. Geol. Congress, Prague, p. 347-366.

Ellis, A.J., and Mahon, W.A.H., 1977, Chemistry and geothermal systems: Academic Press, New York, 392 p.

Fang, S.C., 1978, Sorption and transformation of mercury vapor by dry soil: Environ. Science Tech., v. 12, p. 285-288.

Hem, J.D., 1970a, Chemical behavior of mercury in aqueous media, in Mercury in the environment: U. S. Geol. Survey Prof. Paper 713, p. 19-24.

Hem, J.D., 1970b, Study and interpretation of chemical characteristics of natural water: U. S. Geol. Survey Water Supply Paper 1473, 363 p.

Horsnail, R.F., Nichol, I., and Webb, J.S., 1969, Influence of variations in secondary environment on the metal content of drainage sediments: Colorado School Mines, 64, p. 307-322.

Jonasson, I.R., and Boyle, R.W., 1972, Geochemistry of mercury and origin of natural contaminants of the environment: Can. Inst. Min. Metal., Trans., v. 75, p. 8-15.

Khayretdinov, Z.A., 1971, Gas mercury aureoles: Geochem. Internat., v. 8, p. 412-422.

Klusman, R.W., and Landress, R.A., 1978, Secondary controls on mercury in soils of geothermal areas: Jour. Geochem. Expl., v. 9, no. 1, p. 75-92.

Klusman, R.W., and Landress, R.A., 1979, Mercury in soils of the Long Valley, California, geothermal system: Jour. Volcanol. Geotherm. Res., v. 5, no. 1-2, p. 49-65.

Klusman, R.W., Cowling, S., Culvey, B., Roberts, C., and Schwab, A.P., 1977, Preliminary evaluation of secondary controls on mercury in soils of geothermal districts: Geothermics, in press.

Koga, A., and Noda, T., 1976, Geochemical prospecting in vapor-dominated fields for geothermal exploration: Proc. 2nd U. N. Symposium on Development and Use of Geothermal Resources, v. 1, p. 785-792.

Koksoy, M., Bradshaw, P.M.D., and Tooms, J.S., 1967, Notes on the determination of mercury in geological samples: Can. Inst. Min. Metal., Trans., v. 76, p. B-121-B124.

Landa, E.R., 1978, The retention of metallic mercury vapor by soils: Geochim. Cosmochim., Acta, v. 42, no. 9, p. 1407-1412.

Lawrence, E.F., 1971, Mercury mineralization at the Senator fumaroles, Dixie Valley, Nevada: Geol. Soc. America, Abstr. with Prog., no. 3, p. 147.

Mackay Minerals Research Institute, 1980, Geothermal reservoir assessment case study, northern Basin and Range Province, northern Dixie Valley, Nevada: Rept. prepared for U. S. Dept. of Energy, Contract no. DE-AC08-79ET27006, v. I, 223 p. plus appendices, v.II, map plates, also Univ. Utah Res.Inst. Rept. NV/DV/SR-13.

Matlick, J., and Buseck, P., 1976, Exploration for geothermal areas using mercury: a new geochemical technique: Proc. 2nd U. N. Symposium on Development and Use of Geothermal Resources, v. 1, p. 785-792.

McCarthy, J.H., Jr., 1972, Mercury vapor and other volatile components in the air as guides to ore deposits: Jour. Geochem. Expl., v. 1, no. 2, p. 143-162.

McCarthy, J.H., Jr., Vaughn, W.W., Learned, R.E., and Meuschke, J.L., 1969, Mercury in soil gas and air - a potential tool in mineral exploration: U. S. Geol. Survey Circ. 609, 16 p.

McNerney, J.J., and Buseck, P.R., 1973, Geochemical exploration using mercury vapor: Econ. Geol., v. 68, no. 8, p. 1313-1320.

Meister, L.J., 1967, Seismic refraction study of Dixie Valley, Nevada, in U. S. Air Force Cambridge Research Labs. Spec. Rept., 66-848, 72 p.

Nakagawa, R., 1974, The mercury content in hot springs: Nippon Kagaku Kaishi, p. 71-74.

Nie, N.R., Hull, H.C., Jenkins, J.G., Steinbrenner, K., and Best, D.H., eds., 1975, Statistical package for the social sciences: McGraw-Hill, New York, 675 p.

Phelps, D.W., and Buseck, P.R., 1978, Natural concentrations of mercury in the Yellowstone and Coso Geothermal Fields: Geother. Res. Coun., Trans., v. 2, p. 521-522.

Robertson, D.E., Fruchter, J.S., Ludwick, J.D., Wilkerson, C.L., Crecelius, E.A., and Evans, J.C., 1978, Chemical characterization of gases and volatile heavy metals in geothermal effluents: Geother. Res. Coun., Trans., v. 2, p. 579-582.

Rogers, R.D., and McFarlane, J.C., 1978, Factors influencing the volatilization of mercury from soil: Environ. Protection Agency Rept. no. 600/3-78-054, 13 p.

Sergeyeva, E.I., and Khodakovskiy, I.L., 1969, Physiochemical conditions of formation of native arsenic in hydrothermal deposits: Geochem. Internat., no. 7-8, p. 681-694.

Sillen, L.G., and Martell, A.E., 1964, Stability constants of metal-ion complexes: Chem. Soc. London, Spec. Pub. 17, 754 p.

Sinclair A.J., 1974, Selection of threshold values in geochemical data using probability plots: Jour. Geochem. Expl., v. 3, p. 129-149.

Souto, J.M., 1978, Oahu geothermal exploration: Geother. Res. Coun., Trans., v. 2, p. 605-608.

Tonani, F., 1970, Geochemical methods of exploration for geothermal energy: Proc. U. N. Symposium on Development and Utilization of Geothermal Resources, Pisa, p. 492-515.

Trost, P.B., and Bisque, R.E., 1971, Differentiation of vaporous and ionic mercury in soils: Proc. 3rd Internat. Geochem. Expl. Symposium, Toronto: Can. Inst. Min. Metal., Spec. Volume no. 11, p. 276-278.

Trost, P.B., and Bisque, R.E., 1972, Distribution of mercury in residual soils, in Hartung, R., and Dinman, D.B., eds, Environmental mercury contamination: Ann Arbor Science Pub., p. 178-196.

Vasak, V., and Sedivic, V., 1952, Colorimetric determination of arsenic: Chem. Listy., no. 46, p. 341-344.

White, D.E., 1967, Mercury and base-metal deposits with associated thermal and mineral water, in Barnes, H.L., ed., Geochemistry of hydrothermal ore deposits: Holt,Rinehard and Winston, New York, 575 p.

Whitney, R.A., 1980, Structure-tectonic analysis, in Mackay Minerals Research Institute, Geothermal reservoir assessment case study, northern Basin and Range, northern Dixie Valley, Nevada: Rept. prepared for U. S. Dept. of Energy, Contract no. DE-AC08-79ET 27006, v. I, ch. 3, p. 61-87.

Weissberg, B.G., Browne, P.R.L., and Seward, T.M., 1979, Ore metals in active geothermal systems, in Barnes, H.L., ed., Geochemistry of hydrothermal ore deposits: J. Wiley and Sons, New York, p. 739-780.

Willden, R., and Speed, R., 1974, Geology and mineral deposits of Churchill County, Nevada: Nevada Bur. Mines Geol., Bull. 83, 95 p.

Wright, T., ed., 1977, National Center for Atmospheric Research, Graphics Software, Boulder Colorado.

Chapter 4. PETROCHEMISTRY

By: Elaine J. Bell

4.0 PETROCHEMICAL ANALYSIS

4.1 Introduction

4.1.1 Purpose and Scope

The primary purpose of the petrochemical analysis of the subsurface drill chip samples from the two deep exploratory wells (DF 45-14 and DF 66-21) in Dixie Valley was to identify steam or hot water entries and to delineate the associated geochemical zonations. Secondarily, the data allow for a limited re-evaluation of the integrated model of the Dixie Valley Geothermal System as well for as an evaluation of the technique as an exploration and analytical tool.

The present study is limited to the analysis of available drill chip samples from DF 45-14 and DF 66-21 in Dixie Valley, with elemental analysis for the following five trace elements as indicators of the activity of the geothermal system: lead (Pb), zinc (Zn), arsenic (As), antimony (Sb), and mercury (Hg). Both whole rock samples and heavy mineral fraction separates were analyzed, with the heavy mineral fractions showing geochemical enhancement. The resultant data were evaluated with respect to temperature, depth, lithology, and known or inferred permeable zones (i.e., fracture systems) significant to the fracture-controlled geothermal system.

4.1.2 Methods and Analytical Techniques

The petrochemical analysis to determine distribution of selected elements in samples from deep wells DF 45-14 and DF 66-21, relationship of these elements to geothermal activity, and minerals in which these elements are incorporated involved a four-step process: 1) preparation of whole rock and heavy mineral fraction samples, 2) mineralogic analysis of the heavy mineral fractions, 3) quantitative chemical analysis of whole rock and heavy mineral fraction samples for selected trace elements, and 4) evaluation and reduction of the data.

4.1.2.1 Sample Preparation

Limited volumes of processed drill cutting samples from both DF 45-14 and DF 66-21 were available for this study. These samples represent splits of grab samples originally collected at 10-foot intervals and cleaned and washed of drilling mud and other contaminants by the mud loggers. One-hundred foot composite samples were prepared by combining

five original samples in order to 1) minimize potential random sampling biases of individual grab samples; 2) reduce the number of samples that must be prepared and analyzed to a practical total while maintaining adequate spatial resolution for defining geochemical distribution patterns; and 3) maintain a consistent analytical base for comparison of the petrochemical data with the petrologic data generated by previous analyses of the drill cutting samples (Bard, 1980).

directly lifted from Bamford 1978

Both whole rock and heavy mineral fraction samples were prepared for each 100-foot composite interval. The heavy mineral fractions exhibit enhanced geochemical signatures relative to the whole rock samples. Rock-forming and alteration silicates, essentially lacking hydrothermally derived trace elements, are removed from the samples, leaving a greater than 3.3 specific gravity (+3.3) concentrate containing hydrothermal oxides and sulfides enhanced in the elements of interest. Analysis of whole rock samples for the same sampling intervals can confirm the validity of the heavy mineral fraction analyses and corroborate the location of geochemically anomalous zones.

Heavy mineral fractions were prepared by grinding and sieving each 100-foot composite sample to -80 mesh size to facilitate disaggregation of the particles. A hand magnet was used to separate the magnetic fraction consisting mostly of magnetite with minor residual drill bit shavings. The heavy mineral fraction was separated by settling in methylene iodide (specific gravity 3.3). A minimum of 500 mg of each heavy mineral fraction sample was required to conduct the quantitative analyses for the selected five elements. The amount of +3.3 heavy mineral fraction within a 100-foot composite sample is a function of both the nature (i.e., lithology) and the volume of well cuttings originally supplied to the MMRI for petrographic, petrologic and petrochemical analyses. The lack of sufficient heavy mineral fraction in many of the 100-foot composite samples necessitated the combining of samples into intervals representing as much as 500 feet to obtain the volume of material needed for analysis. This interval compositing results in bias of the sample data for those intervals.

Whole rock samples were prepared for each 100-foot interval by grinding and sieving to -80 mesh size. These samples were then split and, when necessary, combined to correspond to the composited intervals of the +3.3 heavy mineral fractions.

Control samples were prepared for selected whole rock samples and, when sufficient sample was available, for the heavy mineral fractions. These samples were submitted for analysis to provide a check on the accuracy of the analytical technique and to verify internal consistency of the data. In addition, samples of the magnetic fraction of the heavy mineral separates were prepared for analysis in order to evaluate their contribution to the elemental distribution.

4.1.2.2 Mineralogic Analysis

Limited mineralogic studies of the prepared heavy mineral fraction samples were conducted to identify specific minerals and their relative abundances in each interval. Mineral identification was based primarily on petrographic binocular examination under reflected light. Preliminary results were verified and modified by second observer visual scanning. In addition, several minerals were isolated and identified by using standard x-ray powder diffraction camera techniques.

4.1.2.3 Quantitative Elemental Analyses

All whole rock, +3.3 heavy mineral fractions and magnetic fractions, and control samples were submitted to Rocky Mountain Geochemical Corporation, Salt Lake City, for quantitative analysis for lead, zinc, arsenic, antimony, and mercury.

Lead and zinc were determined by atomic absorption; antimony was also determined by atomic absorption following bisulfate fusion. Arsenic determination was made by the colorimetric method discussed in Section 3.1.2. Mercury concentrations were determined by cold vapor generation atomic absorption. Limits of quantitative detection for each element are listed in Table 4-1; minimum reported values for whole rock and for heavy mineral fraction samples are a function of the sample size available for analysis or the minimum concentration of the element in the sample.

4.1.2.4 Data Presentation

4.1.2.4.1 Bar Graph Plots

The distribution of elements within both whole rock and heavy mineral fraction samples for each deep well are depicted by bar graph plots (Plates VI through IX). These histograms are plotted at a scale consistent with the revised data from the petrologic studies of the wells to facilitate

Table 4-1

Detection Limits for Quantitative Trace Analysis

Element	Detection Limit	Minimum Value Reported*
Lead	5 ppm	- 5 ppm for WRS -25 ppm for HMF
Zinc	5 ppm	- 5 ppm for WRS -25 ppm for HMF
Arsenic	5 ppm	- 5 ppm for WRS -25 ppm for HMF
Antimony	1 ppm	- 1 ppm for WRS - 2 ppm for HMF
Mercury	10 ppb	75 ppb for WRS -10 ppb for HMF

* Minimum values reported are function of sample size available for analysis. WRS -- Whole Rock Samples; HMF -- Heavy Mineral Fractions. Minus (-) symbol should be read as 'less than'.

comparison and evaluation of relationships between the various elemental data and the petrology, structure, or other parameters (Plates IV and V).

4.1.2.4.2 Computer Data Reduction

Statistical reduction and analysis of the data utilized portions of the Statistical Package for the Social Sciences (Nie and others, 1975). Subprogram FREQUENCIES developed one-way frequency distributions as absolute, relative and cumulative frequency values; computed descriptive statistics, including mean, standard error, standard deviation, kurtosis and skewness; and generated histograms of the relative frequency distributions of each variable.

The SCATTERGRAM subprogram provides bivariate correlation analysis, generates bivariate scattergram plots, and computes a simple linear regression with the following associated statistical parameters: Pearson product-moment correlation, tests of statistical significance, and the standard error of estimate. Both actual value variables and computed arithmetic variables were analyzed by SCATTERGRAM.

4.1.2.4.3 Log Probability Graphs

Log probability graphs were plotted for each variable and sample type by using the data generated by the FREQUENCIES subprogram and by applying the plotting percentage technique of Koch and Link (1970). These log probability plots were used to verify the statistical data and to aid in the subjective evaluation and interpretations of the bar graph plots and other tabulated data. The log probability plots for each element in both heavy mineral fraction and whole rock samples for DF 45-14 are depicted in Figures 4-14 through 4-23 (Appendix B), and for DF 66-21 are depicted in Figures 4-24 through 4-33 (Appendix B).

4.1.2.4.4 Other

Tables were prepared listing the relative abundance and distribution of minerals in the heavy mineral fraction samples for each well (Tables 4-2 and 4-3, Section 4.2.1), the selected elements in heavy mineral fraction and whole rock samples for each well (Tables 4-5 through 4-8, Section 4.2.2), and the statistical distribution of each selected element in heavy mineral fraction and whole rock samples for DF 45-14 (Tables 4-13 through 4-22, Appendix B) and DF 66-21 (Tables 4-23 through 4-32, Appendix B).

4.1.3 Previous Work

The usefulness of collecting and analyzing solid samples for geochemical signatures and elemental zonations associated with ore deposits has been recognized in previous studies. The trace element zoning and ore deposition by hydrothermal solutions is a response to temperature, pressure or chemical gradients associated with a primary heat source. Skinner and others (1967), Browne and Ellis (1970), Ewers and Keays (1977), and Weissberg and others (1979) have shown that the spectrum of trace elements in geothermal systems is similar to ore-forming hydrothermal solutions.

Bamford (1978) developed techniques for using solid sampling geochemistry to identify trace elements that would be indicative of gradients and zoning around geothermal systems and that would be useful in exploration and evaluation schemes. Bamford and Christensen (1979) and Bamford and others (1980) have continued to test and refine the geochemical exploration assessment techniques for geothermal systems. These techniques are here applied to the Dixie Valley Geothermal System to test the selected elements as indicators of geothermal activity.

4.1.4 Geochemistry of Selected Trace Elements

The following five sections present brief outlines of the geochemical nature of the selected trace elements. While the specific behavior of these elements within geothermal systems (hydrothermal fluids) is not fully understood, elemental characteristics inferred from ore deposits are a valuable aid in interpreting the relationships and distribution of the elements with respect to the geothermal system. The reader is referred to other references, including Barnes (1967, 1979) and Wedepohl (1978), for more detailed discussion of the geochemical behavior of these elements.

4.1.4.1 Lead

Lead ions, naturally occurring in a +2 or +4 valence state, have a high electronegativity that generally relegates them to substitution for potassium or calcium in later formed minerals and concentration in hydrothermal fluids. The tendency of the element to form covalent bonds affects its distribution as a sulfide mineral such that it is not readily dispersed. Galena (PbS) is the primary sulfide mineral; however, about

20 different lead sulfates are recognized. Appreciable lead concentrations are present in fumarole sublimates as the mineral cotunnite ($PbCl_2$) which, under certain conditions, has a higher vapor pressure than the zinc chloride. The ionic radius of lead allows it to substitute for potassium, strontium, barium, and in some cases, calcium or sodium in minerals such as olivine ($(Mg,Fe)_2SiO_4$), pyroxene, and amphibole. Lead is generally present as the mineral galena (PbS), but is also present in lead-arsenic sulfides as well as being a trace element in pyrite (FeS_2) and magnetite (Fe_3O_4).

4.1.4.2 Zinc

Zinc occurs as a +2 ion and forms halides, oxyacid salts or complexes that are highly soluble in water. Zinc forms covalent bonds and is a trace element in many common minerals in which it competes with iron (Fe^{++}). It is generally present in magmatic iron ores such as ilmenite ($FeTiO_3$) and magnetite (Fe_3O_4). In sulfides zinc is associated with very late hydrothermal bodies, being found with copper and lead in sphalerite (ZnS) and galena (PbS) and various complex sulfide minerals. Unlike lead, zinc is very mobile and is generally transported as a chloride complex. In rocks where carbon dioxide is dissolved, as much as 50 percent of the zinc may be in a mobile state. The dispersion patterns of zinc around areas of mineralization are normally distinct. Zinc, along with arsenic, is an indicator of gold deposition. Replacing iron and magnesium in mineral lattices, zinc is a common trace element in magnetite (Fe_3O_4) and diopside ($CaMgSi_2O_6$).

Lead and zinc are distinctly more abundant in acidic and intermediate rocks than in basic or ultrabasic igneous rocks. They generally are progressively deposited outward from an ore zone (halo effect) and may be accompanied by barite ($BaSO_4$). Metamorphism may result in remobilization of these trace elements. Zinc and lead can both be adsorbed from solution by clay minerals.

4.1.4.3 Antimony

Antimony may be present in solution in -3, +3, +5 or 0 valence states, although it is generally present in the +3 state as an ionic complex. This volatile element combines readily with sulfides and may substitute for arsenic and iron in minerals. Antimony becomes enriched in early

stages of magmatic differentiation in sulfide bodies and, in this manner, may be associated with gabbroic rocks. It also accumulates in late stage granitic rocks and in hydrothermal fluids. Precipitation from low-temperature alkaline hydrothermal solutions can be induced by 1) neutralization by carbon dioxide, 2) oxidation, 3) decreasing temperature, or 4) dilution. Antimony may occur as stibnite (Sb_2S_3) with cinnabar (HgS) and pyrite (FeS_2) or as sulfantimonides of copper, lead, zinc, silver or arsenic.

4.1.4.4 Arsenic

The geochemistry of arsenic is discussed in Section 3.1.4.2 with only significant parameters reiterated here. Occurring in three principal oxidation states (+3, +5, 0), this mobile element generally remains hydrolyzed in aqueous solutions. It commonly forms anionic complexes and polymers, particularly with sulfur and oxygen. Arsenic is frequently associated with mercury and, along with zinc, is indicative of gold deposition. It substitutes in mineral lattices for iron and titanium, commonly in magnetite and ilmenite, but also is found as a trace element in galena (PbS), pyrite (FeS_2), chalcopyrite ($CuFeS_2$), pyrrhotite ($Fe_{1-x}S$), and sphalerite (ZnS). Arsenopyrite (FeAsS) is the most abundant arsenic mineral.

4.1.4.5 Mercury

The geochemistry of mercury is discussed in Section 3.1.4.1. Mercury occurs in three principal oxidation states (+1, +2, 0). The relatively high vapor pressure of the element and its compounds is unique. Volatility of mercury is enhanced by the elevated temperatures of hydrothermal systems, and its mobility in the vapor phases allows it to migrate through permeable zones. Mercury is generally found as the sulfide and as a trace element within the lattice of minerals such as pyrite (FeS_2), tourmaline and sphalerite (ZnS).

4.1.5 Acknowledgements

Discussions with Russell W. Juncal, Dennis S. McMurdie and Odin B. Christensen contributed to the development of ideas and helped to focus

the analysis and interpretations of the petrochemical data expressed in this chapter. Dick and Sue Nosker and Mark Chandler are especially thanked for their meticulous efforts in sample preparation. The intensive efforts of Larry T. Larson and D. Burton Slemmons in reviewing and evaluating basic petrologic data were invaluable in developing the detailed base for interpreting the geochemical results. Tom R. Bard assisted with data reduction. Appreciation is extended to Mollie A. Stewart for typing and text preparation and to Loretta Sabini for assistance with computer editing. Technical and editorial review by MMRI and SRC personnel, in particular Larry T. Larson, Russell W. Juncal and Dennis S. McMurdie, significantly improved this chapter.

4.2 Analytical Results

4.2.1 Mineralogic Occurrences

The relative abundance and distribution of minerals in the samples from DF 45-14 and DF 66-21 are listed in Tables 4-2 and 4-3, respectively. These semi-quantitative mineral compositions of the +3.3 heavy mineral fraction samples and the +3.3 magnetic separates were determined by petrographic methods.

Minerals frequently abundant in the +3.3 fraction samples include hematite (Fe_2O_3)/magnetite(Fe_3O_4), pyrite (FeS_2) and epidote ($Ca_2(Al,Fe)_3(OH)(SiO_4)_3$). In addition to these minerals, zircon ($ZrSiO_4$), tourmaline barite(?) ($BaSO_4$), chalcopyrite(?) ($CuFeS_2$), rutile(?) (TiO_2), diopside ($CaMgSi_2O_6$), and garnet $(Mg,Fe)_3Al_2(SiO_4)_2$ are also common in either minor or trace emounts. Various rock-forming silicate minerals and steel shavings are present in minor or trace amounts contaminating the heavy mineral fraction samples. The +3.3 magnetic fraction samples are composed primarily of magnetite and steel shavings with pyrite, ilmenite(?) and various silicate minerals present in either minor or trace amounts as comtaminants.

Ilmenite was not specifically identified in any of the heavy mineral fraction samples. However, its presence in at least several intervals is suspected since it was tentatively identified as a trace mineral in the magnetic fraction of DF 66-21 and leucoxene was identified during petrographic analysis of whole rock samples (Bard, 1980). Similarly, x-ray fluorescence data and the identification of leucoxene in whole rock

Table 4-2

RELATIVE ABUNDANCE AND DISTRIBUTION OF MINERALS IN DF 45-14 HEAVY MINERAL FRACTIONS

DEPTH	MAJOR	MINOR	TRACE
100-200	Hematite/Magnetite	Epidote	Tourmaline, Barite(?)
200-300	Hematite/Magnetite	Epidote	Pyrite, Tourmaline
300-400	Hematite/Magnetite	Epidote	Tourmaline, Garnet
400-500	Hematite/Magnetite	Epidote, Pyrite	Tourmaline, Zircon(?), Chalcopyrite(?)
500-700	Pyrite, Hematite/Magnetite	Tourmaline	Chalcopyrite(?)
700-800	Pyrite	Limonite	Epidote, Chalcopyrite(?)
800-900	Pyrite	Hematite/Magnetite	Epidote
900-1000	Pyrite, Magnetite/Hematite		Epidote, Chalcopyrite(?)
1000-1100	Magnetite/Hematite	Epidote, Pyrite	
1100-1300	Pyrite	Hematite/Magnetite	Epidote, Tourmaline, Garnet(?)
1300-1400	Pyrite	Hematite/Magnetite	Tourmaline(?), Chalcopyrite(?)
1400-1600	Pyrite	Hematite/Magnetite	(?) others
1600-1800	Pyrite, Hematite/Magnetite	Epidote	
1800-1900	Pyrite, Hematite/Magnetite	Epidote	
1900-2200	Pyrite, Hematite/Magnetite	Epidote	
2200-2400	Pyrite, Hematite/Magnetite	Epidote, Barite(?)	
2400-2700	Pyrite	Hematite/Magnetite	Epidote
2700-2900	Pyrite	Hematite/Magnetite	Tourmaline
2900-3000	Pyrite	Hematite/Magnetite	
3000-3200	Pyrite	Hematite/Magnetite	
3200-3300	Hematite	Pyrite, Tourmaline(?)	Magnetite
3300-3500	Pyrite	Hematite/Magnetite	Epidote
3500-3700	Pyrite	Hematite/Magnetite	Epidote
3700-4000	Pyrite	Epidote	Hematite/Magnetite
4000-4100	Epidote(?)	Magnetite	Pyrite, Tourmaline(?), Chalcopyrite(?)
4100-4200	Epidote(?)	Hematite/Magnetite	Pyrite
4200-4500	Hematite/Magnetite	Pyrite	Epidote, (?) other
4500-4900	Pyrite	Hematite/Magnetite	Epidote, Barite(?), (?) other
4900-5400	Pyrite	Hematite/Magnetite	Epidote, Barite(?)
5400-5700	Pyrite	Hematite/Magnetite	Epidote, Barite(?)
5700-5900	Pyrite	Hematite/Magnetite	Epidote
5900-6400	Pyrite	Hematite/Magnetite	Epidote
6400-6900	Pyrite	Hematite/Magnetite	Rutile(?), Zircon(?), Epidote
6900-7400	Pyrite	Hematite/Magnetite	Zircon, Garnet(?), (?) others
7400-7700	Pyrite	Hematite/Magnetite	Tourmaline, Epidote, (?) others
7700-8100	Pyrite, Magnetite/Hematite	Hematite/Magnetite	Tourmaline, Zircon, Epidote, (?) others
8100-8500	Pyrite	Hematite/Magnetite	Epidote
8500-9000	Pyrite	Hematite/Magnetite	Epidote, Barite(?)
Magnetic fraction (5000-7000)	Magnetite/Hematite	Pyrite	Tourmaline, (?) other

Note:
(?) following mineral name indicates tentative identification; (?) other indicates unidentified mineral present.

Table 4-3

RELATIVE ABUNDANCE AND DISTRIBUTION OF MINERALS IN DF 66-21 HEAVY MINERAL FRACTIONS

DEPTH	MAJOR	MINOR	TRACE
135-700	Hematite	Magnetite	Epidote, Pyrite, Diopside
700-900	Hematite	Magnetite	Epidote, Diopside
900-1200	Hematite	Magnetite	Epidote, Diopside
1200-1500	Hematite	Magnetite	Epidote, Diopside
1500-1700	Hematite	Magnetite	Epidote, Diopside
1700-2000	Hematite	Magnetite	Epidote, Diopside
2000-2400	Hematite	Magnetite	Epidote, Diopside
2400-2700	Hematite	Magnetite, Diopside	Epidote
2700-3000	Hematite	Magnetite	Epidote, Diopside
3000-3200	Hematite	Magnetite, Tourmaline	Epidote, Pyrite, Diopside
3200-3400	Hematite	Magnetite, Tourmaline	Epidote, Zircon, Diopside, Rutile(?), (?) other
3400-3700	Hematite	Magnetite, Tourmaline Diopside	Epidote, Zircon
3700-4000	Hematite	Magnetite, Tourmaline	Epidote, Diopside
4000-4100	Hematite	Magnetite, Tourmaline	Diopside
4100-4200	Hematite	Magnetite, Tourmaline	Epidote, Diopside
4200-4300	Hematite	Magnetite, Tourmaline	Pyrite
4300-4400	Hematite	Magnetite, Pyrite Tourmaline	
4400-4500	Pyrite, Tourmaline	Magnetite	Cinnabar(?), (?) other
4500-4600	Hematite/Magnetite	Pyrite	
4600-4800	Pyrite	Magnetite	Rutile, Garnet, Tourmaline
4800-4900	Hematite/Magnetite	Pyrite	Garnet(?)
4900-5200	Hematite/Magnetite	Pyrite	Gold, Tourmaline
5200-5400	Hematite/Magnetite	Pyrite, Epidote	Diopside, Tourmaline
5400-5800	Epidote,Hematite	Pyrite	Magnetite, Tourmaline, Diopside
5800-6100	Epidote,Tourmaline	Pyrite, Magnetite	(?) other
6100-6200	Epidote	Pyrite, Tourmaline	Diopside
6200-6500	Epidote, Pyrite	Tourmaline, Magnetite	Diopside, Zircon(?), (?) other
6500-6600	Epidote, Pyrite	Tourmaline, Hematite	Diopside, Hornblende(?), Corundum(?)
6600-6800	Pyrite	Tourmaline	Rutile, Epidote, (?) other
6800-7100	Pyrite	Epidote, Hematite	Tourmaline, Magnetite, Diopside
7100-7400	Pyrite	Epidote, Hematite	Tourmaline, Magnetite, Diopside
7400-7600	Pyrite	Epidote, Hematite	Magnetite
7600-7800	Pyrite		Epidote, Hematite
7800-8200	Pyrite		Diopside, Hematite
8200-8600	Pyrite		Hematite
8600-8900	Pyrite	Magnetite, Diopside	Epidote, Tourmaline, Zircon, (?) other
8900-9400	Pyrite		Epidote, Tourmaline, Diopside, Corundum(?)
9400-9780	Pyrite	Diopside, Tourmaline	Epidote, Magnetite
Magnetic fraction	Magnetite/Steel		Epidote, Tourmaline, Ilmenite(?)

Note:
(?) following mineral name indicates tentative identification; (?) other indicates unidentified mineral present.

samples (Bard, 1980) suggest the possible presence of ilmenite in DF 45-14. The presence of sphene ($CaTiSiO_5$) is also suspected since it too was identified during petrographic analysis of whole rock samples.

The presence of other significant minerals is suspected in a number of zones, particularly in DF 66-21, based upon the drill logs and petrographic analysis of the whole rock samples. These minerals and the respective approximate depths are indicated in Table 4-4.

Pyrite and magnetite are present as both primary and secondary minerals distributed throughout both wells. Primary pyrite is generally present as euhedral or subhedral grains in veins; primary magnetite is generally present as euhedral or subhedral igneous grains or in vein fillings. Secondary pyrite and magnetite are generally alteration products of ferromagnesian silicate minerals. Crystalline pyrite and magnetite are commonly partially or completely replaced by pseudomorphous hematite.

Epidote occurs within veins, as an alteration product of ferromagnesian silicates in association with magnetite, or within altered plagioclase grains.

Mineralogical hosts for the selected trace elements can be inferred from the geochemical behavior of these elements (Section 4.1.4). The trace elements have been adsorbed or incorporated into solid solution in pyrite and base metal sulfides or in oxide minerals (e.g., arsenic in pyrite or hematite), have formed discrete sulfide phases (e.g., mercury in cinnabar or lead in galena), or have been incorporated into silicate phases (e.g., zinc in diopside). The significantly enhanced concentrations of these trace elements in the heavy mineral fractions support the assumption that they are contained in sulfides, oxides and other +3.3 mineral phases.

The distribution and relative abundance of the mineral phases in the heavy mineral fraction samples (Tables 4-2 and 4-3) distinguish various zones or intervals within each well as summarized in Figures 4-1 and 4-2. In DF 45-14 (Figure 4-1) a shallow iron oxide-rich zone is replaced below 500 feet by a sulfide-rich zone in which pyrite is the major mineral. Within the pyrite zone, a number of subzones can be distinguished based on the changes in relative abundances of the various non-metallic minerals (i.e., silicates and barite). Significant intervals include 1600 to 2400 feet in which epidote is a minor rather than a

Table 4-4

Mineral Occurrences

Well	Mineral	Depth(s) in feet*	Reference
DF 45-14	Cinnabar (HgS)	900, 1300(?), 1600(?), 1900-2000(?), 4100, 5900(?), 9000(?)	Drill Log (DL)
	Arsenopyrite (FeAsS)	5300(?), 5700(?), 6300(?)	Petrographic Analysis (PA)
	Pyrrhotite ($Fe_{1-X}S$)	5600-5800(?)	PA
DF 66-21	Malachite ($Cu_2(CO_3)(OH)_2$)	700(?), 1000, 1400-1600, 1700, 4200	DL
	Galena (PbS)	1000 6600	DL PA
	Cinnabar (HgS)	1500-1600, 7600, 8800 6600, 7600	DL PA
	Bornite (Cu_5FeS_4)	5000, 5500	DL
	Marcasite (FeS_2)	5500	DL
	Arsenopyrite (FeAsS)	4600(?)	PA

*(?) following depth indicates tentative mineral identification rather than uncertain depth.

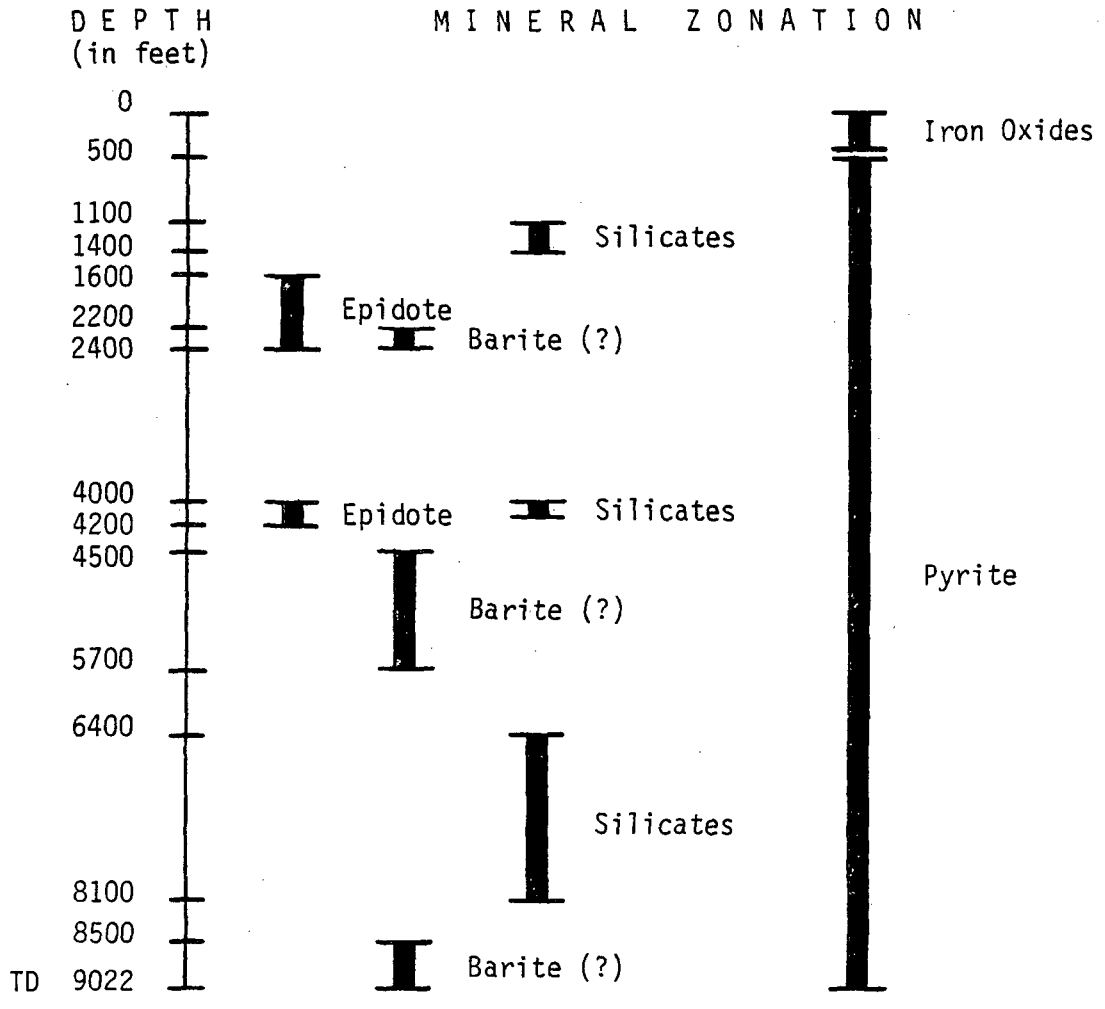

Figure 4-1. Zonation of mineral occurrences in DF 45-14 heavy mineral fraction samples.

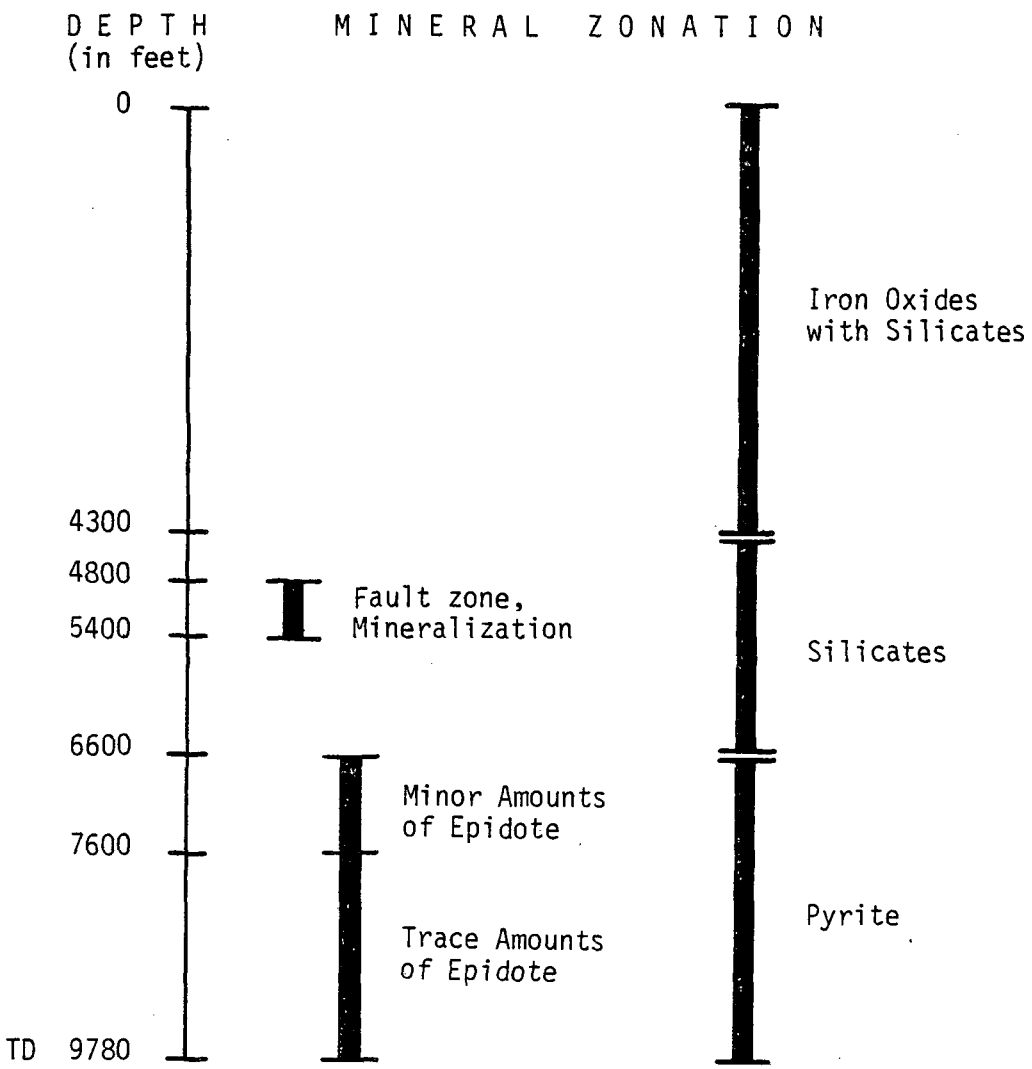

Figure 4-2. Zonation of mineral occurrences in DF 66-21 heavy mineral fraction samples.

trace mineral and 4000 to 4200 feet in which epidote is a major constituent. Barite is significant from 2200 to 2400 feet, from 4500 to 5700 feet and from 8500 feet to total depth of the well (9022 feet). Associations of silicate minerals including epidote, tourmaline, garnet, rutile, and zircon are notable in the following intervals: 1100 to 1400 feet, 4000 to 4100 feet, and 6400 to 8100 feet.

In DF 66-21 (Figure 4-2), an iron oxide-rich zone with minor or trace amounts of various silicate minerals (epidote, diopside, and tourmaline) extends to a depth of 4300 feet. With the appearance of significant pyrite from 4300 to 4400 feet, an intermediate zone starts which is dominated primarily by various silicate minerals to a depth of 6600 feet. Within this intermediate zone from 4800 to 5400 feet is a major mineralized fracture system. Below 6600 feet to total depth of the well is a pyrite dominated zone in which a subdivision at 7600 feet can be based on a decrease in epidote from minor to trace amounts. The possible significance of these mineral distribution zones in both DF 45-14 and DF 66-21 will be discussed in a later section.

4.2.2 Elemental Distribution

4.2.2.1 General

Distributions of the selected trace elements in +3.3 heavy mineral fraction and whole rock composite samples were determined for wells DF 45-14 and DF 66-21 to allow for comparison of the geochemical signature patterns and the known physical characteristics of the geothermal system. For DF 45-14 composite interval samples from 100 feet to a depth of 9022 feet were analyzed; Table 4-5 lists the results for the heavy mineral fraction samples and Table 4-6 lists the results for the whole rock samples. For DF 66-21 composite interval samples from 135 feet to a depth of 9780 feet were analyzed; Table 4-7 and Table 4-8 list the results for the heavy mineral fraction and whole rock samples, respectively. Plates VI through IX present bar graph plots of these data.

Frequency distributions of these data as plotting percentages are presented on log probability plots in Figures 4-14 through 4-33 (Appendix B), with Tables 4-13 through 4-32 (Appendix B) listing corresponding statistical data and specific lithologies for each value increment. Anomalous population threshold values (Table 4-9) for each trace element in both heavy mineral fraction and whole rock samples for each well were

Table 4-5

Distribution of Selected Elements in DF 45-14 Heavy Mineral Fractions

Depth Interval (in Feet)	Lead (ppm)	Zinc (ppm)	Arsenic (ppm)	Antimony (ppm)	Mercury (ppm)	Temperature (°F)
0100 0200	00425	00375	00220	0014	00.125	105
0200 0300	00075	00400	00220	0022	00.010	112
0300 0400	00125	00075	00200	0016	00.010	121
0400 0500	00025	00375	00620	0192	07.400	130
0500 0700	00050	00125	00780	0338	04.800	141
0700 0800	00050	00025	01000	0836	13.800	151
0800 0900	00075	00025	00920	0384	16.700	156
0900 1000	00075	00025	00550	0104	01.700	163
1000 1100	00075	00050	00780	0514	00.100	169
1100 1300	00075	00075	06000	0500	02.100	175
1300 1400	00475	00075	06500	0338	00.270	180
1400 1600	00100	00075	03800	0214	09.100	187
1600 1800	00075	00100	00880	0074	00.375	197
1800 1900	00050	00150	01600	0106	01.100	205
1900 2200	00075	00075	00580	0046	00.570	213
2200 2400	00100	02000	00500	0024	-ND-	223
2400 2700	00175	00650	00900	0032	00.010	231
2700 2900	00150	00100	00650	0020	00.010	240
2900 3000	00150	00100	00750	0014	00.010	246
3000 3100	00075	00175	00780	0012	00.010	248
3100 3200	00150	00075	00420	0002	00.010	251
3200 3300	00150	00050	00175	0002	00.200	255
3300 3500	00250	00175	00200	0002	00.270	260
3500 3700	00200	00300	00650	0008	00.235	268
3700 4000	00125	00175	00800	0036	00.360	277
4000 4100	00050	00150	00400	0014	00.185	284
4100 4200	00025	00125	00125	0002	00.185	287
4200 4500	00325	00325	01500	0022	00.270	298
4500 4900	00425	00200	01300	0020	00.380	314
4900 5400	00475	00600	01000	0016	00.585	327
5400 5700	02200	04100	00400	0020	00.395	336
5700 5900	00200	01200	00200	-ND-	00.185	340
5900 6400	02200	00800	00600	0006	00.965	346
6400 6900	03000	00875	00450	0004	01.400	353
6900 7400	02200	01200	00275	0002	01.800	360
7400 7700	00325	00175	00250	0002	00.505	366
7700 8100	00680	00200	00225	0002	01.600	372
8100 8500	03700	00800	00520	0012	01.600	377
8500 9022	02500	00300	00480	0420	-ND-	379
Magnetic fraction (5000-7000)	00025	00025	00800	0304	09.600	

ND = No Data

Table 4-6

Distribution of Selected Elements in DF 45-14 Whole Rock Samples

Depth Interval (in Feet)	Lead (ppm)	Zinc (ppm)	Arsenic (ppm)	Antimony (ppm)	Mercury (ppm)	Temperature (°F)
0300 0400	00035	00050	00020	0002	00.300	121
0400 0600	00020	00065	00050	0010	03.100	130
0600 0700	00015	00045	00085	0024	06.000	141
0700 0800	00015	00045	00145	0046	07.400	151
0800 0900	00010	00040	00070	0021	03.300	156
0900 1000	00015	00040	00060	0012	01.400	163
1000 1100	00015	00025	00080	0029	00.460	169
1100 1300	00015	00020	00350	0036	02.900	175
1300 1400	00025	00135	00760	0022	02.300	180
1400 1600	00010	00020	00230	0016	00.940	187
1600 1800	-ND-	-ND-	-ND-	-ND-	-ND-	197
1800 1900	00010	00025	00065	0006	00.220	205
1900 2200	*00015*	*00030*	*00025*	*0003*	*00.220*	213
2200 2300	00010	00025	00005	0001	00.225	220
2300 2400	00005	00025	00005	0001	00.240	224
2400 2700	00010	00025	00015	0001	00.245	231
2700 2900	00010	00025	00010	0001	00.245	240
2900 3000	00015	00020	00025	0001	00.270	246
3000 3100	00015	00025	00030	0001	00.250	248
3100 3200	00020	00055	00010	0001	00.190	251
3200 3300	00025	00070	00005	0001	00.180	255
3300 3500	00020	00035	00005	0001	00.220	260
3500 3700	00025	00060	00025	0001	00.180	268
3700 4000	00015	00055	00020	0001	00.225	277
4000 4100	00015	00050	00010	0001	00.240	284
4100 4200	00015	00060	00070	0001	00.240	287
4200 4500	00025	00070	00040	0001	00.245	298
4500 4900	00020	00075	00015	0001	00.195	314
4900 5400	00030	00100	00010	0001	00.310	327
5400 5700	-ND-	-ND-	-ND-	-ND-	-ND-	336
5700 5900	00030	00120	00010	0001	00.360	340
5900 6400	00045	00085	00010	0001	00.320	346
6400 6900	00030	00070	00010	0001	00.345	353
7000 7100	00025	00060	00005	0001	00.350	357
7300 7400	00115	00085	00005	0001	00.190	360
7400 7700	00025	00090	00005	0001	00.185	366
7700 8100	00035	00055	00005	0001	00.225	372
8100 8500	*00040*	*00070*	*00005*	0001	00.075	377
8500 9022	00030	00060	00005	0001	00.260	379

ND = No Data

Table 4-7

Distribution of Selected Elements in DF 66-21 Heavy Mineral Fractions

Depth Interval (in Feet)	Lead (ppm)	Zinc (ppm)	Arsenic (ppm)	Antimony (ppm)	Mercury (ppm)	Temperature (°F)
0135 0700	00025	00125	00075	0014	02.300	206
0700 0900	00025	00100	00050	0016	01.300	232
0900 1200	00025	00250	00025	0006	00.400	241
1200 1500	00025	00100	00050	0008	00.285	250
1500 1700	00025	00125	00050	0002	01.400	254
1700 2000	00025	00175	00050	0002	00.375	259
2000 2400	09500	00250	00175	0004	13.000	267
2400 2700	00025	00050	00050	0006	00.435	275
2700 3000	00050	00050	00250	0014	05.500	283
3000 3200	00050	00050	00125	0008	00.225	291
3200 3400	00050	00050	00075	0006	00.315	294
3400 3700	00050	00050	00100	0002	01.800	298
3700 4000	00075	00075	00100	0016	42.000	303
4000 4100	00025	00025	00050	0024	43.000	306
4100 4200	00025	00025	00075	0024	21.000	307
4200 4300	00025	00050	00250	0008	37.000	308
4300 4400	00025	00025	00025	0004	02.500	310
4400 4500	00025	00100	00200	0088	16.000	311
4500 4600	00025	00050	00050	0002	10.300	313
4600 4800	00025	00050	00050	0156	19.000	315
4800 4900	00025	00050	00025	0002	00.260	317
4900 5200	01200	11500	00225	0048	00.105	318
5200 5400	00025	00050	00025	0002	00.680	319
5400 5800	00250	00100	00005	-ND-	00.435	321
5800 6100	00025	00025	00780	0010	03.500	324
6100 6200	00025	00025	00025	0002	00.695	326
6200 6500	00025	00125	00075	0002	00.750	327
6500 6600	00025	00025	00050	0002	02.300	329
6600 6800	00025	00025	00125	0006	01.600	330
6800 7100	00025	00100	01200	0014	00.660	332
7100 7400	00075	00050	00175	0020	01.800	333
7400 7600	13500	00520	00200	1600	13.400	334
7800 8200	01000	00950	00520	0068	07.200	335
8200 8600	06000	00125	00480	0048	00.730	336
8600 8900	00650	00175	00320	0008	00.305	336
8900 9400	01100	00150	00420	0002	00.995	-ND-
9400 9780	01200	01300	00100	0018	08.600	-ND-
Magnetic	00025	00125	00025	0002	05.500	
fractions	00025	00125	00025	0002	06.100	

ND = No Data

Table 4-8

Distribution of Selected Elements in DF 66-21 Whole Rock Samples

Depth Interval (in Feet)	Lead (ppm)	Zinc (ppm)	Arsenic (ppm)	Antimony (ppm)	Mercury (ppm)	Temperature (°F)
0135 0700	00020	00050	00005	0001	00.130	206
0700 0900	00015	00035	00005	0001	00.180	232
0900 1200	00010	00035	00010	0001	00.095	241
1200 1400	00005	00040	00005	0001	00.165	250
1400 1700	00005	00045	00010	0001	00.130	254
1700 2000	00005	00050	00005	0001	00.200	259
2000 2400	00065	00075	00010	0001	00.120	267
2400 2700	00005	00050	00010	0001	00.140	275
2700 3000	00010	00055	00005	0001	00.160	283
3000 3200	00010	00055	00005	0001	00.150	291
3200 3400	00010	00040	00010	0001	00.195	294
3400 3700	00010	00060	00005	0001	00.140	298
3700 4000	00010	00060	00005	0001	00.120	303
4000 4100	00015	00050	00010	0003	00.130	306
4100 4200	00020	00065	00015	0002	00.190	307
4200 4300	00015	00045	00020	0002	00.280	308
4300 4400	00010	00035	00010	0002	00.300	310
4400 4500	00010	00025	00010	0006	00.720	311
4500 4600	00010	00020	00005	0007	00.460	313
4600 4800	00020	00015	00005	0002	00.235	315
4800 4900	00015	00020	00005	0005	00.180	317
4900 5200	00045	00055	00005	0004	00.150	318
5200 5400	00020	00010	00005	0002	00.105	319
5400 5800	00010	00010	00005	0001	00.085	321
5800 6100	00020	00010	00050	0001	00.125	324
6100 6200	00020	00010	00005	0001	00.255	326
6200 6500	00020	00015	00005	0001	00.125	327
6500 6600	00020	00010	00010	0001	00.685	329
6600 6800	00005	00005	00005	0001	00.265	330
6800 7100	00005	00025	00030	0003	00.330	332
7100 7400	00010	00020	00005	0002	00.260	333
7400 7600	00015	00035	00005	0001	00.200	334
7600 7800	00020	00065	00010	0001	00.130	335
7800 8200	00020	00060	00005	0002	00.115	335
8200 8600	00040	00075	00005	0001	00.175	336
8600 8900	00030	00070	00005	0001	00.105	336
8900 9400	00030	00080	00005	0001	00.175	-ND-
9400 9780	00025	00065	00005	0001	00.155	-ND-

ND = No Data

Table 4-9

Threshold Values of Anomalous Populations

Well	Sample Type*	Element	Threshold Value
DF 45-14	HMF	Lead	1500 ppm
		Zinc	** (1500 PPM)
		Arsenic	2000 ppm
		Antimony	80 ppm or 250 ppm
		Mercury	2500 ppb
DF 45-14	WR	Lead	60 ppm
		Zinc	** (100 ppm)
		Arsenic	100 ppm
		Antimony	15 ppm
		Mercury	600 ppb
DF 66-21	HMF	Lead	400 ppm or 2000 ppm
		Zinc	700 ppm
		Arsenic	** (275 ppm)
		Antimony	300 ppm
		Mercury	4 ppm
DF 66-21	WR	Lead	** (45 ppm)
		Zinc	**
		Arsenic	** (15 ppm)
		Antimony	** (5.5 ppm)
		Mercury	400 ppb

** Double asterisk denotes a log normal population; when a (value) is provided, it signifies a possible anomalous population threshold with uncertainty based upon the small size of the data set.

determined from the log probability plots. It should be noted that a number of plots are interpreted as indicating only one log-normal population. However, the small size of the data sets in some cases makes identification of anomalous populations uncertain; tentative threshold values are indicated for these log probability plots.

By applying these threshold values to their respective data sets, anomalous intervals can be identified and evaluated. Tables 4-10 and 4-11 list the anomalous trace element concentrations in DF 45-14 and DF 66-21, respectively. The spatial relationships and relative values of these anomalous intervals are depicted in Figures 4-3 through 4-6.

4.2.2.2 DF 45-14

Three distinct zones are distinguishable in DF 45-14 (Figure 4-3). The first, extending from 400 feet to a depth of 1600 feet, is characterized by concentrations of arsenic, antimony and mercury. Arsenic is restricted to below 1100 feet; antimony is fairly evenly distributed throughout the zone but shows a maximum anomaly occurring above 1000 feet; and mercury is restricted to the interval above 1000 feet with the exception of a 6.6 ppm anomaly from 1400 to 1600 feet. Similar relationships among the anomalous concentrations of these three elements within the whole rock samples also define this zone (Figure 4-4). This spatial-value relationship is consistent with the geochemical behavior of these elements. The mercury, being more volatile, occurs as a halo above the arsenic, with antimony reflecting an affinity for both elements.

The second zone extends from 5400 feet to a depth of 7400 feet and is characterized by anomalous lead concentrations in the heavy mineral fraction samples (Figure 4-3). Secondary confirmation of this zone is provided by tentative zinc anomalies in both heavy mineral fraction and whole rock samples from 5400 to 5700 feet and a 55 ppm lead anomaly in the whole rock sample from 7300 to 7400 feet (Figure 4-4).

The third zone extends from 8100 feet to the total depth of the well (9022 feet) and is defined solely by anomalous lead concentrations in the heavy mineral fraction samples (Figure 4-3). No anomalous arsenic, antimony or mercury concentrations occur in either the second or third zones. This is consistent with the geochemical behavior of these elements.

Table 4-10

Anomalous Trace Element Concentrations in DF 45-14

Element	Threshold Values* HMF; WR in ppm	Depth Interval in feet	Anomalous Concentrations* (Actual - Threshold Value) HMF	WR in ppm
Lead	1500; 60	5400 - 5700	700	--
		5900 - 6400	700	--
		6400 - 6900	1500	--
		6900 - 7400	700	--
		7300 - 7400	--	55
		8100 - 8500	2200	--
		8500 - TD	1000	--
Zinc	(1500); (100)	1300 - 1400	--	(35)
		2200 - 2400	(500)	--
		5400 - 5700	(2600)	--
		5700 - 5900	--	(20)
Arsenic	2000; 100	700 - 800	--	45
		1100 - 1300	4000	250
		1300 - 1400	4500	660
		1400 - 1600	1800	130
Antimony	250; 15	500 - 700	88	--
		600 - 700	--	9
		700 - 800	586	31
		800 - 900	134	6
		1000 - 1100	264	14
		1100 - 1300	250	21
		1300 - 1400	88	7
		1400 - 1600	--	1
Mercury	2.5; 0.6	400 - 500	4.9	--
		400 - 600	--	2.5
		500 - 700	2.3	--
		600 - 700	--	5.7
		700 - 800	11.3	6.8
		800 - 900	14.2	2.7
		900 - 1000	--	0.8
		1100 - 1300	--	2.3
		1300 - 1400	--	1.7
		1400 - 1600	6.6	0.34

*Values given in parentheses indicate tentative anomalous population; see Table 4-9. HMF - Heavy Mineral Fraction; WR - Whole Rock.

Table 4-11

Anomalous Trace Element Concentrations in DF 66-21

Element	Threshold Values* HMF; WR in ppm	Depth Interval in feet	Anomalous Concentrations* (Actual - Threshold Value) HMF	WR in ppm
Lead	2000; (45)	2000 - 2400	--	(20)
		2200 - 2400	7500	--
		7400 - 7600	11500	--
		8200 - 8600	4000	--
Zinc	700; (**)	4900 - 5200	10800	(**)
		7800 - 8200	250	(**)
		9400 - TD	600	(**)
Arsenic	(275); (15)	4200 - 4300	--	(5)
		5800 - 6100	(515)	(35)
		6800 - 7100	(925)	(15)
		7800 - 8200	(245)	--
		8200 - 8600	(205)	--
		8600 - 8900	(45)	--
		8900 - 9400	(145)	--
Antimony	300; (5.5)	4400 - 4500	--	(0.5)
		4500 - 4600	--	(1.5)
		7400 - 7600	1300	--
Mercury	4.0; 0.400	2200 - 2400	9.0	--
		2700 - 3000	1.5	--
		3700 - 4000	38.0	--
		4000 - 4100	39.0	--
		4100 - 4200	17.0	--
		4200 - 4300	33.0	--
		4400 - 4500	12.0	0.320
		4500 - 4600	6.3	0.620
		4600 - 4800	15.0	--
		6500 - 6600	--	0.285
		7400 - 7600	9.4	--
		7800 - 8200	3.2	--
		9400 - TD	4.6	--

*Values given in parentheses indicate tentative anomalous populations; see Table 4-9. HMF - Heavy Mineral Fraction; WR - Whole Rock.

**Indicates single log-normal population; no anomalous values.

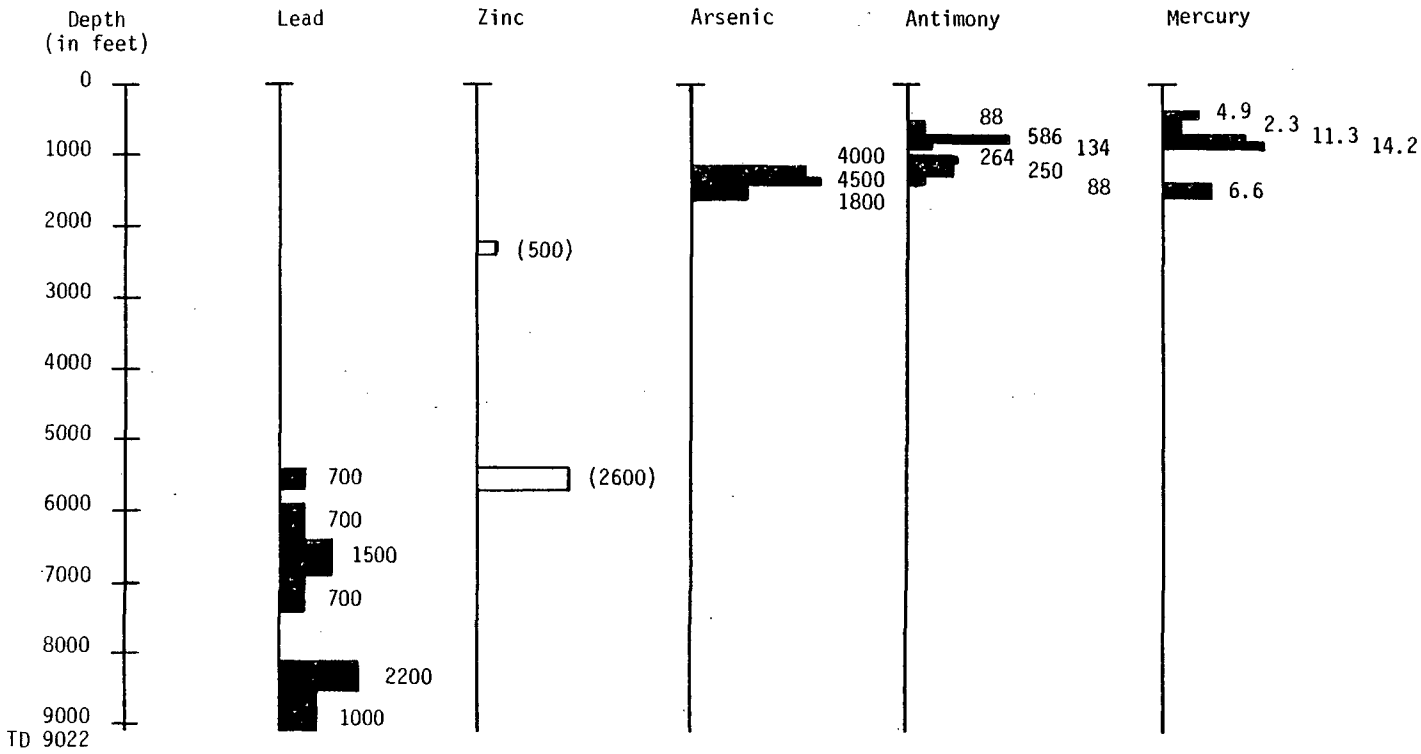

Figure 4-3. Anomalous concentrations of selected trace elements in DF 45-14 heavy mineral fraction samples.

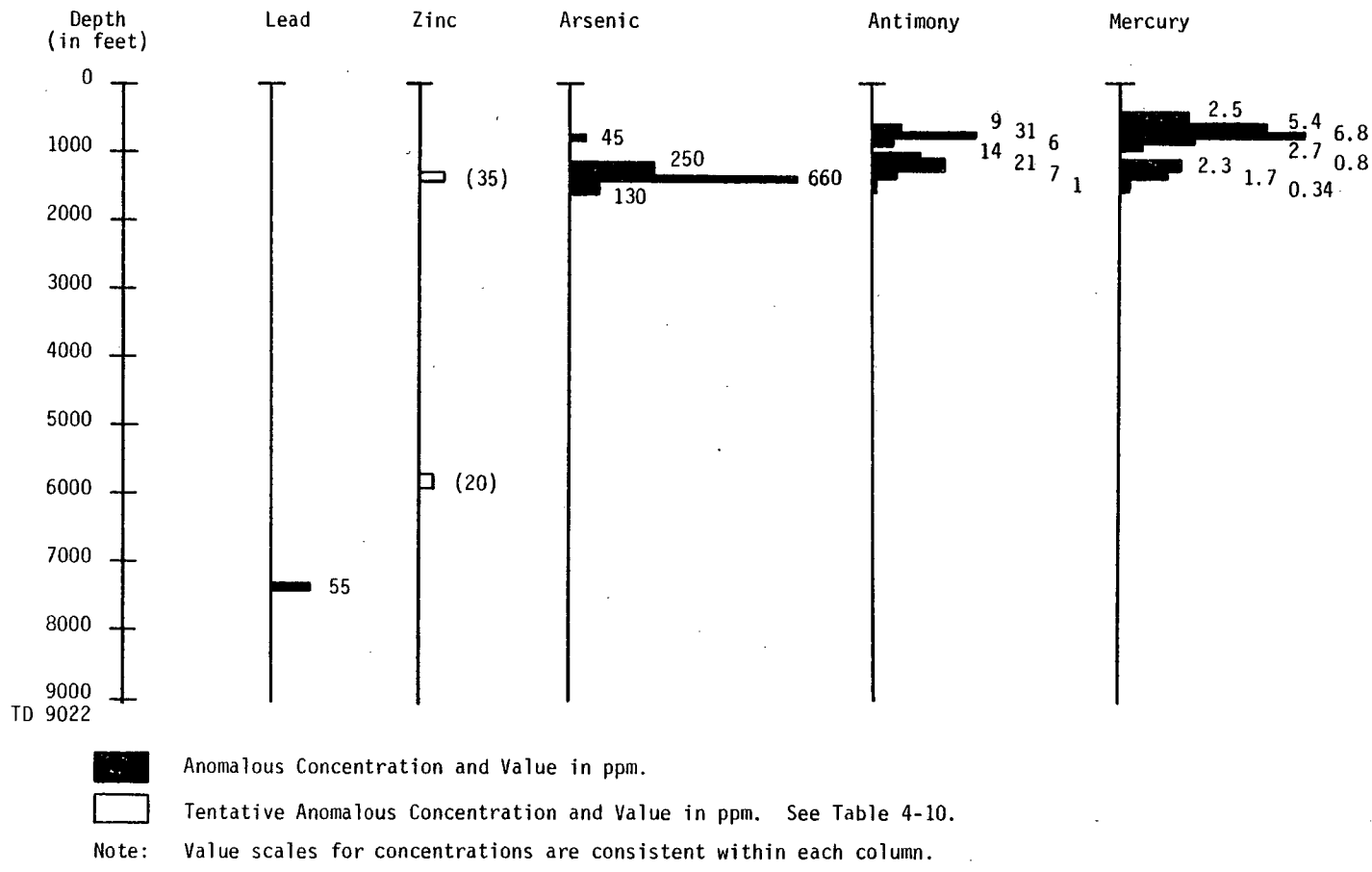

Figure 4-4. Anomalous concentrations of selected trace elements in DF 45-14 whole rock samples.

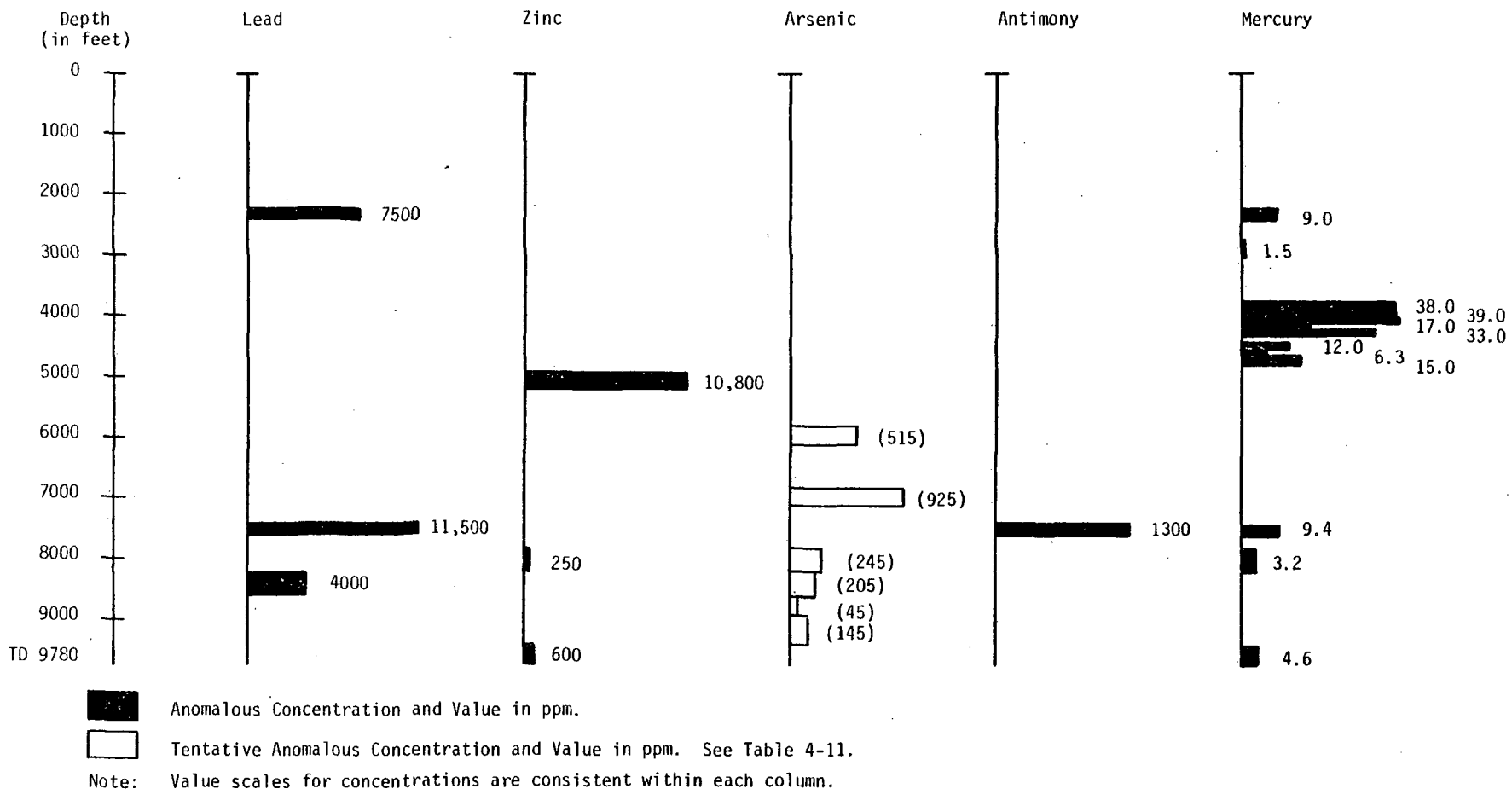

Figure 4-5. Anomalous concentrations of selected trace elements in DF 66-21 heavy mineral fraction samples.

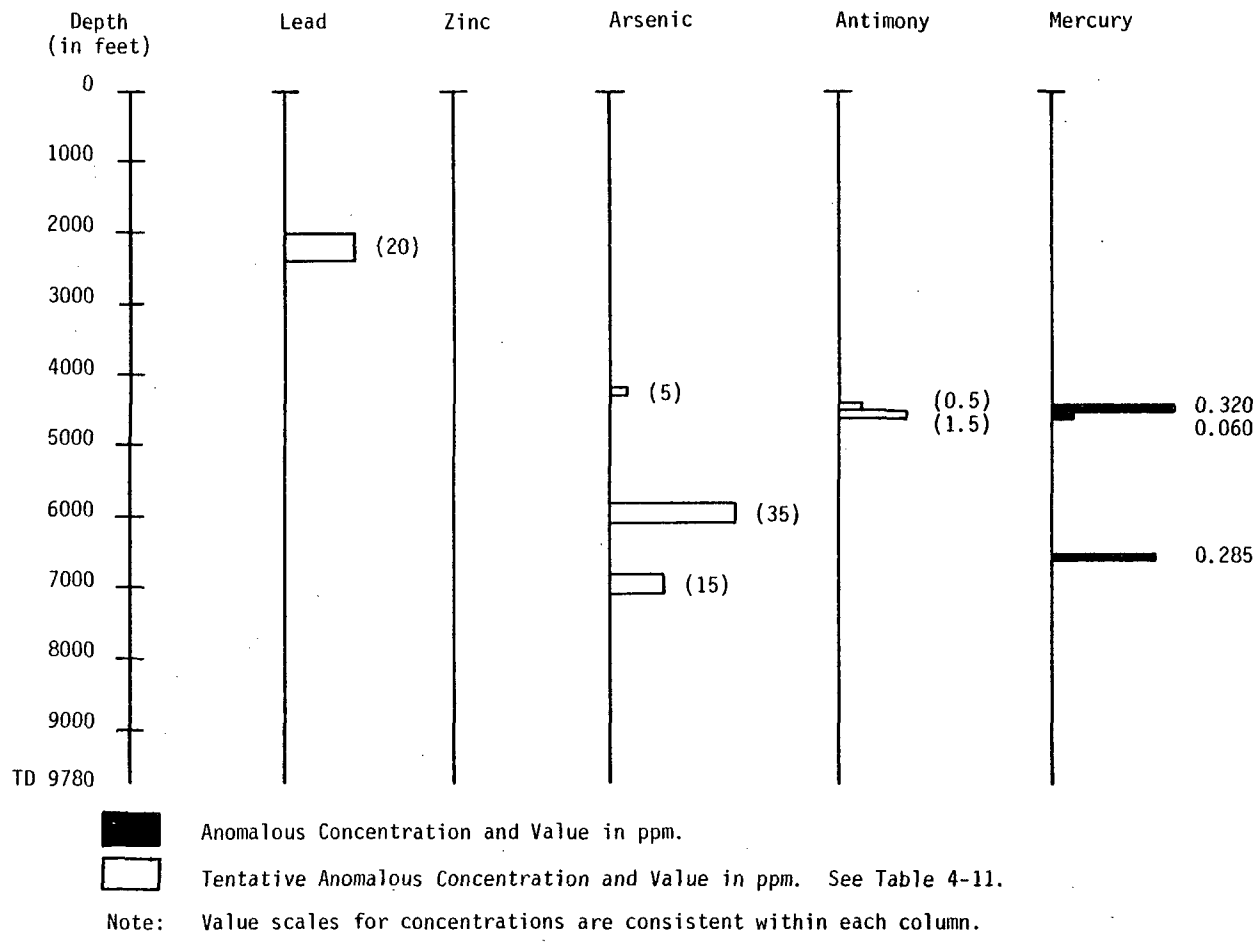

Figure 4-6. Anomalous concentrations of selected trace elements in DF 66-21 whole rock samples.

4.2.2.3 DF 66-21

In DF 66-21, a number of zones can also be defined by the spatial distribution and correspondence of anomalous concentrations of the trace elements (Figures 4-5 and 4-6). It should be noted that the patterns are not as distinct as in DF 45-14, nor as simple. In addition, the respective trace element abundances for whole rock samples in DF 66-21, with the exception of mercury, appear to be log-normal populations (Figure 4-29 through 4-33, Appendix B), that is, that no anomalous concentrations are present and only very tentative interpretations could be made in identifying possible lead, arsenic and antimony anomalies. This is also true for arsenic concentrations in the heavy mineral fraction samples (Figure 4-26, Appendix B).

The following zones can be identified in DF 66-21 (Figure 4-5): 1) a zone from 2200 to 2400 feet characterized by anomalous lead and mercury concentrations; 2) a zone from 3700 to 4800 feet characterized by anomalous mercury concentrations ranging up to 39 ppm in heavy mineral fraction samples, with anomalous concentrations of mercury also occurring in whole rock samples between 4400 and 4600 feet; 3) a zone from 4900 to 5200 feet characterized by a 10,800 ppm anomalous zinc concentration; 4) a zone from 7400 to 7600 feet characterized by anomalous concentrations of lead (11,500 ppm), antimony (1300 ppm) and mercury (9.4 ppm); 5) a zone from 7800 to 8200 feet characterized by anomalous concentrations of zinc (250 ppm) and mercury (3.2 ppm); 6) a zone from 8200 to 8600 feet characterized by a 400 ppm anomalous lead concentration; and 7) a zone from 9400 feet to total depth of the well (9780 feet) characterized by anomalous concentrations of zinc (600 ppm) and mercury (4.6 ppm). In addition, a zone can also be distinguished at 6500 to 6600 feet characterized by a minor (0.285 ppm) anomalous mercury concentration in whole rock samples (Figure 4-6). Unlike DF 45-14, these zones exhibit apparent discordant trace element geochemistry that poses a problem of interpretation. The significance of these anomalous trace element concentration zones is discussed in a later section.

4.2.3 Reservoir Zoning

4.2.3.1 General

The distribution of the selected trace elements may also be viewed using the concepts of the reservoir, self-sealed and peripheral zones.

As applied by Bamford and others (1980), the zones may generally be characterized as follows:

The reservoir zone exhibits temperatures greater than 206°C (400°F) with predominantly convective heat transfer. Arsenic and zinc concentrations are enriched, while lead is constant or only slightly enriched, and mercury concentrations remain low.

The self-sealed zone is characterized physically in the rock by alteration, limonite and sulfide accumulation, and/or siliceous and carbonate cement, as well as by the absence of significant surface leakage of fluids. Chemically the outer portion of the self-sealed zone is characterized by high zinc enrichments and arsenic enrichment, with the inner self-sealed zone characterized by arsenic and lesser amounts of zinc. The entire self-sealed zone is characterized by very high mercury enrichment. In general, an outer halo assemblage of erratic low-level mercury and arsenic anomalies, usually associated with locally anomalous concentrations of zinc (and manganese), grades into a zone of increasing mercury concentrations to a region of continuous anomalous arsenic with minor zinc.

The overlying peripheral zone generally exhibits zinc enrichment and physically exhibits slight to moderate evidence of hydrothermal activity. Localized zoning around hot water entries or sealed fracture zones may occur in any or all of these zones.

The distribution of the selected trace elements in DF 45-14 (Plates VI and VII) and DF 66-21 (Plates VIII and IX) and the known physical characteristics of the wells (Plates IV and V) can be subjectively interpreted with respect to the reservoir, self-sealed and peripheral zone concepts. Figure 4-7 depicts these zones as interpreted for the two wells.

4.2.3.2 DF 45-14

In DF 45-14, a peripheral zone, extending to approximately 4100 feet, is characterized by low lead and zinc with arsenic, antimony and mercury concentrations localized with respect to a series of interbedded tuffaceous units which display evidence of secondary mineralization, recrystallization and fracture filling -- i.e., a localized self-sealed zone.

The self-sealed zone extends from about 4100 feet to total depth of the well. This zone is characterized by high lead concentrations with

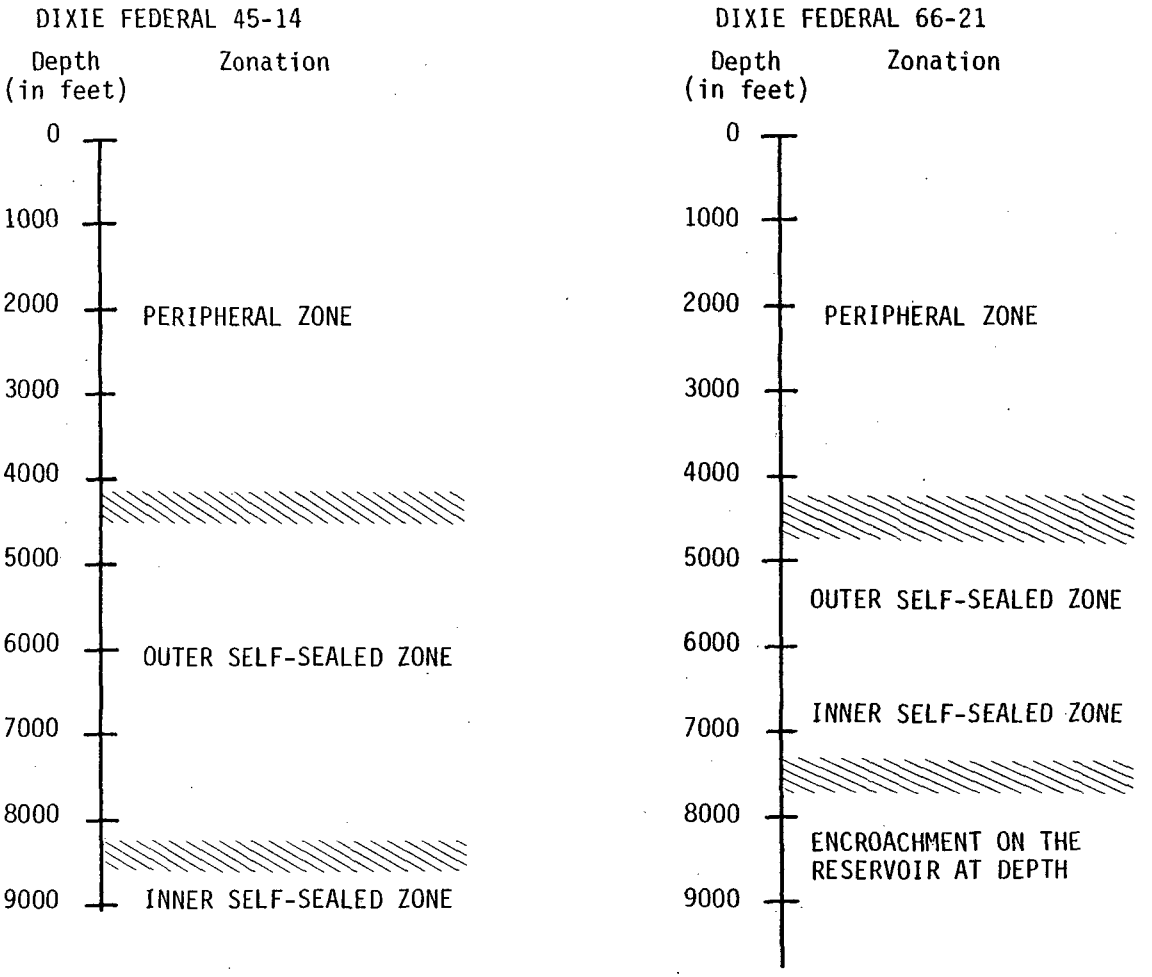

Figure 4-7. Reservoir zoning model for DF 45-14 and DF 66-21.

zinc. The arsenic is high but decreasing somewhat with depth as antimony increases. Mercury concentrations increase with depth. A tentative gradational boundary from outer to inner self-sealed zone is placed between 8100 to 8500 feet. Lead and zinc remain fairly constant and both arsenic and antimony are enriched. Physical evidence for hydrothermal activity within the well (Bard, 1980) is consistent with the zoning concepts. In addition, the presence of fracture zones (Plate IV) with barite (?) deposition (Figure 4-1) and very limited production within the self-sealed zone suggest that self-sealing has occurred and may be continuing.

4.2.3.3 DF 66-21

In DF 66-21, a peripheral zone is identified above about 4300 feet and is characterized by low lead concentrations and constant concentrations of zinc, arsenic, antimony and mercury. Anomalous lead and mercury concentrations, with some enrichment of arsenic, occur between 2000 and 2400 feet associated with the upper boundary of a red clay-alluvial sequence. This concentration may reflect the low permeability of the clay with deposition from aqueous solutions or adsorption by clays of the vapor transported elements. The very high mercury concentration near the base of the peripheral zone probably reflects adsorption on the fine-grained alteration minerals from remobilization or direct vapor transport generated by a major fracture system at 4700 to 5100 feet (Bard, 1980).

The self-sealed zone extends below about 4300 feet with a very broad gradation from outer to inner self-sealed zone. Mercury, zinc and arsenic concentrations characterize the outer self-sealed zone. In the inner self-sealed zone mercury and arsenic increase somewhat while zinc concentrations remain fairly constant. Below about 7500 feet the self-sealed zone begins to encroach on a possible reservoir zone at depth. This encroachment is evidenced by a general increase in mercury, high arsenic and lead concentrations, and significant concentrations of zinc. Localized zoning present within the self-sealed zone is associated with active and sealed fractures (e.g., about 5000 feet, 8000 to 8400 feet, 9400 to 9700 feet). Physical evidence for hydrothermal activity within the well (Bard, 1980) is consistent with the zoning concepts.

The zoning depicted in Figure 4-7 for DF 45-14 and DF 66-21 was tested by scattergram statistical analysis. Figures 4-8 and 4-9 depict the scattergrams for depth versus zinc bivariate analysis for whole rock

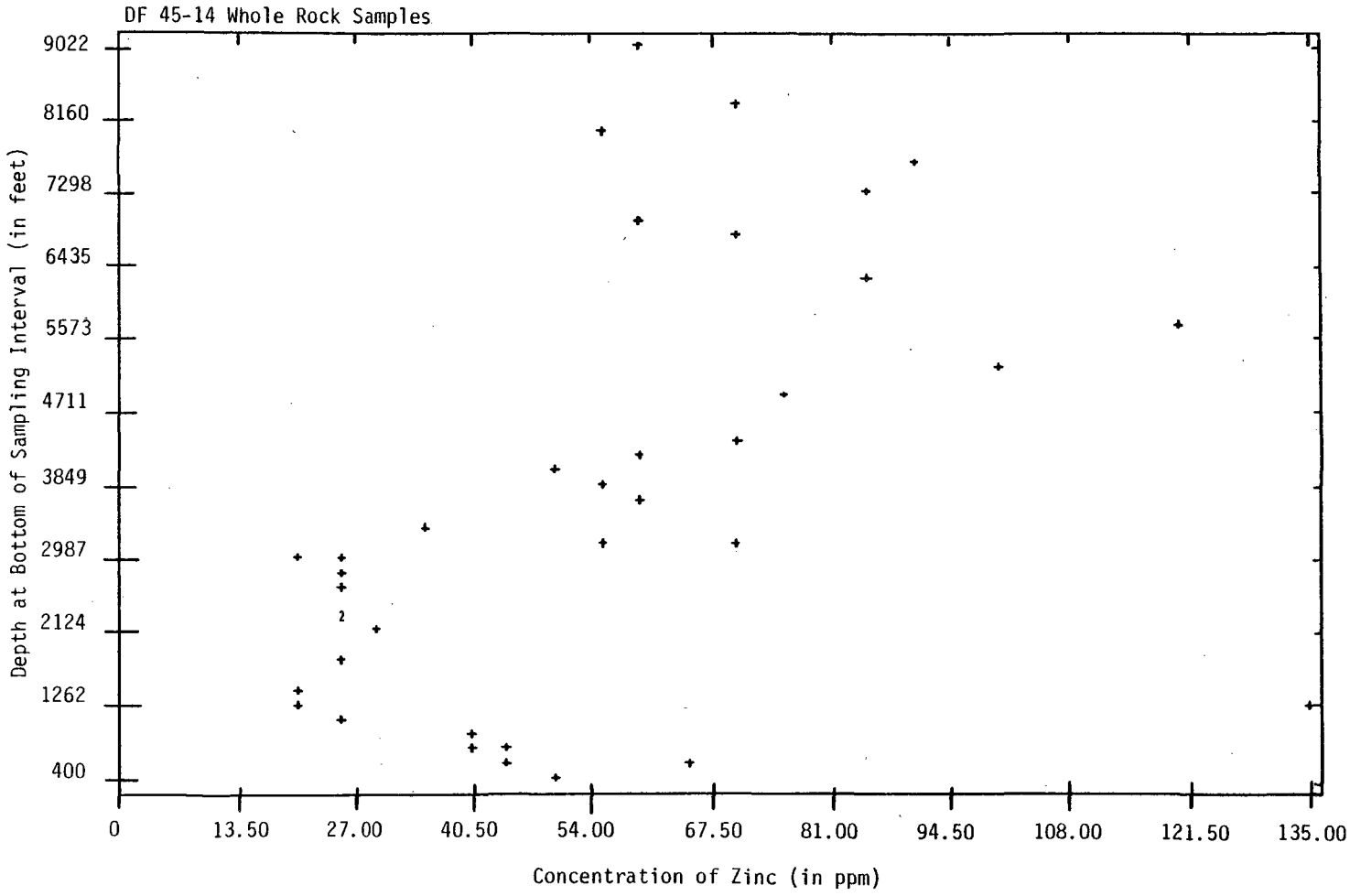

Figure 4-8. Scattergram plot of bivariate analysis of zinc with respect to depth (as bottom of sampling interval) for DF 45-14 whole rock samples.

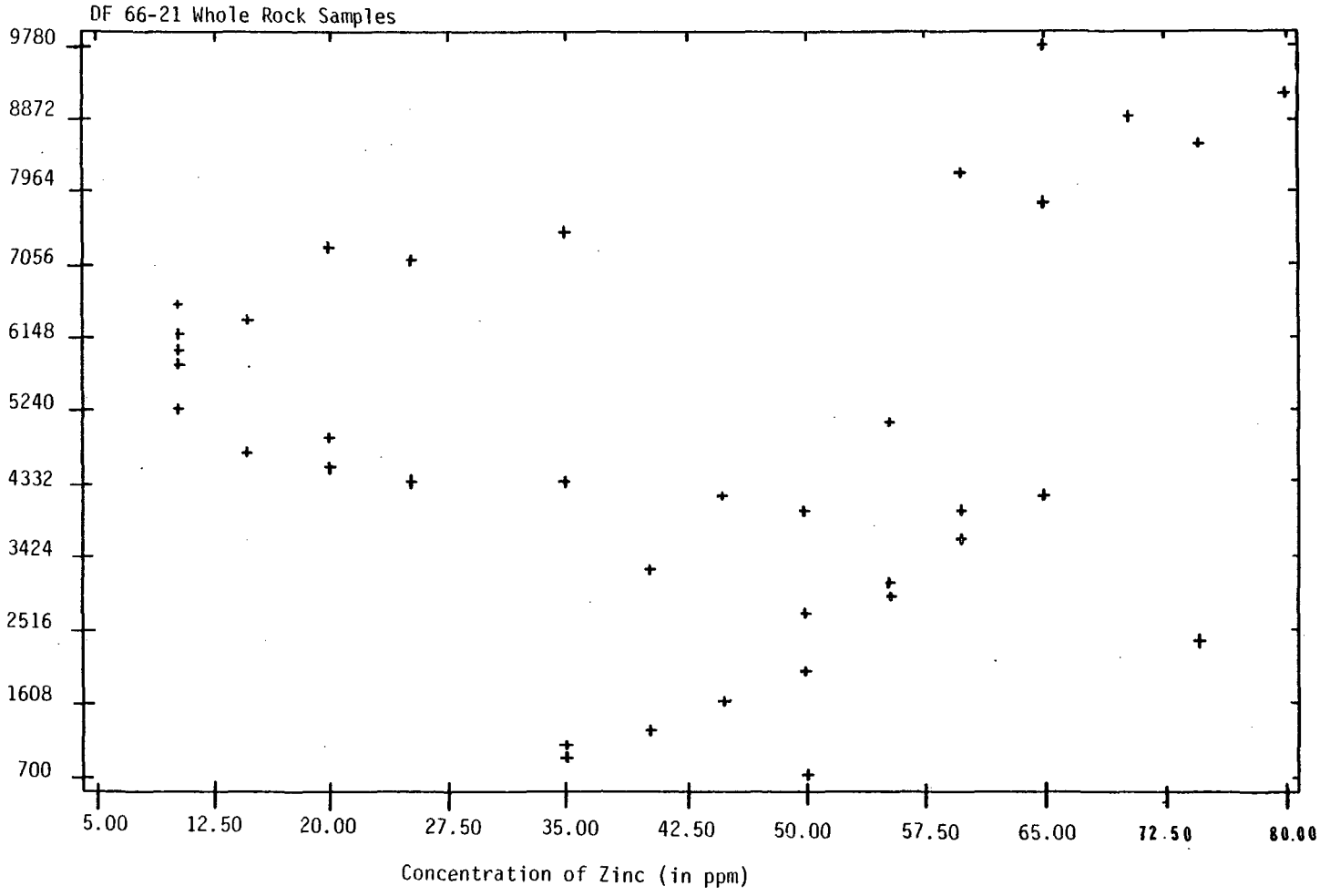

Figure 4-9. Scattergram plot of bivariate analysis of zinc with respect to depth (as top of sampling interval) for DF 66-21 whole rock samples.

samples in the two wells. While the scatter and overlap on the diagrams is a function of gradational boundaries and localized zoning, the divisions between the generalized zones are consistent with those subjectively determined. Similar results are obtained by using computed algebraic variables, such as zinc + arsenic + mercury as depicted in Figures 4-10 and 4-11. Since the general trends of the element concentrations in the heavy mineral fraction samples are reflected by the whole rock sample values, similar scattergram plots can be generated for corresponding data sets but are not included here.

4.2.4 An Alternate Interpretation

4.2.4.1 General

The reservoir zoning interpretation (Figure 4-7) is based on general trends and corresponding concentrations of the selected trace elements. This interpretation is not, however, totally compatible with a zonation based on mineral occurrences in the heavy mineral fraction samples (Figures 4-1 and 4-2) or anomalous concentrations of the selected trace elements (Figures 4-3 through 4-6). For this reason, and because the reservoir zoning technique is still in a formative phase, an alternate interpretation of the wells based on the petrochemical data as well as the physical characteristics of the wells is offered.

Figures 4-12 and 4-13 depict composite logs of DF 45-14 and DF 66-21, respectively, including selected physical parameters and both the mineral occurrences and anomalous concentrations of trace elements in the heavy mineral fraction samples.

4.2.4.2 DF 45-14

The pyrite dominated portion of DF 45-14 reflects the pervasive influence of the geothermal system. Within the pyrite-rich zone, intervals characterized secondarily by epidote and/or barite(?) correlate with intervals of fracture systems (Figure 4-12) and indicate that more intense hydrothermal activity has occurred in the fracture systems and rocks adjacent to them.

The zones of intense hydrothermal activity, as reflected by anomalous concentrations of the trace elements, suggest two different influences. The 400 to 1600 feet interval is characterized by high arsenic concentrations and an overlying halo of high mercury concentration with

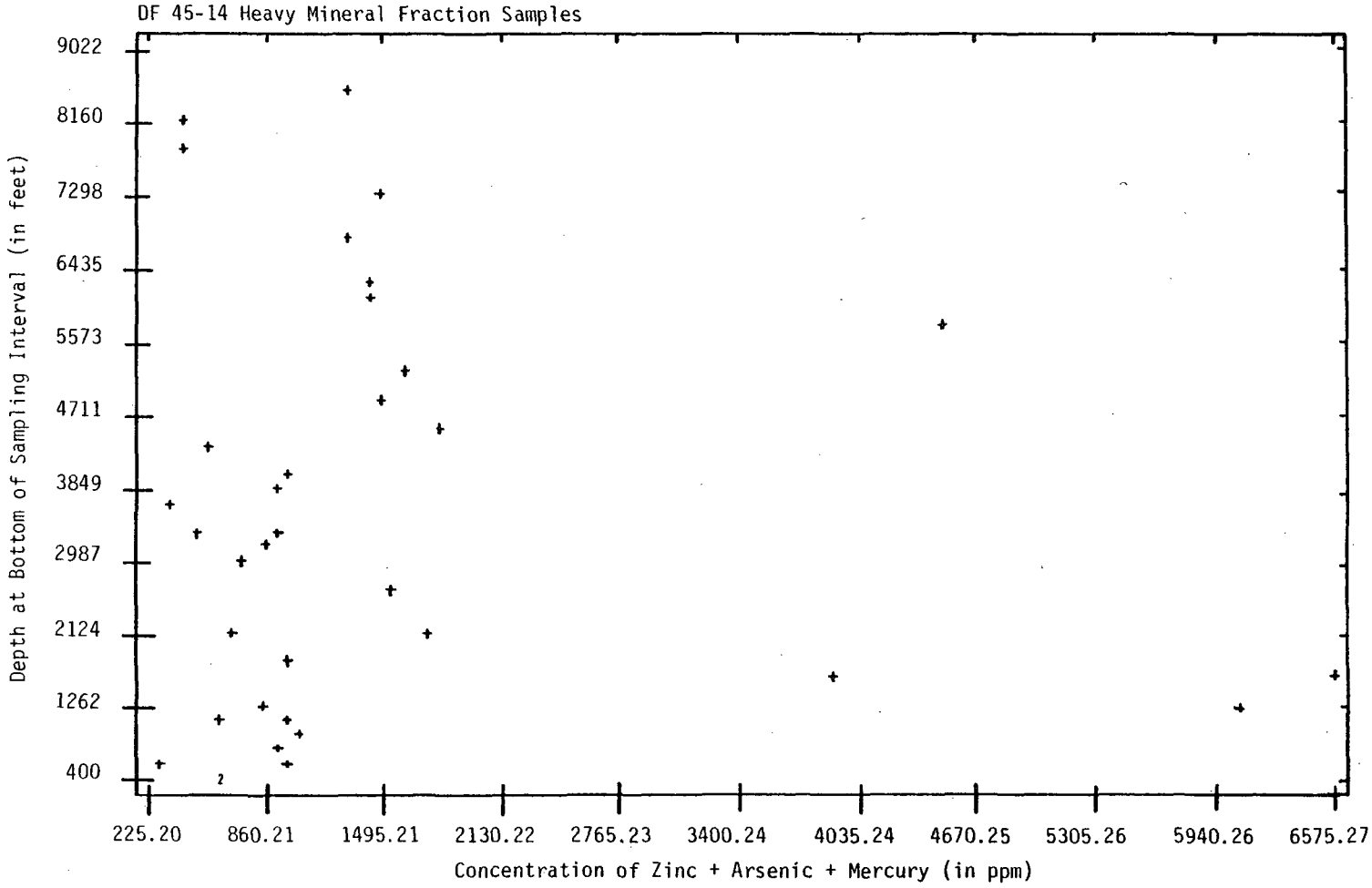

Figure 4-10. Scattergram plot of computed variable (zinc + arsenic + mercury) with respect to depth (as bottom of sampling interval) for DF 45-14 heavy mineral fraction samples.

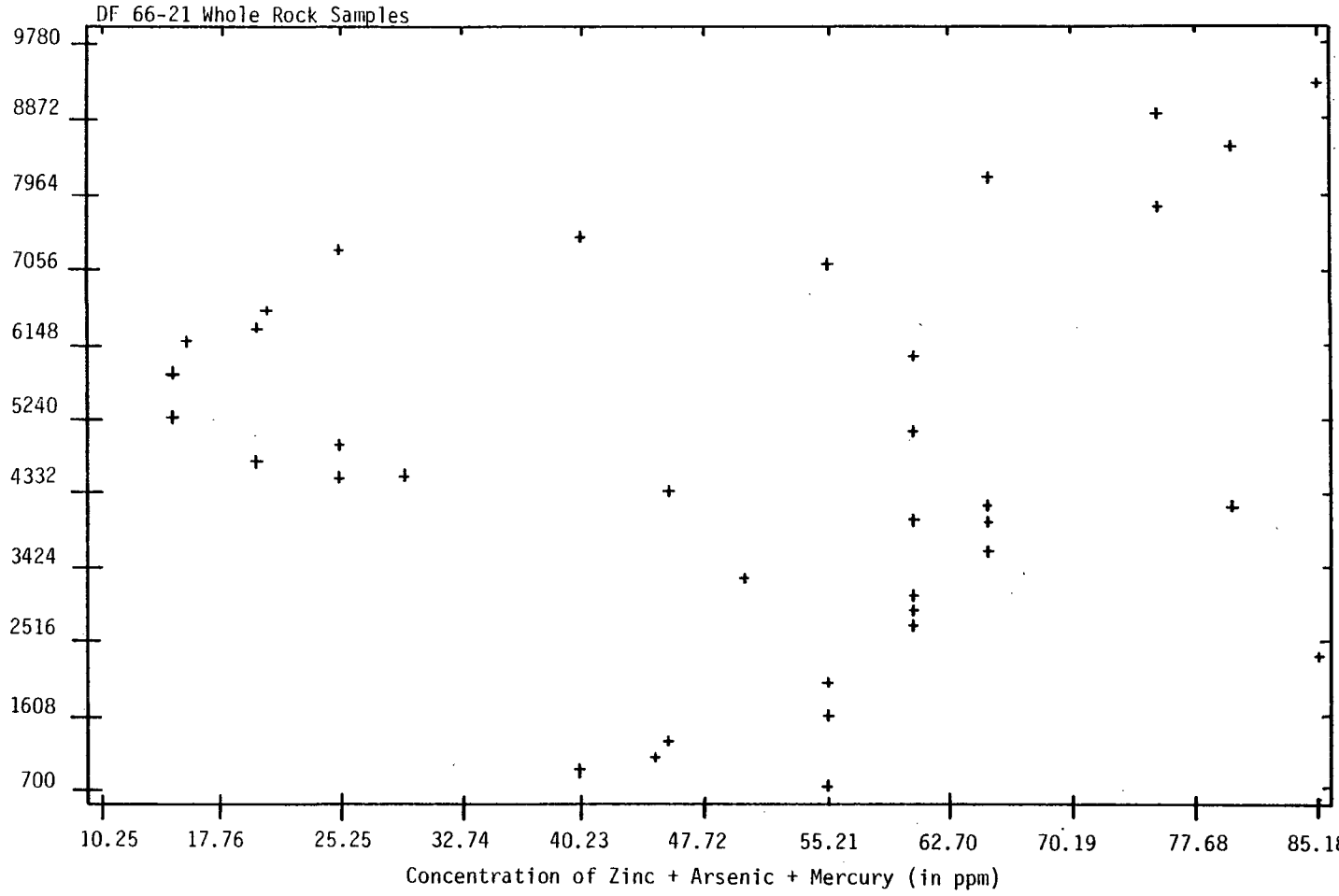

Figure 4-11. Scattergram plot of computed variable (zinc + arsenic + mercury) with respect to depth (as bottom of sampling interval) for DF 66-21 whole rock samples.

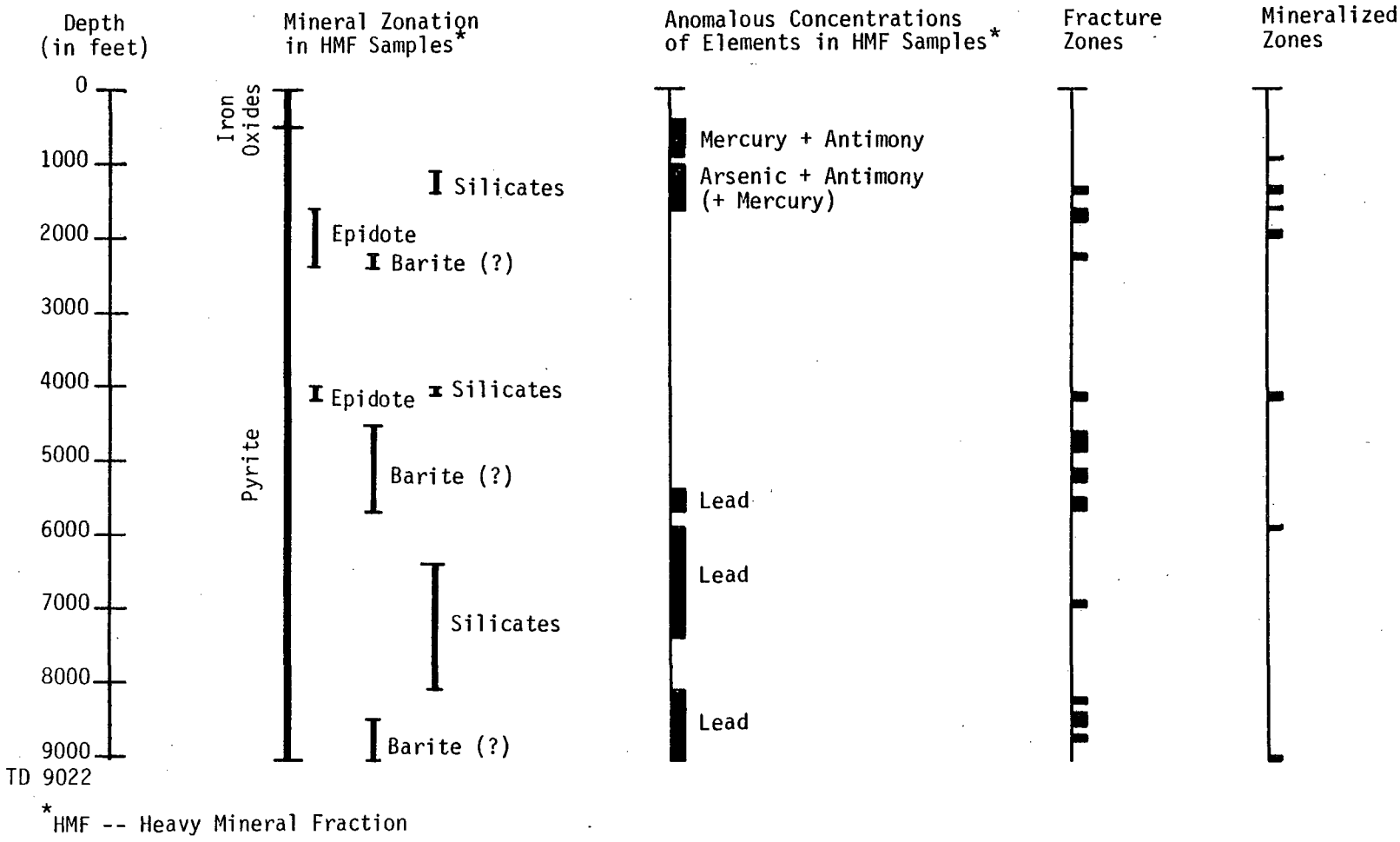

Figure 4-12. Composite of logs for DF 45-14 indicating selected physical parameters, mineral occurrences and anomalous element concentrations in heavy mineral fraction samples.

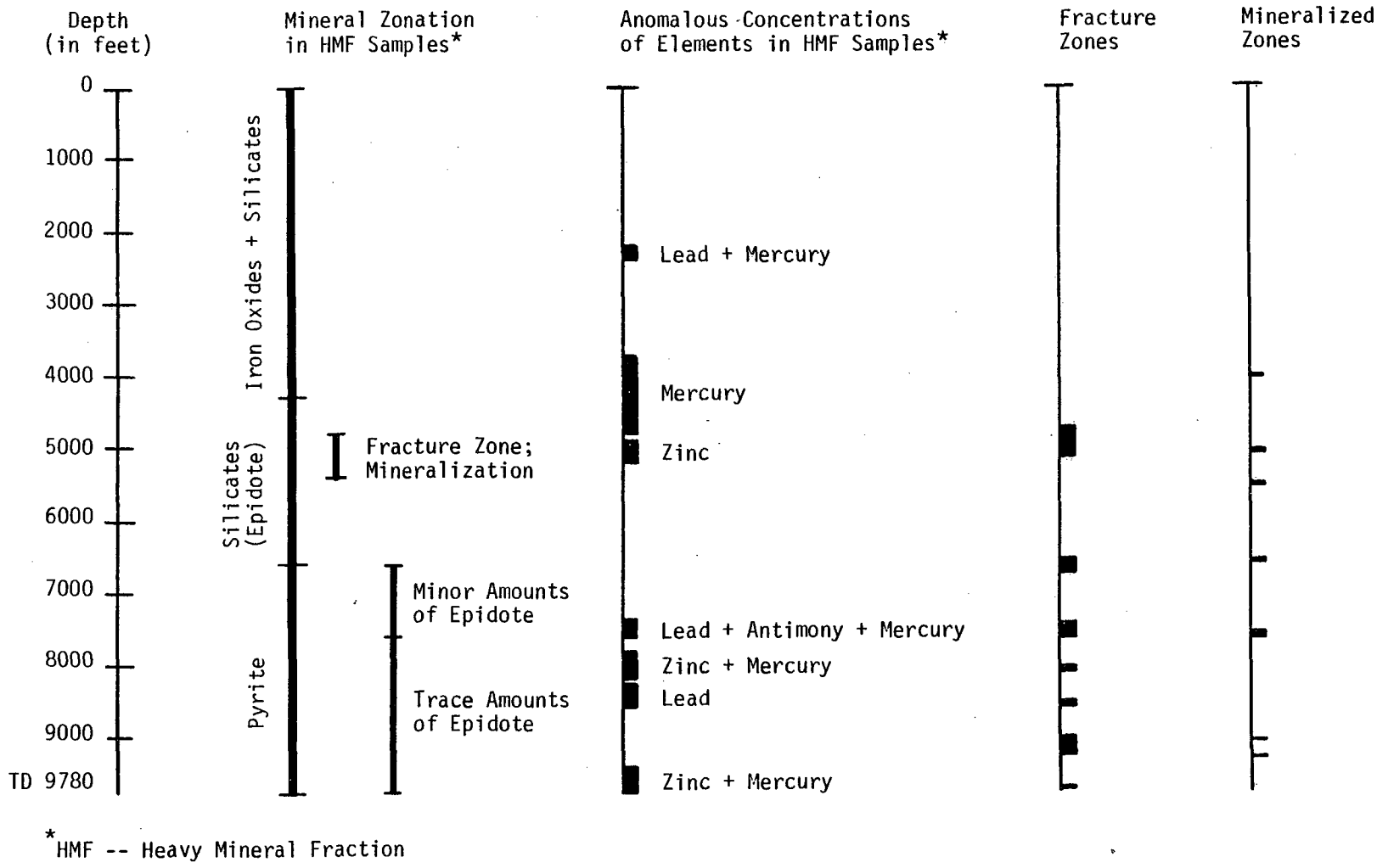

Figure 4-13. Composite of logs for DF 66-21 indicating selected physical parameters and the mineral occurrences and anomalous concentrations of elements in heavy mineral fraction samples.

antimony fairly uniformly distributed throughout the interval. This zone is interpreted as being a product of fracture-controlled permeability with the hydrothermal fluids migrating from the reservoir at depth through fractures associated with the tuffaceous units between 1300 and 1800 feet. Bacause of the geochemical behavior of the selected trace elements, it is believed that they were probably carried by the fluids through the fracture zone, and deposited in sulfide and silicate +3.3 mineral phases. The mercury, being more volatile and subject to vapor transport, occurs as a halo in the overlying interval (400-900 feet) probably due to adsorbtion by, or incorporation into, the +3.3 mineral phase.

A second probable influence of the geothermal system in DF 45-14 is reflected in the anomalous concentrations of lead present in the lower portions of the well (Figure 4-12): 700 to 1500 ppm in the interval from 5400 to 7400 feet and 1000 to 2200 ppm in the interval from 8100 to 9022 feet. These lead concentrations are interpreted as lead halos overlying the reservoir or heat source at depth, just as lead halos are similarly associated with ore deposits. This idea is further supported by the presence of barite(?) in fracture zones corresponding to portions of the anomalous lead intervals. The magnitude of the lead anomalies suggests that they probably developed over a relatively long time period, and that the larger anomaly (up to 2200 ppm) from 8100 to 9022 feet may be due to secondary enrichment by halo migration toward the heat source as it cooled. This cooling of the heat source may have been caused by age or by a decrease in connection to the heat source whether from self-sealing of the conduits or possibly from tectonic adjustments that may have closed the conduits. Alternatively, the high lead concentrations may reflect enrichment from fluids migrating through the fracture zones within the interval from 8100 to 9022 feet.

The degree of cementation and fracture-filling within most of the recognized major fault zones and in the numerous minor fractures encountered in the well is also indicative of significant decrease in connection with the reservoir at depth, with the exception of several intervals, most notably from 8100 feet to the bottom of the well.

4.2.4.3 DF 66-21

In contrast, DF 66-21 is interpreted as a more dynamic system with significant connection with the reservoir and a developing geochemical

signature. The anomalous lead (7500 ppm) and mercury (9.0 ppm) concentrations in the interval 2200 to 2400 feet (Figure 4-13) associated with the top of a red clay-alluvial sequence are interpreted as being deposited from aqueous solutions or adsorbed from vapor transport by +3.3 heavy mineral phases at the low-permeability boundary produced by the clay content. The source for the lead and mercury is uncertain; there may be an unrecognized fracture system in the overlying alluvial sequence, or more likely, thermal fluids released in the alluvium may be flowing through the ground water system with downward percolation inhibited by the impermeable clay.

From the lowermost portion of the clay-alluvial sequence to the total depth of the well at 9780 feet, the rocks show an increasingly pervasive influence of the geothermal system: silicate minerals (primarily epidote) with minor pyrite are replaced by a pyrite dominated assemblage. Within the silicate dominated zone is a major active fault system between 4800 and 5400 feet. An anomalous concentration of zinc (10,800 ppm) marks the most active portion of the fault zone where, during drilling, hot fluids under high pressure were encountered. The most significant indication of mineralization in this interval is the presence of flakes of native gold in the heavy mineral fraction sample. A halo of mercury with anomalous concentrations ranging from 6.3 to 39.0 ppm overlies the fault zone, with maximum concentrations occurring in the lowermost portion of the red clay-alluvium sequence. These maximum mercury concentrations are the result of adsorption of the vapor transported mercury by fine-grained +3.3 mineral phases in the base of the clay sequence, with upward migration of the volatile mercury limited by the impermeability of the clay.

Below 5400 feet are four zones containing anomalous element concentrations (Figure 4-13) interpreted as being the result of active migration of thermal fluids through fracture zones. Anomalous lead (11,500 ppm), antimony (1300 ppm) and mercury (9.4 ppm) concentrations are associated with a mineralized fracture zone in the interval 7400 to 7600 feet. A 250 ppm zinc and 3.2 ppm mercury anomaly is associated with a fracture zone identified at 8000 to 8100 feet. The fracture zone encountered at the bottom of the well (9780 feet) is associated with anomalous concentrations of zinc (600 ppm) and mercury (4.6 ppm). The range of concentrations for lead (4000 to 11,500 ppm), zinc (250 to 10,800 ppm), and

mercury (3.2 to 39 ppm) is believed to be related to possible variations in fluid compositions and may also reflect the significance of the fracture zone as a conduit; i.e., the more open a fracture zone, the greater volume of fluid it conducts and the greater the concentration of elements. For example, the mineralized fracture zone at 6500 to 6750 feet exhibits no anomalous element concentrations and is basically closed by calcite fracture-filling and veining.

4.3 Conclusions and Recommendations

4.3.1 *Significance of the Interpretations*

Both reservoir zoning and petrochemical analysis can be used as methods of interpreting the trace element geochemistry exhibited by DF 45-14 and DF 66-21 in Dixie Valley. In DF 45-14, distinct peripheral and inner and outer self-sealed zones can be identified based on general trends and corresponding concentrations of the trace element geochemistry. The outer self-sealed zone is approximately 4000 feet thick and the inner self-sealed zone extends from about 8500 feet to beyond the bottom of the well (9022 feet). Self-sealing has occurred with either partial or complete sealing of localized zones within the peripheral and self-sealed zones of DF 45-14.

In DF 66-21, the peripheral zone is distinct and extends to a depth of approximately 4300 feet. Below this depth lies the self-sealed zone with the boundary between the outer and inner self-sealed zones being gradational and poorly defined within the interval from 4300 to 7500 feet where the inner self-sealed zone begins encroaching upon the reservoir at depth. This encroachment zone extends beyond the bottom of the well (9780 feet). Self-sealing of localized zones is generally restricted to minor fracture systems, with most major fracture systems still serving as active fluid conduits.

By applying petrochemical analysis, relationships between the trace element geochemistry and the physical characteristics of the well, in particular the locations of fracture and mineralized zones, can be defined. In DF 45-14, two diverse effects of the geothermal system are identified: the first is a fracture-controlled arsenic-mercury concentration in the upper portion of the well and the second is a broad halo of lead concentrations overlying the reservoir, with possible secondary enrichment as a result of fracture-controlled fluid migration.

In DF 66-21 a number of zones can be defined with various combinations of anomalous trace elements; these are essentially fracture-controlled. Most of the fractures are still active conduits for the thermal fluids with the magnitude of the anomalous concentration values possibly related to the fluid composition or to the significance of the conduit.

The reservoir zoning and the petrochemical analysis techniques generate models of the two deep wells that are generally consistent and significant with respect to developing an understanding of the history of the Dixie Valley Geothermal System. In general, DF 45-14 represents a longer history of geothermal activity: the reservoir zones are more distinct and extend over larger depth intervals; self-sealing is more complete; a halo of anomalous lead concentrations has developed in the lower portions of the well that, while it may be secondarily enriched by fracture-controlled fluids, is a pervasive concentration; and fluid migration through fracture systems is limited. DF 66-21 exhibits a younger, more dynamic history of geothermal activity: while the peripheral zone is well defined, the self-sealed zone extends over a relatively narrow depth interval and has not yet developed geochemical signatures which differentiate well-defined outer and inner self-sealed zones; the inner self-sealed zone encroaches on the reservoir at depth; fracture zones are generally not self-sealed and actively conduct significant volumes of thermal fluids; and anomalous trace element concentrations exist in fairly narrow intervals associated primarily with active fracture systems.

This interpretation is based solely on the present level of knowledge of the two deep wells. It can not be over-emphasized that DF 45-14 and DF 66-21 represent a very limited sampling of the Dixie Valley Geothermal System. With the collection of additional data as suggested in the following section or with refinement of the data presently available, these interpretations can and should be re-evaluated.

4.3.2 Recommendations

1) Core samples should be taken at selected intervals in the wells. This would provide definitive identification of the specific mineral assemblages and the inter-granular relationships amoung the various mineral phases, and would allow for estimation of the amount of mixing and contamination that affects drill chip samples.

2) Other trace elements in the samples should be examined. Based on the models of Bamford and others (1980) for Roosevelt Hot Springs, KGRA, manganese may prove useful. In addition, since the thermal waters in DF 45-14 and DF 66-21 contain relatively high concentrations of boron (Bohm and others, 1980) it might prove to be a useful indicator element for the Dixie Valley system. Since boron is not selectively concentrated in sulfide phases, whole rock sampling may prove sufficient.

3) While an examination and interpretation of the trace element geochemistry of DF 45-14 and DF 66-21 has proven quite useful in understanding these portions of the reservoir and confirming prior data, testing of the technique should continue. Other methods, besides reservoir zoning and petrochemical analysis, should be developed for interpreting this type of data as it is applied to new wells drilled in Dixie Valley.

4.4 References

Bard, T.R., 1980, Petrologic alteration studies, in Mackay Minerals Research Institute, Geothermal reservoir assessment case study, northern Basin and Range Province, northern Dixie Valley, Nevada: Report for the U.S. Dept of Energy, Contract no. DE-AC08-79ET27006, ch. 4, p. 88-158.

Bamford, R.W., 1978, Geochemistry of solid material from two U.S. geothermal systems and its application to exploration: Univ. Utah Res. Inst., Earth Science Lab. Rept. 6, DOE contract no. EY-76-S-97-1601, 196 p.

Bamford, R.W., and Christensen, O.D., 1979, Multielement geochemical exploration data for the Cove Fort-Sulpherdale Known Geothermal Resource Area, Beaver and Millard Counties, Utah: Univ. Utah Res. Inst., Earth Sciences Lab. Rept. 19, DOE contract no. DE-AC07-78ET28392, 47 p.

Bamford, R.W., Christensen, O.D., and Capauno, R.M., 1980, Multielement geochemistry of solid material in geothermal systems and its applications, Part 1: The hot-water system at the Roosevelt Hot Springs KGTA, Utah: Univ. Utah Res. Inst., Earth Sciences Lab. Rept. 30, DOE contract no. DE-AC03-79ET27002, 168 p.

Barnes, H.L., ed., 1967, Geochemistry of hydrothermal ore deposits: Holt, Rinehard and Winston, New York.

Barnes, H.L., ed., 1979, Geochemistry of hydrothermal ore deposits: John Wiley and Sons, New York, 798 p.

Browne, P.R.L., and Ellis, A.J., 1970, The Ohaki-Broadlands hydrothermal area, New Zealand: Mineralogy and related geochemistry: Am. Jour. Sci., v. 269, p. 97-131.

Ewers, G.R., and Keays, R.R., 1977, Volatile and precious metal zoning in the Broadlands Geothermal Field, New Zealand: Econ. Geol., v. 72, p. 1337-1354.

Koch, G.S., Jr., and Link, R.F., 1970, Statistical analysis of geologic data: John Wiley and Sons, New York, v. I, 375 p.

Mackay Minerals Research Institute, 1980, Geothermal reservoir assessment case study, northern Basin and Range Province, northern Dixie Valley, Nevada: Rept. prepared for U.S. Dept. of Energy, contract no. DE-AC08-79ET27006, v. I, 223 p. plus appendices; v. II, map plates; also Univ. Utah Res. Inst. Rept NV/DV/SR-13.

Nie, N.H., Hull, C.H., Jenkins, J.G., Steinbrenner, K., and Best, D.H., 1975, Statistical package for the social sciences: McGraw-Hill, New York, 675 p.

Skinner, B.J., White, D.E., Rose, H.J., and Mays, R., 1967, Sulfides associated with the Salton Sea geothermal brine: Econ. Geol., v. 62, p. 316-330.

Wedepohl, K.H., ed., 1978, Handbook of geochemistry: Springer-Verlag, New York.

Weissberg, B.G., Browne, P.R.L., and Seward, T.M., 1979, Ore metals in active geothermal systems, in Barnes, H.L., ed., Geochemistry of hydrothermal ore depoits: John Wiley and Sons, New York, p. 739-780.

Chapter 5. DIXIE VALLEY GEOTHERMAL SYSTEM

By: Elaine J. Bell

5.0 DIXIE VALLEY GEOTHERMAL SYSTEM

5.1 Introduction

The purpose of the MMRI program of investigation was to develop a model for the geothermal system in Dixie Valley. An initial model based on existing data, was modified and refined to develop an integrated model incorporating data derived from four fields of study: structure-tectonics, petrology, hydrology and hydrogeochemistry, and shallow temperature survey (Mackay Minerals Research Institute, 1980). With the development of new data derived from soil geochemistry and petrochemistry, as presented in the preceeding chapters of this report, the integrated model of the Dixie Valley Geothermal System can be re-evaluated.

A brief summary of the integrated model, an evaluation of the model based on the soil geochemistry and petrochemistry and recommendations for investigations considered necessary for futher refinement and verification of the model are presented in the following sections.

5.2 Integrated Model of the Dixie Valley Geothermal System

The Dixie Valley Geothermal System appears to be the result of regionally high mantle heat flow through a thin crust, with preferential conduits for fluid migration structurally controlled by major basement faults and by Basin and Range extensional faults. Figure 5-1 depicts the spatial relationships among the major structural elements in Dixie Valley, with a generalized cross-section of the model shown in Figure 5-2. Production zones may be found in association with any of several lithologies, such as the Humboldt gabbroic complex or Triassic metasediments, if there is communication by fracture or fault zones with the reservoir at depth and sufficient fluid to transport the heat. A detailed discussion of the model is presented by Bell and others (1980a).

5.3 Evaluation of the Integrated Model

The data and conclusions derived from the soil geochemistry and petrochemistry are generally consistent with the integrated model of the Dixie Valley Geothermal System. Mercury and arsenic soil geochemical distributions confirm the location, trend and significance of known structures as conduits for migration of thermal fluids to the surface. In addition, geochemical trends also suggest the location and orientation of suspected or inferred structures within the study area that have

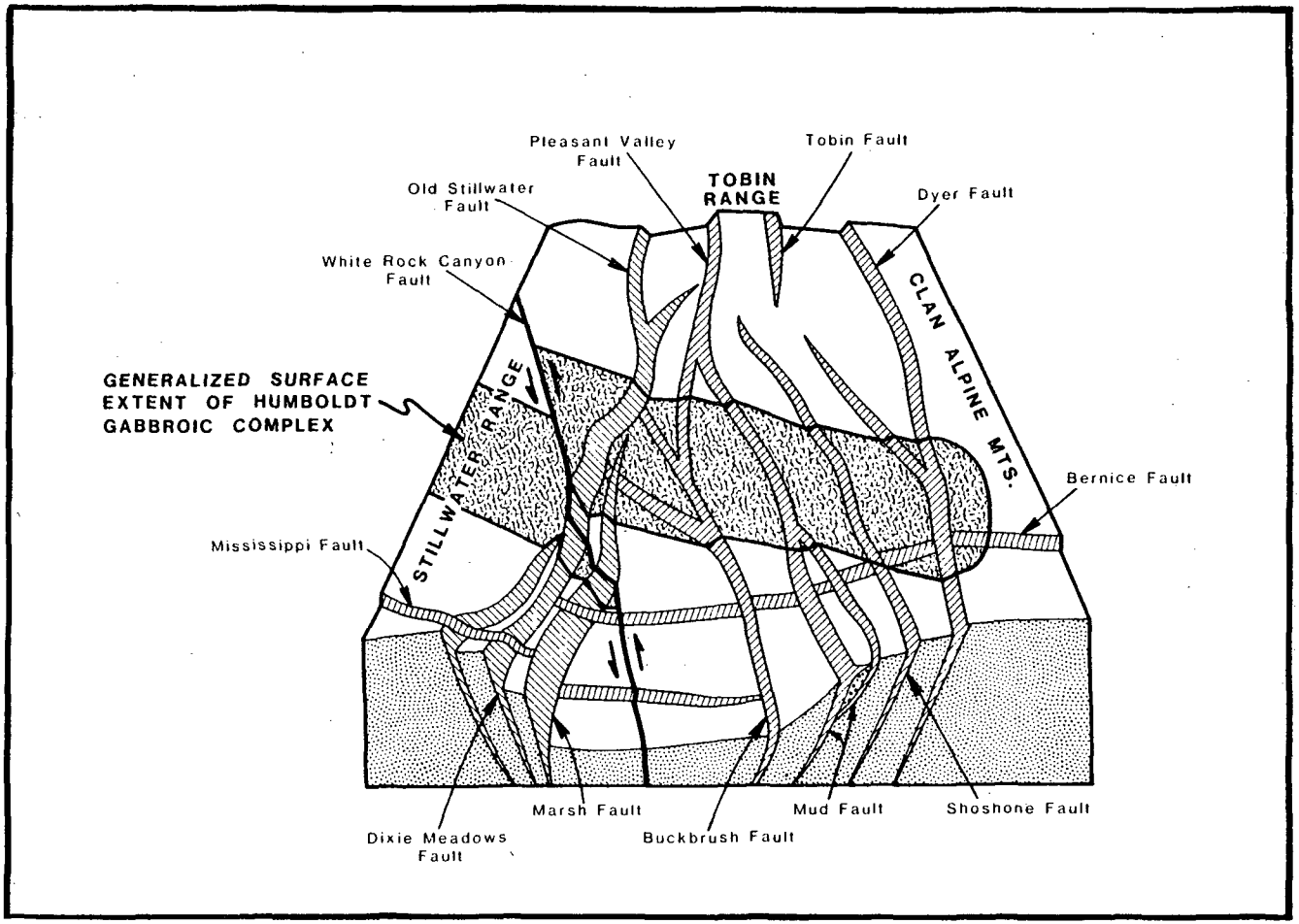

Figure 5-1. Three dimensional view of integrated model of the Dixie Valley Geothermal System.

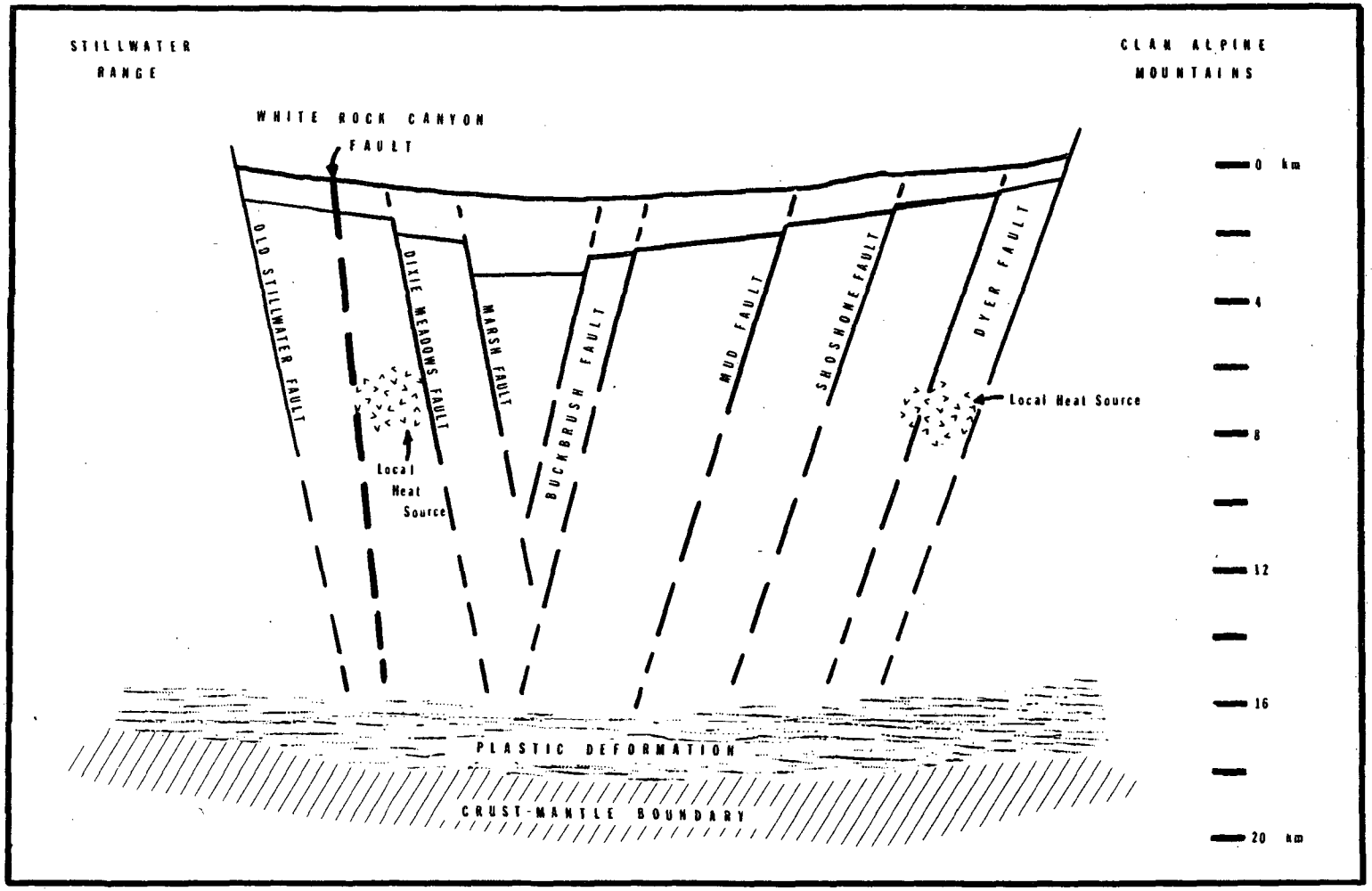

Figure 5-2. Generalized east-west cross-section of the integrated model of the Dixie Valley Geothermal System. Structural elements (faults) are propagated downward from the surface through the valley fill (alluvium with intercalated volcanics) and into the underlying undifferentiated bedrock and then projected through the zone of brittle failure.

significance with respect to proven production areas or natural surface manifestations of the geothermal system.

The general distribution of selected trace elements (reservoir zoning) and the specific zones distinguished by anomalous trace element concentrations (petrochemical analysis) confirm the significance of structural controls of fluid migration in the subsurface. Additionally, the petrochemistry suggests a possible interpretation of the dynamics of the reservoir. DF 45-14 is located in an area with a longer history of geothermal activity that has resulted in reduced interaction with and connection to the reservoir. DF 66-21, however, exhibits a younger, more dynamic history with significant fracture zones actively conducting thermal fluids migrating from the reservoir at depth.

5.4 Recommendations

Recommendations for further studies necessary to test and refine the model of the Dixie Valley Geothermal System have previously been made (Bell and others, 1980b). The importance of conducting these types of investigations is emphasized here, along with the recommendation that both soil geochemical and petrochemical studies be continued and expanded in Dixie Valley as new wells are drilled.

5.5 References

Bell, E.J., Slemmons, D.B., Whitney, R.A., Bard, T.R., Jacobson, R.L., Campana, M.E., Juncal, R.W., Larson, L.T., Bohm, B.W., and Ingraham, N.L., 1980a, Models of the Dixie Valley Geothermal System, in Mackay Minerals Research Institute, Geothermal reservoir assessment case study, northern Basin and Range Province, northern Dixie Valley, Nevada: Rept. prepared for U.S. Dept. of Energy, Contract no. DE-AC08-79ET27006, v. I, Ch. 7, p. 206-217

Bell, E.J., Campana, M.E., Jacobson, R.L., Larson, L.T., Slemmons, D.B., Bard, T.R., Bohm, B.W., Ingraham, N.L., Juncal, R.W., and Whitney, R.A., 1980b, Evaluation of the integrated model of the Dixie Valley Geothermal System, in Mackay Minerals Research Institute, Geothermal reservoir assessment case study, northern Basin and Range Province, northern Dixie Valley, Nevada: Rept. prepared for U.S. Dept. of Energy, Contract no. DE-AC08-79ET27006, v. I, ch. 8, p. 218-223.

Mackay Minerals Research Institute, 1980, Geothermal reservoir assessment case study, northern Basin and Range Province, northern Dixie Valley, Nevada: Rept. prepared for U.S. Dept of Energy, Contract no. DE-AC08-79ET27006, v. I, 223 p. plus appendices, v. II, map plates; also Univ. Utah Res. Inst. Rept. NV/DV/SR-13.

Appendix A. SOIL GEOCHEMICAL DATA

Sample #	Hg ppb	As ppm
1	104	25
2	56	45
3	96	15
4	40	30
5	32	35
6	28	65
7	72	10
8	64	15
9	96	10
10	60	15
11	68	25
12	48	60
13	8	40
14	16	45
15	88	15
16	56	15
17	116	20
18	392	50
19	76	20
20	16	40
21	24	15
22	8	45
23	56	25
24	60	20
25	176	20
26	976	55
27	488	40
28	108	25
29	168	30
30	80	35
31	8	25
32	16	30
33	60	40
34	28	15
35	152	30
36	232	35
37	272	25
38	2120	80
39	180	30
40	88	20
41	16	85
42	20	10
43	4	15
44	24	25
45	8	30
46	24	15
47	40	25
48	56	25
49	64	30
50	56	35
51	104	25

Sample #	Hg ppb	As ppm
52	36	25
53	76	15
54	16	30
55	68	15
56	76	25
57	44	15
58	8	15
59	28	20
60	16	15
61	8	15
62	8	20
63	16	15
64	28	5
65	28	10
66	28	10
67	44	15
68	44	15
69	52	15
70	64	20
71	108	10
72	36	10
73	32	25
74	36	20
75	16	15
76	24	25
77	24	20
78	4	10
79	144	25
80	72	15
81	80	10
82	156	20
83	96	10
84	12	20
85	116	15
86	128	25
87	60	10
88	108	10
89	188	15
90	120	20
91	68	15
92	80	10
93	88	15
94	80	15
95	116	15
96	88	15
97	52	10
98	376	30
99	120	15
100	24	10
101	96	15
102	40	10

Sample #	Hg ppb	As ppm
103	132	15
104	36	15
105	40	15
106	68	10
107	44	10
108	28	15
109	4	20
110	108	10
111	24	5
112	92	15
113	12	5
114	8	10
115	8	15
116	32	15
117	48	25
118	36	10
119	32	5
120	32	5
121	24	5
122	16	5
123	108	10
124	84	10
125	52	10
126	24	5
127	12	5
128	32	5
129	12	80
130	12	35
131	8	35
132	28	5
133	72	5
134	20	5
135	24	5
136	12	20
137	48	15
138	84	10
139	52	10
140	28	10
141	8	20
142	8	25
143	12	40
144	12	45
145	36	15
146	20	15
147	60	5
148	92	35
149	132	15
150	44	10
151	68	10
152	68	5
153	64	20

Sample #	Hg ppb	As ppm
154	24	20
155	24	25
156	16	10
157	12	50
158	32	25
159	104	15
160	272	10
161	84	15
162	136	25
163	56	10
164	32	5
165	120	25
166	140	45
167	64	25
168	20	25
169	28	25
170	12	15
171	8	15
172	28	10
173	164	15
174	232	25
175	104	20
176	92	15
177	148	20
178	60	10
179	152	1
180	100	20
181	68	35
182	8	10
183	16	15
184	16	10
185	8	10
186	12	15
187	24	20
188	24	15
189	12	20
190	28	15
191	56	10
192	56	10
193	156	10
194	68	15
195	84	5
196	32	5
197	16	10
198	36	5
199	36	10
200	96	10
201	64	5
202	40	5
203	36	10
204	48	15
205	28	15

Sample #	Hg ppb	As ppm
206	40	30
207	28	25
208	176	5
209	48	10
210	36	5
211	56	5
212	120	10
213	40	35
214	120	10
215	56	15
216	88	15
217	40	10
218	40	10
219	24	10
220	0	5
221	28	15
222	40	15
223	16	35
224	60	25
225	80	10
226	76	5
227	112	35
228	100	5
229	104	5
230	68	5
231	56	5
232	108	5
233	104	10
234	120	10
235	56	5
236	168	10
237	48	15
238	40	15
239	48	15
240	40	10
241	36	10
242	40	25
243	32	15
244	28	15
245	32	10
246	40	5
247	56	15
248	44	10
249	28	10
250	12	5
251	20	40
252	28	15
253	36	10
254	72	20
255	24	10
256	120	15
257	156	25

Sample #	Hg ppb	As ppm
258	132	15
259	164	10
260	100	10
261	120	15
262	160	15
263	116	15
264	160	10
265	124	10
266	108	15
267	140	10
268	160	15
269	176	10
270	160	15
271	144	20
272	68	15
273	52	40
274	40	15
275	72	15
276	48	15
277	40	15
278	72	35
279	48	20
280	48	15
281	56	30
282	56	15
283	36	15
284	64	15
285	40	40
286	40	115
287	156	35
288	4	15
289	56	30
290	48	30
291	32	10
292	76	25
293	72	35
294	24	5
295	32	10
296	32	15
297	44	15
298	88	20
299	96	20
300	56	10
301	108	25
302	56	25
303	12	10
304	32	15
305	32	10
306	0	10
307	48	10
308	160	15
309	68	15

Sample #	Hg ppb	As ppm
310	28	10
311	36	15
312	16	15
313	88	10
314	40	10
315	32	15
316	40	10
317	44	15
318	72	25
319	36	15
320	96	15
321	48	10
322	76	15
323	212	15
324	6280	10
325	1080	20
326	1400	25
327	12760	15
328	400	50
329	1720	35
330	1240	10
331	388	15
332	364	10
333	48	35
334	248	15
335	76	25
336	64	10
337	40	10
338	32	10
339	84	10
340	24	10
341	40	15
342	80	15
343	36	15
344	72	15
345	28	35
346	88	25
347	40	10
348	20	10
349	88	10
350	44	40
351	156	15
352	84	15
353	116	15
354	120	15
355	60	15
356	204	15
357	116	15
358	56	25
359	56	15
360	168	5

Sample #	Hg ppb	As ppm
361	560	5
362	84	15
363	44	5
364	220	15
365	40	15
366	56	10
367	92	10
368	96	10
369	40	10
370	40	5
371	48	5
372	72	15
373	104	10
374	80	15
375	288	10
376	68	10
377	96	15
378	56	15
379	64	5
380	284	10
381	256	10
382	188	20
383	480	15
384	64	85
385	60	15
386	296	15
387	40	15
388	64	15
389	64	5
390	32	10
391	56	10
392	28	10
393	48	10
394	40	15
395	52	15
396	48	10
397	72	15
398	48	10
399	68	10
400	28	10
401	16	10
402	112	15
403	64	10
404	32	10
405	56	10
406	256	225
407	76	5
408	240	40
409	16	15
410	32	15
411	60	5
412	48	10

Sample #	Hg ppb	As ppm
413	56	10
414	40	10
415	28	10
416	36	10
417	36	10
418	12	10
419	40	10
420	68	10
421	28	10
422	24	10
423	24	10
424	76	10
425	16	10
426	16	10
427	36	10
428	44	10
429	16	10
430	84	15
431	64	10
432	104	15
433	56	10
434	16	10
435	68	15
436	40	10
437	96	10
438	12	10
439	40	20
440	40	10
441	56	15
442	56	20
443	112	35
444	48	10
445	36	15
446	4	1
447	0	1
448	36	5
449	16	1
450	84	15
451	92	15
452	184	10
453	68	10
454	104	15
455	172	20
456	104	15
457	56	15
458	172	15
459	72	10
460	52	25
461	232	25
462	284	35
463	172	30
464	216	25

Appendix B. PETROCHEMICAL DATA

Table 4-12

Lithologic Symbols

Symbol	Lithologic Symbol
A	Alluvium
A/c	Alluvium with clay
T	Tuff
A/B	Andesite/Basalt
G	Granodiorite Intrusive
QA	Quartz Arenite
M/M	Metasiltstone/Metashale
G/D	Gabbro/Diorite Intrusive
MZ	Mineralized Zone
FZ	Fault Zone

Table 4-13

Lead Distribution in DF 45-14 Heavy Mineral Fractions

Lead (ppm)	Absolute Frequency	Plotting Percentage	Lithology*
25	2	4.2	A
50	4	14.4	A; T; G/D
75	8	34.7	T; A/B; A; M/M
100	2	39.8	T; A/B
125	2	44.9	M/M; A; G/D
150	4	55.1	M/M
175	1	57.6	M/M
200	2	62.7	M/M; FZ
250	1	65.2	M/M
325	2	70.3	M/M; QA; G/D; FZ
425	2	75.4	M/M; A; G/D; FZ
475	2	80.5	M/M; T; A/B; FZ
680	1	83.0	M/M; G/D
2200	3	90.7	M/M; QA; G/D; T; FZ
2500	1	93.2	QA; M/M; FZ
3000	1	95.8	QA; M/M; FZ
3700	1	98.3	M/M; G/D; FZ

Mean 555.2 Std Err 149.9 Std Dev 936.0 Median 146.9
Kurtosis 3.6 Skewness 2.2

*Refer to Table 4-12 for explanation of symbols.

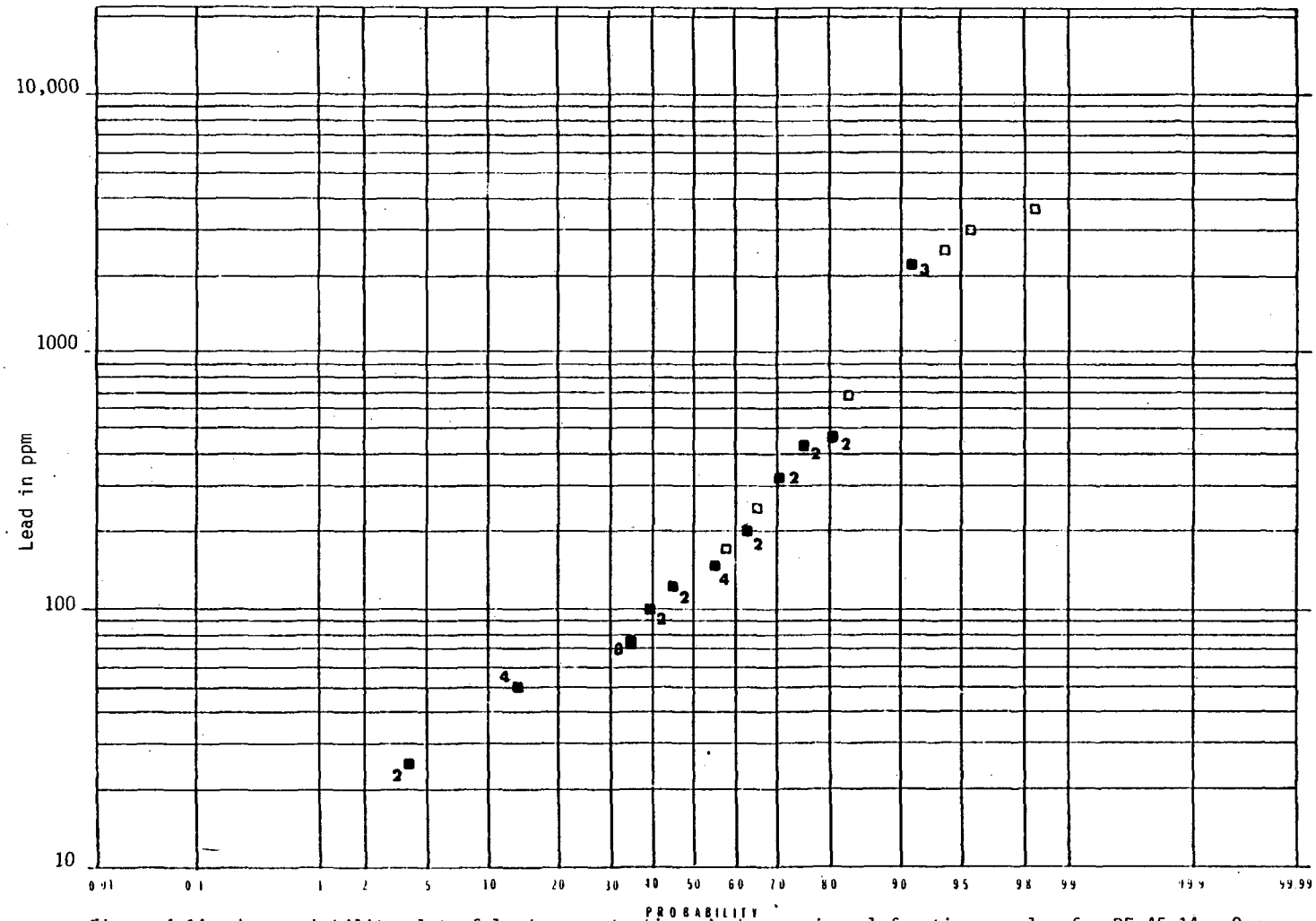

Figure 4-14. Log probability plot of lead concentrations in heavy mineral fraction samples for DF 45-14. Open squares indicate single sample value; solid squares indicate multiple sample values.

Table 4-14

Zinc Distribution in DF 45-14 Heavy Mineral Fractions

Zinc (ppm)	Absolute Frequency	Plotting Percentage	Lithology*
25	3	6.8	A; T
50	2	11.9	A; T; M/M
75	6	27.1	T; A/B; A; M/M
100	3	34.7	M/M; T; A/B
125	2	39.8	A; G/D; M/M
150	2	44.9	T; A/B; G/D
175	4	55.1	M/M; QA; G/D
200	2	60.2	M/M; G/D; FZ
300	2	65.2	M/M; QA; G/D; FZ
325	1	67.8	M/M; G/D
375	2	72.9	A
400	1	75.4	A
600	1	77.9	M/M; FZ
650	1	80.5	M/M; T
800	2	85.6	M/M; FZ
875	1	88.1	QA; M/M; FZ
1200	2	93.2	M/M; FZ
2000	1	95.8	T; A/B
4100	1	98.3	M/M; FZ

Mean 432.7 Std Err 117.0 Std Dev 730.8 Median 171.9

Kurtosis 17.1 Skewness 3.8

*Refer to Table 4-12 for explanation of symbols.

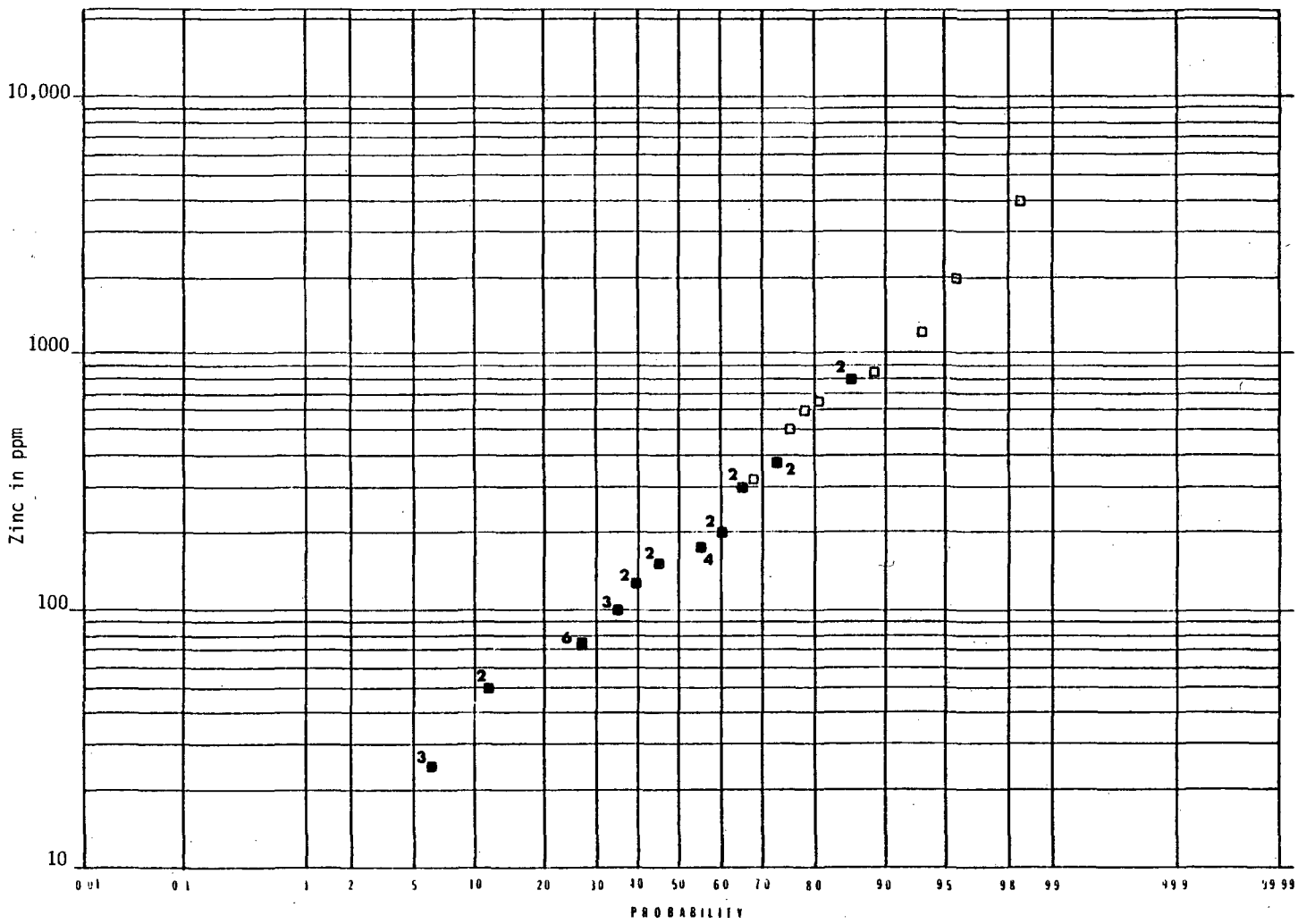

Figure 4-15. Log probability plot of zinc concentrations in heavy mineral fraction samples for DF 45-14. Open squares indicate single sample value; solid squares indicate multiple sample values.

Table 4-15

Arsenic Distribution in DF 45-14 Heavy Mineral Fractions

Arsenic (ppm)	Absolute Frequency	Plotting Percentage	Lithology*
125	1	1.7	G/D
175	1	4.2	M/M
200	3	11.9	M/M; A; FZ
220	2	16.9	A
225	1	19.5	M/M; G/D
250	1	22.0	M/M; QA; G/D
275	1	24.6	QA; T; FZ
400	2	29.7	M/M; G/D; FZ
420	1	32.2	M/M
450	1	34.7	QA; M/M
480	1	37.3	QA; M/M; FZ
500	1	39.8	T; A/B
520	1	42.2	M/M; FZ
550	1	44.9	A
580	1	47.4	T; A/B
600	1	50.0	M/M; QA; G/D
620	1	52.5	A
650	2	57.6	M/M
750	1	60.2	M/M
780	3	67.8	A; M/M; T
800	1	70.3	M/M; G/D
880	1	72.9	T; A/B
900	1	75.4	M/M; T
920	1	77.9	A
1000	2	83.0	T; A
1300	1	85.6	M/M; G/D; FZ
1500	1	88.1	M/M; G/D
1600	1	90.7	T; A/B
3800	1	93.2	T; A/B
6000	1	95.8	T; A
6500	1	98.3	T; A/B; A

Mean 979.5 Std Err 222.5 Std Dev 1389.5 Median 600.0

Kurtosis 10.2 Skewness 3.2

*Refer to Table 4-12 for explanation of symbols.

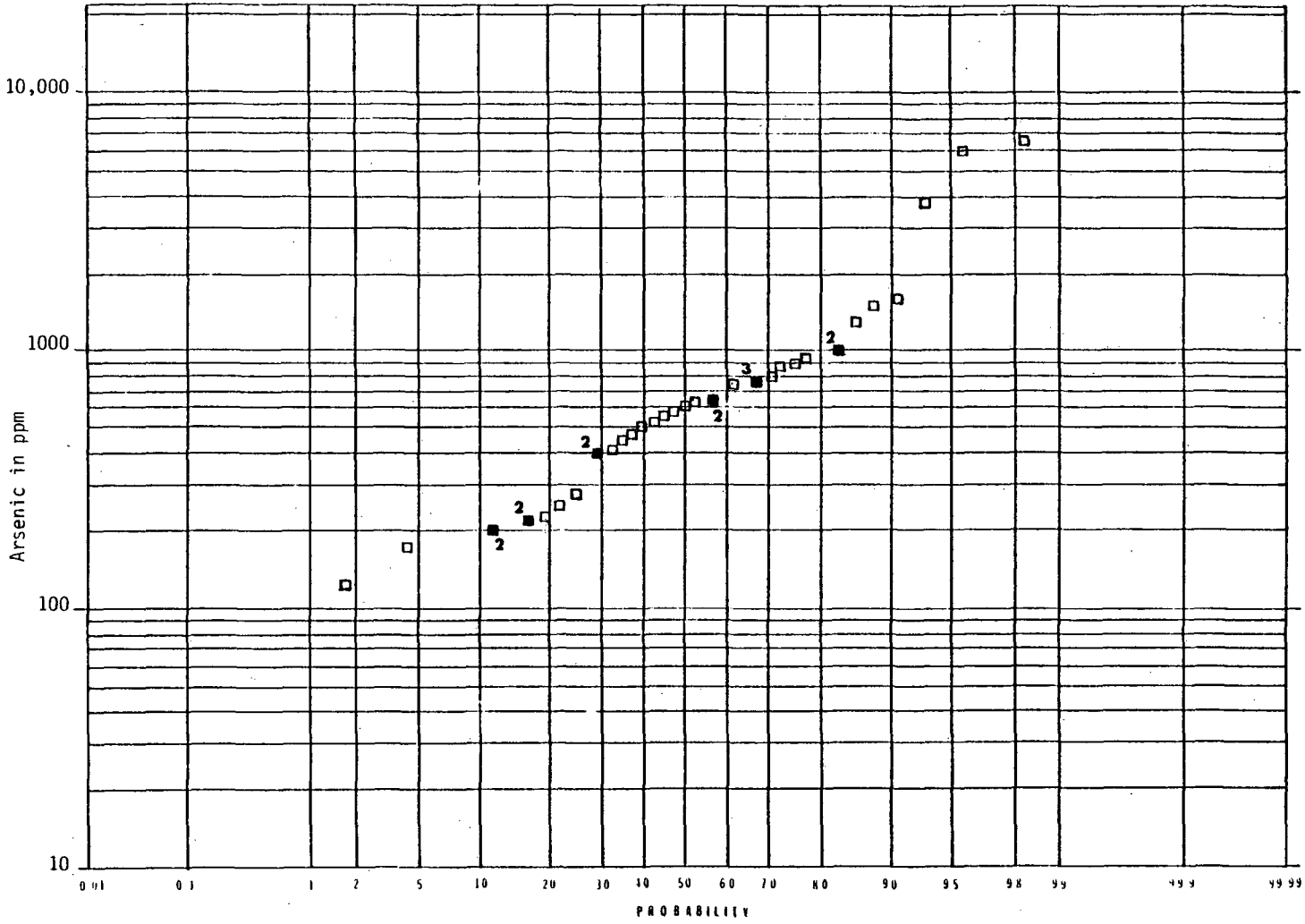

Figure 4-16. Log probabiltiy plot of arsenic concentrations in heavy mineral fraction samples for DF 45-14. Open squares indicate single sample value; solid squares indicate multiple sample values.

Table 4-16

Antimony Distribution in DF 45-14 Heavy Mineral Fractions

Antimony (ppm)	Absolute Frequency	Plotting Percentage	Lithology*
2	7	17.4	M/M; QA; G/D; FZ
4	1	20.0	M/M; QA
6	1	22.6	M/M; QA; T
8	1	25.2	M/M
12	2	30.4	M/M; FZ
14	3	38.3	M/M; G/D; A
16	2	43,5	M/M; A; FZ
20	3	51.3	M/M; G/D; FZ
22	2	56.5	M/M; A; G/D
24	1	59.1	T; A/B
32	1	61.7	M/M; T
36	1	64.3	M/M; G/D
46	1	66.9	T; A/B
74	1	69.5	T; A/B
104	1	72.2	A
106	1	74.8	T; A/B
192	1	77.4	A
214	1	80.0	T; A/B; A
338	2	85.2	A; T; A/B
384	1	87.8	A; T
420	1	90.4	QA; M/M; FZ
500	1	93.0	A; T
514	1	95.7	A
836	1	98.3	T

Mean 115.6 Std Err 31.3 Std Dev 192.9 Median 20.3
Kurtosis 4.5 Skewness 2.1

*Refer to Table 4-12 for explantion of symbols.

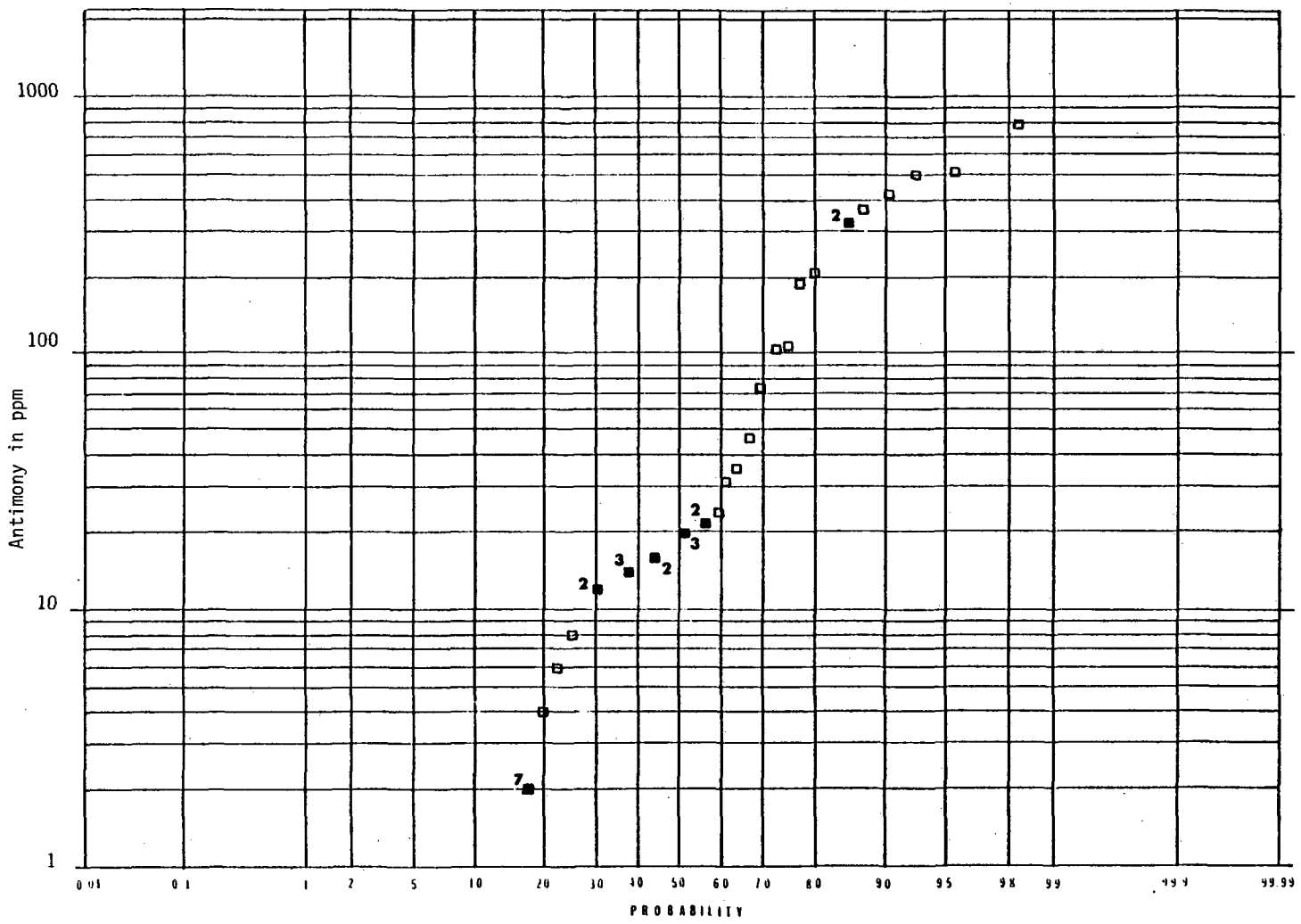

Figure 4-17. Log probability plot of antimony concentrations in heavy mineral fraction samples for DF 45-14. Open squares indicate single sample value; solid squares indicate multiple sample values.

Table 4-17

Mercury Distribution in DF 45-14 Heavy Mineral Fractions

Mercury (ppm)	Absolute Frequency	Plotting Percentage	Lithology*
0.01	7	17.9	A; M/M
0.1	1	20.5	A
0.125	1	23.2	A
0.185	3	31.3	G/c; M/M; FZ
0.200	1	33.9	M/M
0.235	1	36.6	M/M
0.270	3	44.6	M/M; A; T
0.360	1	47.3	M/M; G/D
0.375	1	50.0	T; A/B
0.380	1	52.7	M/M; G/D; FZ
0.395	1	55.4	M/M; FZ
0.505	1	58.0	M/M; QA; G/D
0.570	1	60.7	T; A/B
0.585	1	63.4	M/M; G/D; T; FZ
0.965	1	66.1	M/M; QA; T
1.1	1	68.8	T; A/B
1.4	1	71.4	QA; M/M; FZ
1.6	2	76.8	M/M; G/D
1.7	1	79.5	A
1.8	1	82.1	QA; T; FZ
2.1	1	84.8	A; T
4.8	1	87.5	A
7.4	1	90.2	A
9.1	1	92.9	T; A/B; A
13.8	1	95.5	T
16.7	1	98.2	A; T

Mean 1.9 Std Err 0.6 Std Dev 3.8 Median 0.4

Kurtosis 8.1 Skewness 2.9

*Refer to Table 4-12 for explantion of symbols.

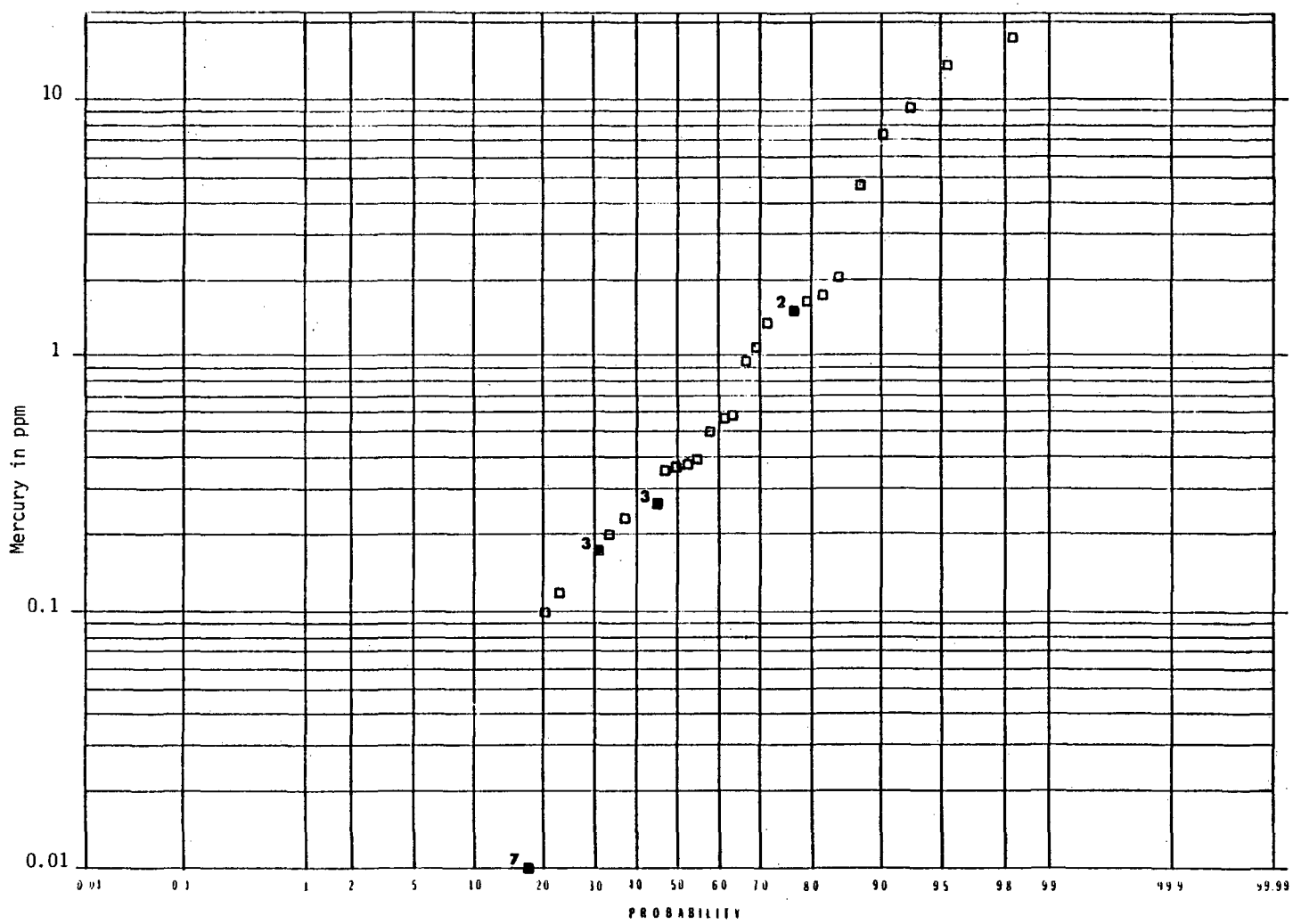

Figure 4-18. Log probability plot of mercury concentrations in heavy mineral fraction samples for DF 45-14. Open squares indicate single sample value; solid squares indicate multiple sample values.

Table 4-18

Lead Distribution in DF 45-14 Whole Rock Samples

Lead (ppm)	Absolute Frequency	Plotting Percentage	Lithology*
5	1	1.8	T
10	6	17.9	T; A/B; A; M/M
15	11	47.3	M/M; A; T; A/B
20	4	58.0	M/M; A; G/D; FZ
25	6	74.1	M/M; QA; G/D; T; A/B
30	4	84.8	M/M; QA; G/D; FZ
35	2	90.2	M/M; A; G/D
40	1	92.9	M/M; G/D; FZ
45	1	95.5	M/M; QA/ T
115	1	98.3	QA

Mean 22.9 Std Eff 2.9 Std Dev 18.1 Median 18.1

Kurtosis 18.8 Skewness 3.8

*Refer to Table 4-12 for explanation of symbols.

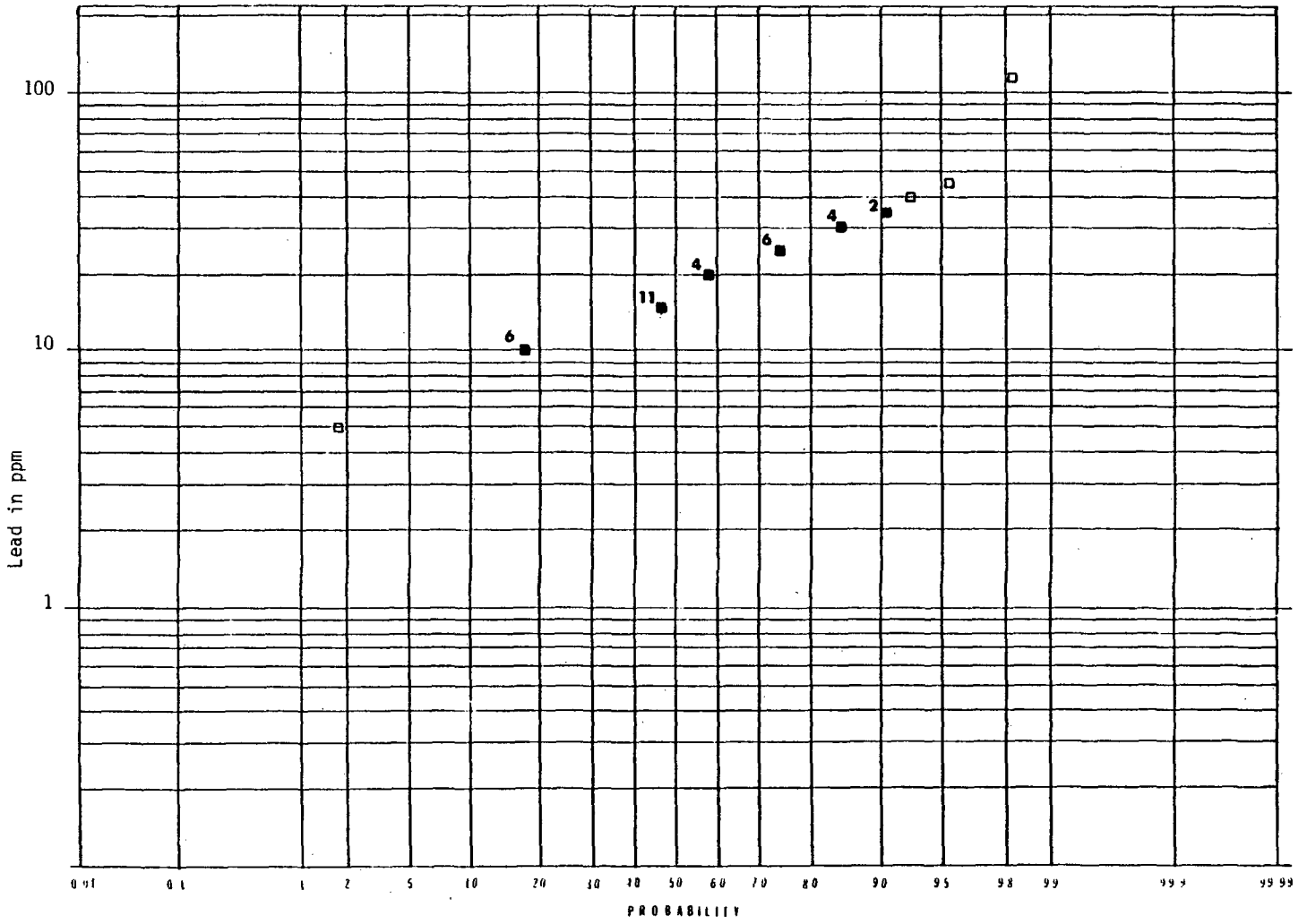

Figure 4-19. Log probability plot of lead concentrations in whole rock samples for DF 45-14. Open squares indicate single sample value; solid squares indicate nultiple sample values.

Table 4-19

Zinc Distribution in DF 45-14 Whole Rock Samples

Zinc (ppm)	Absolute Frequency	Plotting Percentage	Lithology*
20	3	7.1	M/M; T; A/B; A
25	7	25.9	M/M; T; A/B; A
30	1	28.6	T; A/B
35	1	31.2	M/M
40	2	36.6	A; T
45	2	42.0	T; A
50	2	47.3	A; G/D
55	3	55.4	M/M; G/D
60	4	66.1	M/M; QA; G/D; FZ
65	1	68.8	A
70	4	79.5	M/M; QA; G/D; FZ
75	1	82.1	M/M; G/D; FZ
85	2	87.5	QA; M/M; T
90	1	90.2	QA; M/M
100	1	92.9	M/M; FZ
120	1	95.5	M/M; FZ
135	1	98.2	T; A/B; A

Mean 54.3 Std Err 4.6 Std Dev 28.3 Median 53.3
Kurtosis 0.8 Skewness 0.9

*Refer to Table 4-12 for explanation of symbols.

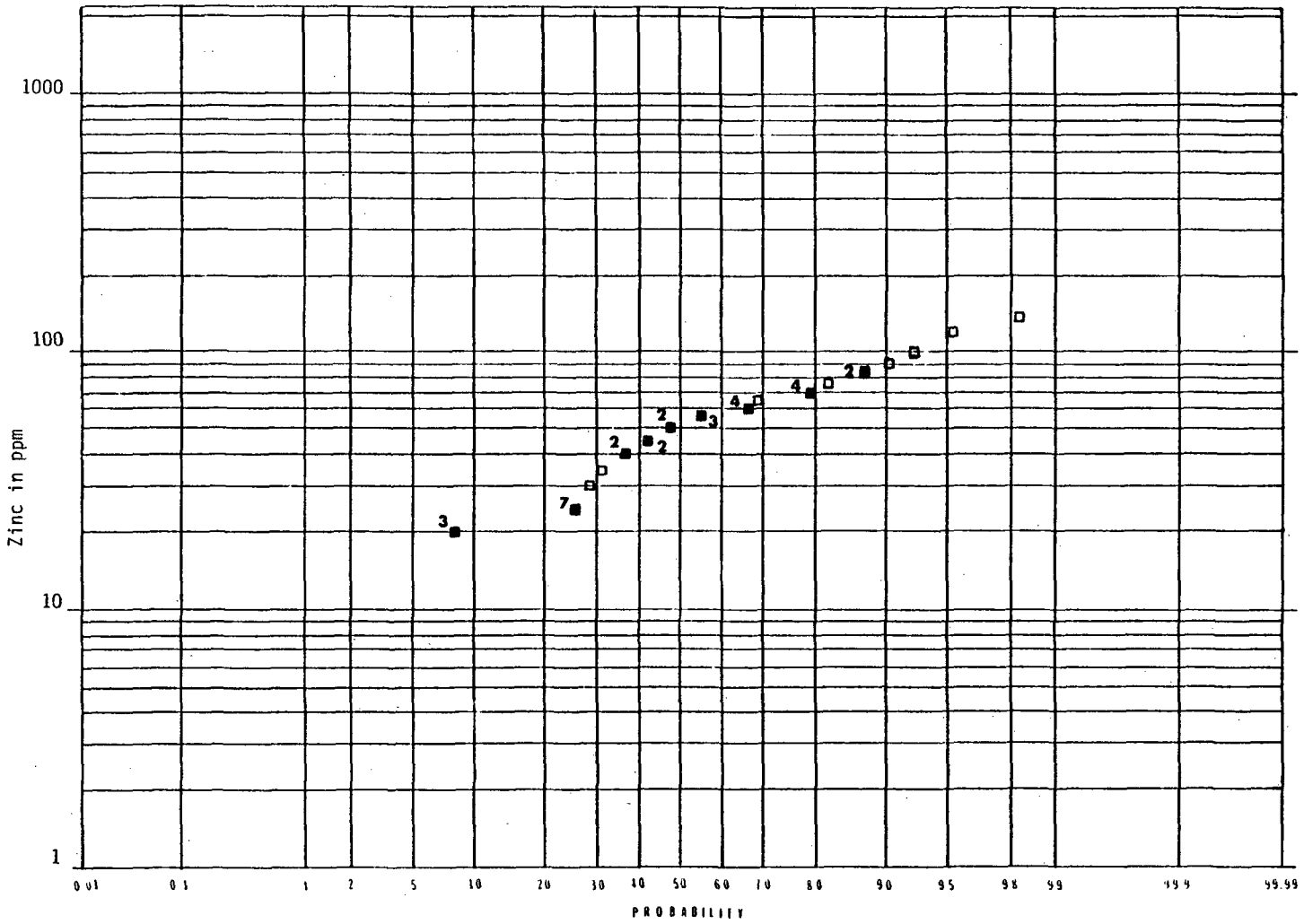

Figure 4-20. Log probability plot of zinc concentrations in whole rock samples for DF 45-14. Open squares indicate single sample value; solid squares indicate multiple sample values.

Table 4-20

Arsenic Distribution in DF 45-14 Whole Rock Samples

Arsenic (ppm)	Absolute Frequency	Plotting Percentage	Lithology*
5	10	25.9	M/M;QA;T;A/B;G/D;FZ
10	7	44.6	M/M; QA; T; G/D; FZ
15	2	50.0	M/M; T; G/D; FZ
20	2	55.4	M/M; A; G/D
25	3	63.4	M/M; T; A/B
30	1	66.1	M/M
40	1	68.8	M/M; G/D
50	1	71.4	A
60	1	74.1	A
65	1	76.8	T; A/B
70	2	82.1	T; G/D; A
80	1	84.8	A
85	1	87.5	A
145	1	90.2	T
230	1	92.9	T; A/B
350	1	95.5	T; A
760	1	98.2	T; A/B; A

Mean 62.2 Std Err 22.5 Std Dev 136.6 Median 16.3
Kurtosis 19.9 Skewness 4.2

*Refer to Table 4-12 for explanation of symbols.

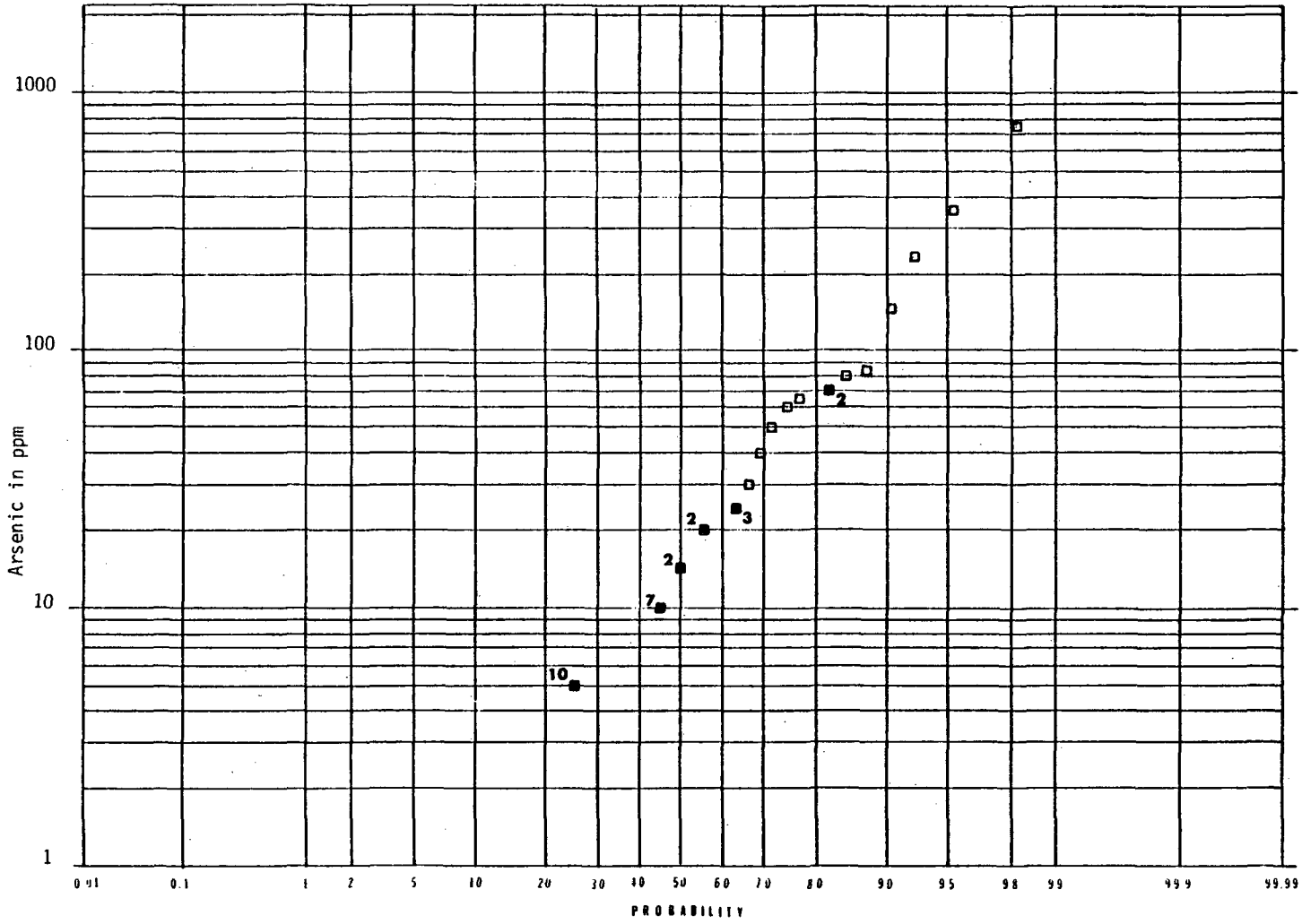

Figure 4-21. Log probability plot of arsenic concentrations in whole rock samples for DF 45-14. Open squares indicate single sample value; solid squares indicate multiple sample values.

Table 4-21

Antimony Distribution in DF 45-14 Whole Rock Samples

Antimony (ppm)	Absolute Frequency	Plotting Percentage	Lithology*
1.0	25	66.1	M/M;Q/A;T;A/B;G/D;FZ
2.0	1	68.8	A
3.0	1	71.4	T; A/B
6.0	1	74.1	T; A/B
10.0	1	76.8	A
12.0	1	79.5	A
16.0	1	82.1	T; A/B
21.0	1	84.8	A; T
22.0	1	87.5	T; A/B; A
24.0	1	90.2	A
29.0	1	92.9	A
36.0	1	95.5	A; T
46.0	1	98.2	T

Mean 6.8 Std Err 1.9 Std Dev 11.3 Median 1.2

Kurtosis 3.8 Skewness 2.1

*Refer to Table 4-12 for explanation of symbols.

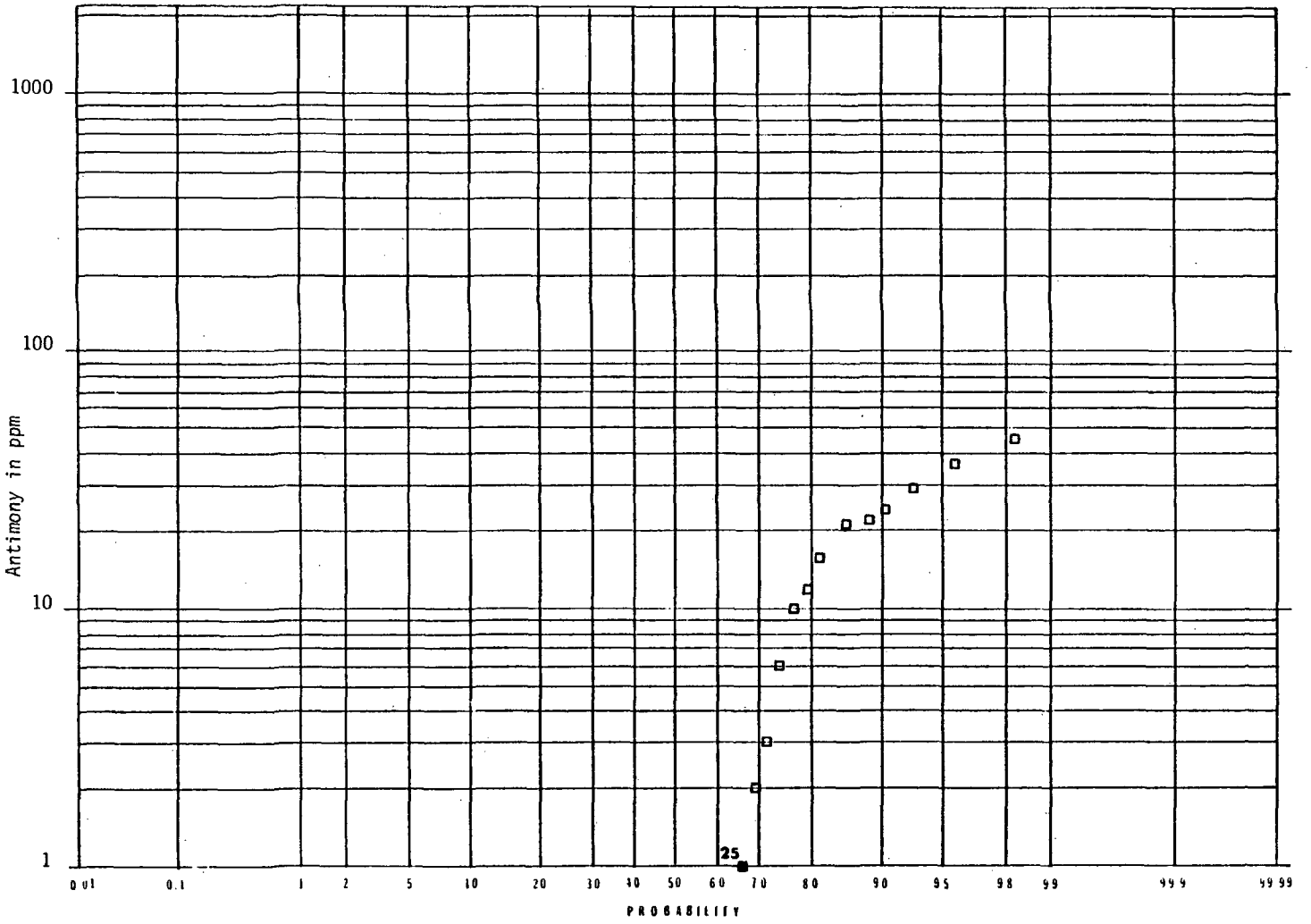

Figure 4-22. Log probability plot of antimony concentrations in whole rock samples for DF 45-14. Open squares indicate single sample value; solid squares indicate multiple sample values.

Table 4-22

Mercury Distribution in DF 45-14 Whole Rock Samples

Mercury (ppm)	Absolute Frequency	Plotting Percentage	Lithology*
0.075	1	1.8	M/M; FZ
0.180	2	7.1	M/M
0.185	1	9.8	QA; M/M; G/D
0.190	2	15.1	M/M; QA
0.195	1	17.9	M/M; G/D; FZ
0.220	3	25.9	T; A/B; M/M
0.225	3	33.9	M/M; T; A/B; G/D
0.240	3	42.0	T; A/B; M/M; G/D
0.245	3	50.0	M/M; G/D
0.250	1	52.7	M/M
0.260	1	55.4	M/M; QA; FZ
0.270	1	58.0	M/M
0.300	1	60.7	A
0.310	1	63.4	M/M; F/D; R; FZ
0.320	1	66.1	M/M; QA; G/D; T
0.345	1	68.8	QA; M/M
0.350	1	71.4	QA; T
0.360	1	74.1	M/M; T; FZ
0.460	1	76.8	A
0.940	1	79.5	T; A/B; A
1.4	1	82.1	A
2.3	1	84.8	T; A
2.9	1	87.5	A; T
3.1	1	90.2	A
3.3	1	92.9	A; T
6.0	1	95.5	A
7.4	1	98.2	T

Mean 0.9 Std Err 0.3 Std Dev 1.6 Median 0.3

Kurtosis 7.9 Skewness 2.8

*Refer to Table 4-12 for explanation of symbols.

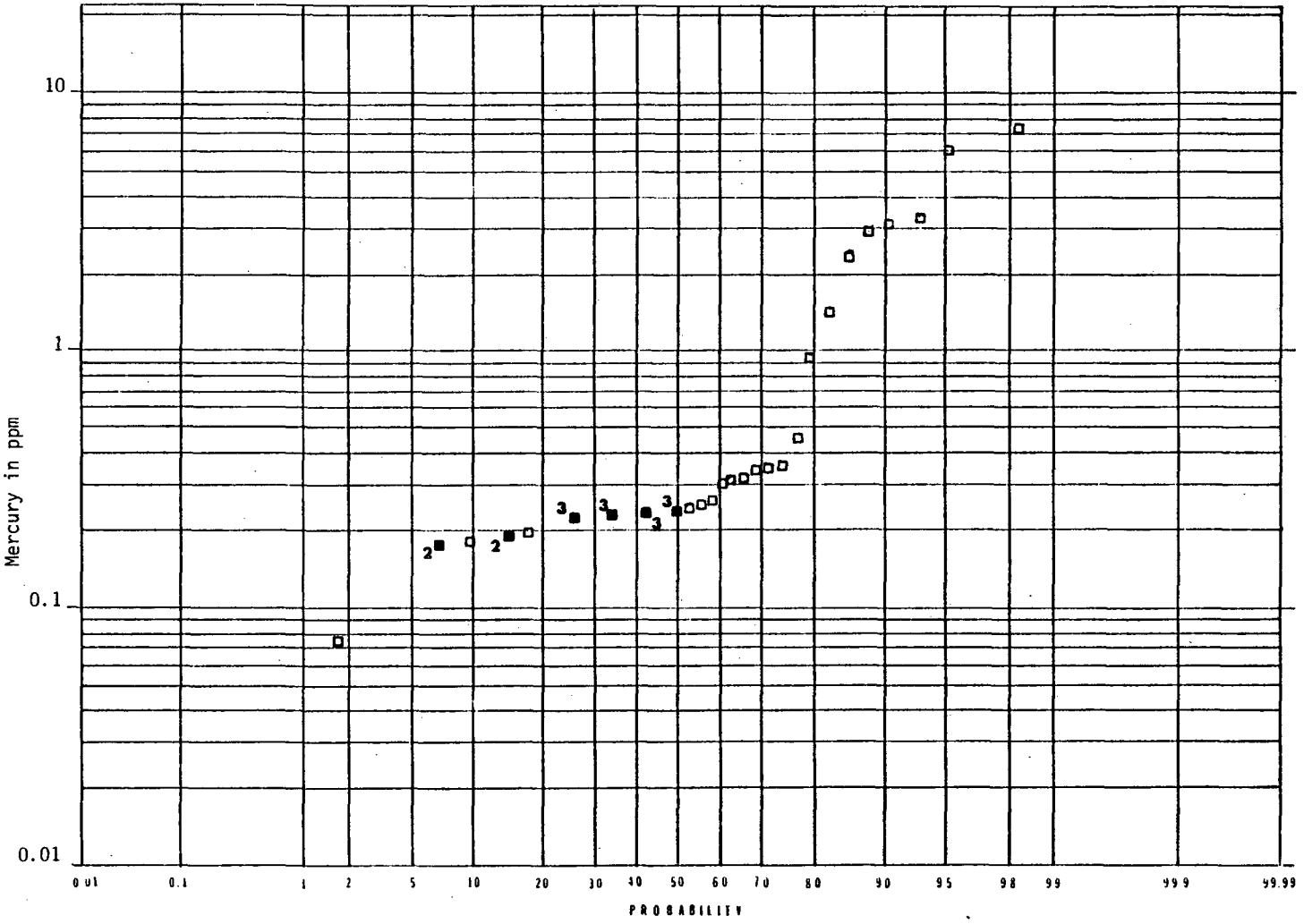

Figure 4-23. Log probability plot of mercury concentrations in whole rock samples for DF 45-14. Open squares indicate single sample value; solid squares indicate multiple sample values.

Table 4-23

Lead Distribution in DF 66-21 Heavy Mineral Fractions

Lead (ppm)	Absolute Frequency	Plotting Percentage	Lithology*
25	22	58.0	A; A/c; T; A/B; G
50	4	68.7	A/c
75	2	74.1	A/c; G; QA; FZ
250	1	76.8	G
650	1	79.5	M/M
1000	1	82.1	M/M; G
1100	1	84.8	M/M; G/D; FZ; MZ
1200	2	90.2	M/M; G
6000	1	92.8	M/M
9500	1	95.5	A; A/c
13500	1	98.3	QA; MZ; FZ

Mean 954.1 Std Err 458.8 Std Dev 2791.0 Median 33.5

Kurtosis 13.4 Skewness 3.7

*Refer to Table 4-12 for explanation of symbols.

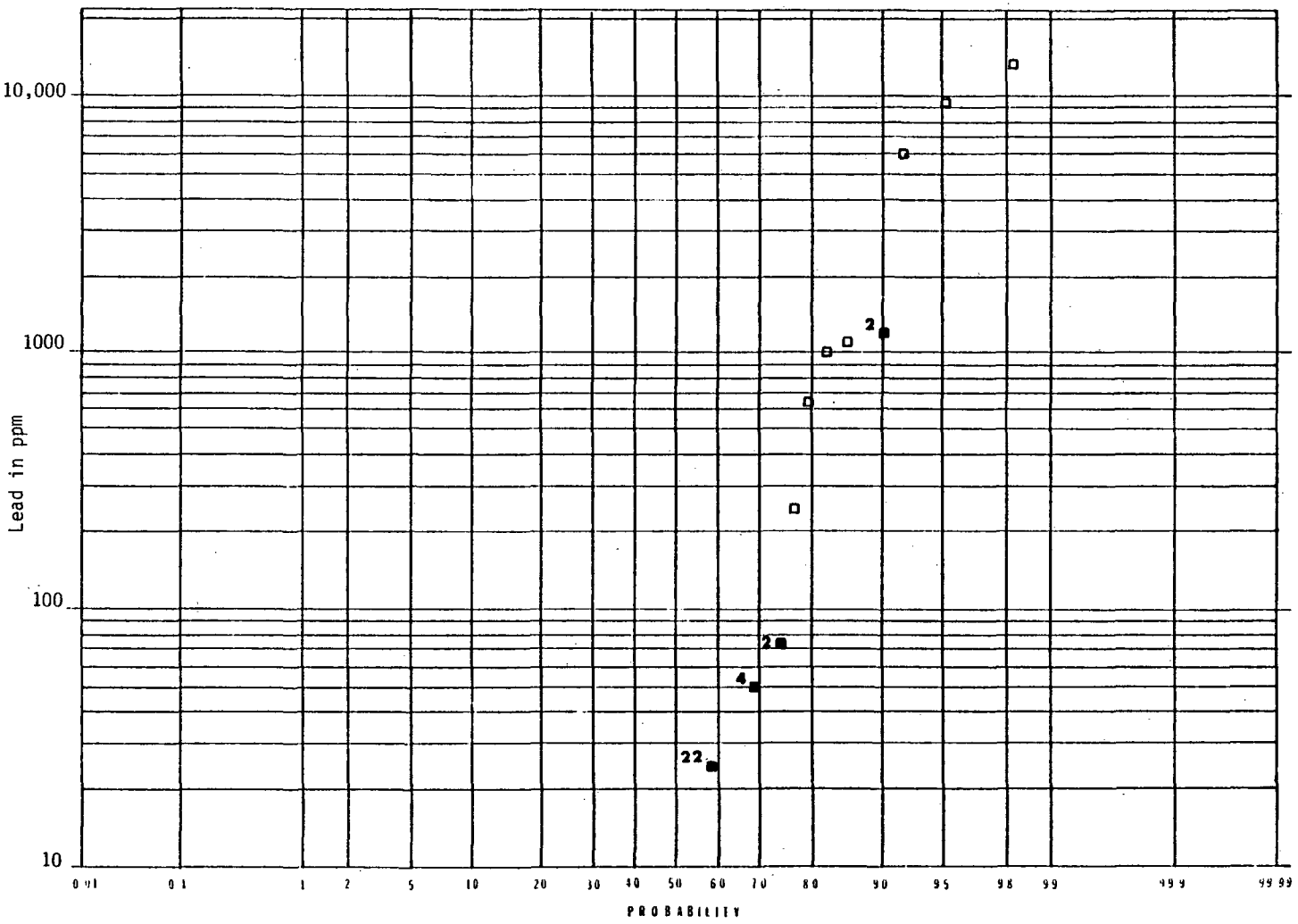

Figure 4-24. Log probability plot of lead concentrations in heavy mineral fraction samples for DF 66-21. Open squares indicate single sample value; solid squares indicate multiple sample values.

Table 4-24

Zinc Distribution in DF 66-21 Heavy Mineral Fractions

Zinc (ppm)	Absolute Frequency	Plotting Percentage	Lithology*
25	7	17.8	G; A; A/B; T; MZ; FZ
50	11	47.3	A/c; A/B; T; FZ; G
75	1	50.0	A/B; T; FZ
100	5	63.4	G; A; QA; A/B
125	4	74.1	A; G; M/M
150	1	76.8	M/M; G; G/D; MZ; FZ
175	2	82.1	M/M; A; G
250	2	87.5	A; A/c
520	1	90.2	G; QA; FZ
950	1	92.8	M/M; G
1300	1	95.5	M/M; G; G/D
11500	1	98.3	A/B; T; FZ

Mean 461.4 Std Err 310.0 Std Dev 1882.6 Median 75.0
Kurtosis 35.5 Skewness 5.9

*Refer to Table 4-12 for explanation of symbols.

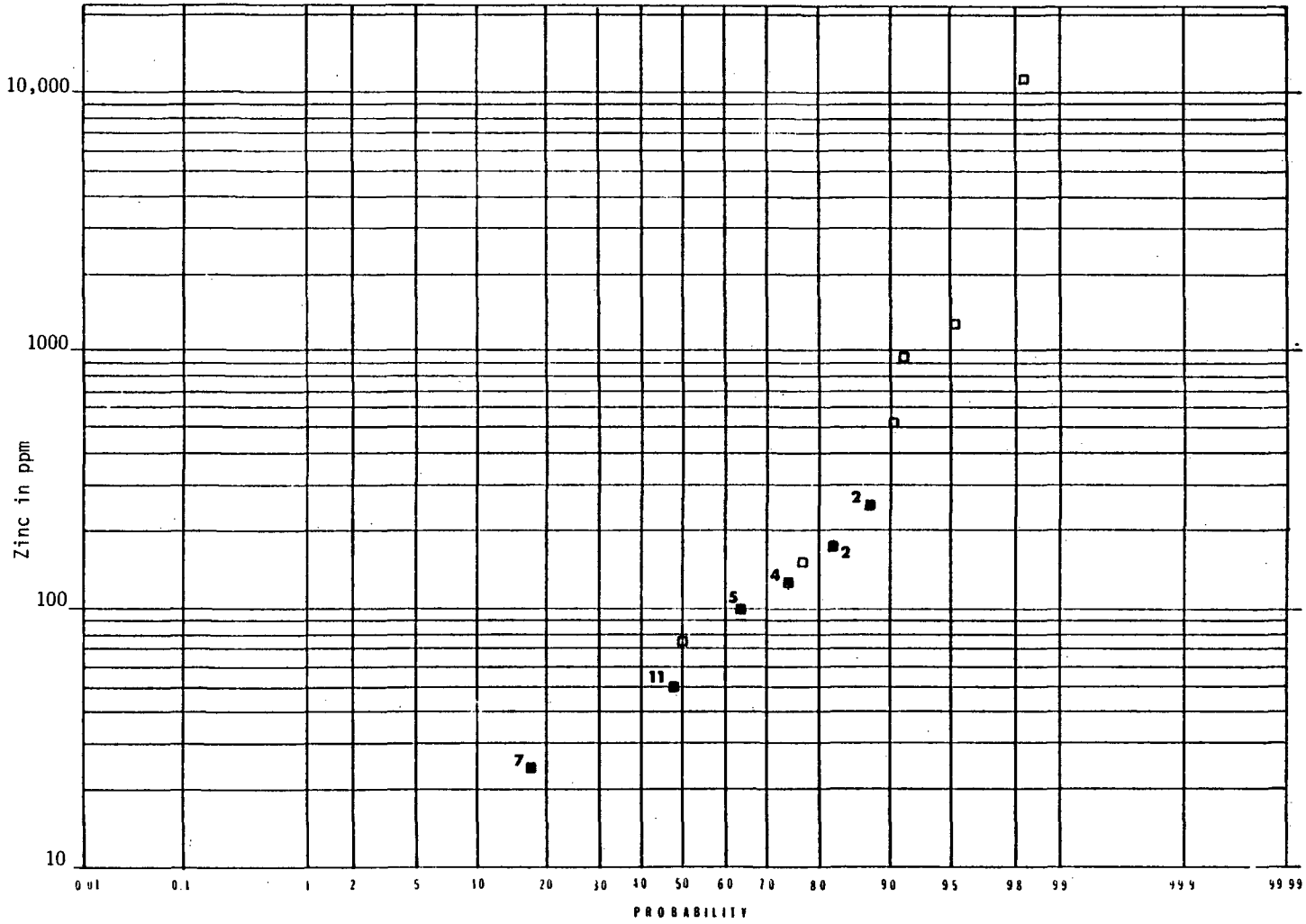

Figure 4-25. Log probability plot of zinc concentrations in heavy mineral fraction samples for DF 66-21. Open squares indicate single sample value; solid squares indicate multiple sample values.

Table 4-25

Arsenic Distribution in DF 66-21 Heavy Mineral Fractions

Arsenic (ppm)	Absolute Frequency	Plotting Percentage	Lithology*
5	1	1.7	G
25	5	15.2	A; A/B; T; G; FZ
50	9	39.3	A; A/c; A/B; T; FZ; G
75	4	50.0	A; A/c; G
100	3	58.0	A/c; M/M; G
125	2	63.4	A/c; QA; MZ; FZ
175	2	68.8	G; QA; A; A/c
200	2	74.1	G; QA; A/B; T; FZ
225	1	76.8	A/B; T; FZ
250	2	82.1	A/c; A/B; T
320	1	84.8	M/M; G
420	1	87.5	M/M; G; G/D; MZ; FZ
480	1	90.2	M/M
520	1	92.9	M/M; G
780	1	95.5	G
1200	1	98.3	QA; G; MZ; FZ

Mean 179.1 Std Err 39.4 Std Dev 239.7 Median 82.5
Kurtosis 9.2 Skewness 2.8

*Refer to Table 4-12 for explanation of symbols.

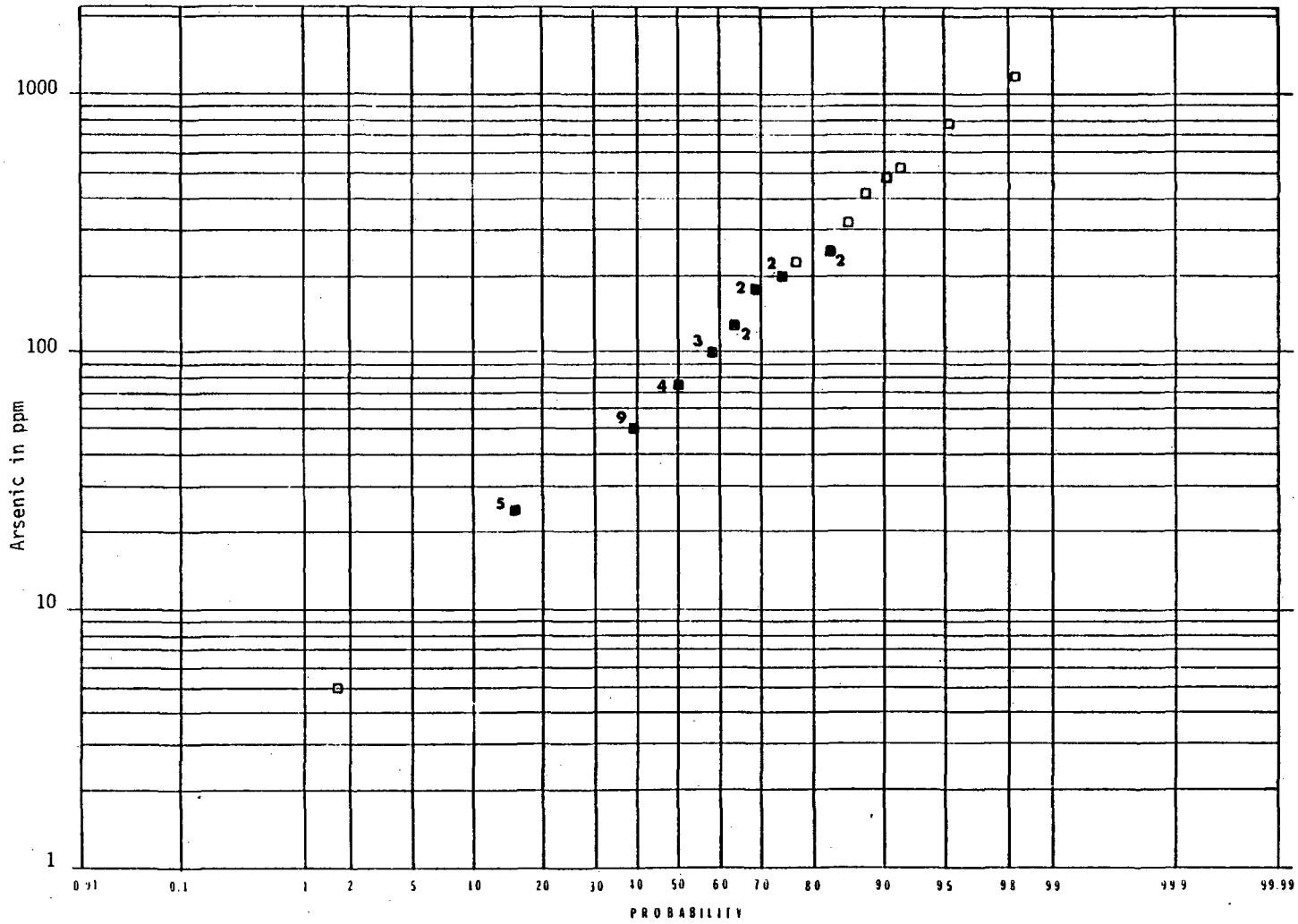

Figure 4-26. Log probability plot of arsenic concentrations in heavy mineral fraction samples for DF 66-21. Open squares indicate single sample value; solid squares indicate multiple sample values.

Table 4-26

Antimony Distribution in DF 66-21 Heavy Mineral Fraction

Antimony (ppm)	Absolute Frequency	Plotting Percentage	Lithology*
2	10	26.6	G;A;A/c;A/B;T;M/M;MZ;FZ
4	2	32.1	A; A/c; A/B; T
6	4	43.1	A; A/c; QA; MZ; FZ
8	4	54.1	A; A/c; A/B; T; M/M
10	1	56.9	G
14	3	65.1	A; A/c
16	2	70.6	A/c
18	1	73.4	M/M; G
20	1	76.1	G; QA
24	2	81.7	A/c
48	2	87.2	M/M; A/B; T; FZ
68	1	89.9	M/M; G
88	1	92.7	A/B; T; FZ
156	1	95.4	A/B; T; FZ
1600	1	98.3	G; QA; FZ

Mean 62.8 Std Err 44.2 Std Dev 265.3 Median 8.0

Kurtosis 35.0 Skewness 5.9

*Refer to Table 4-12 for explanation of symbols.

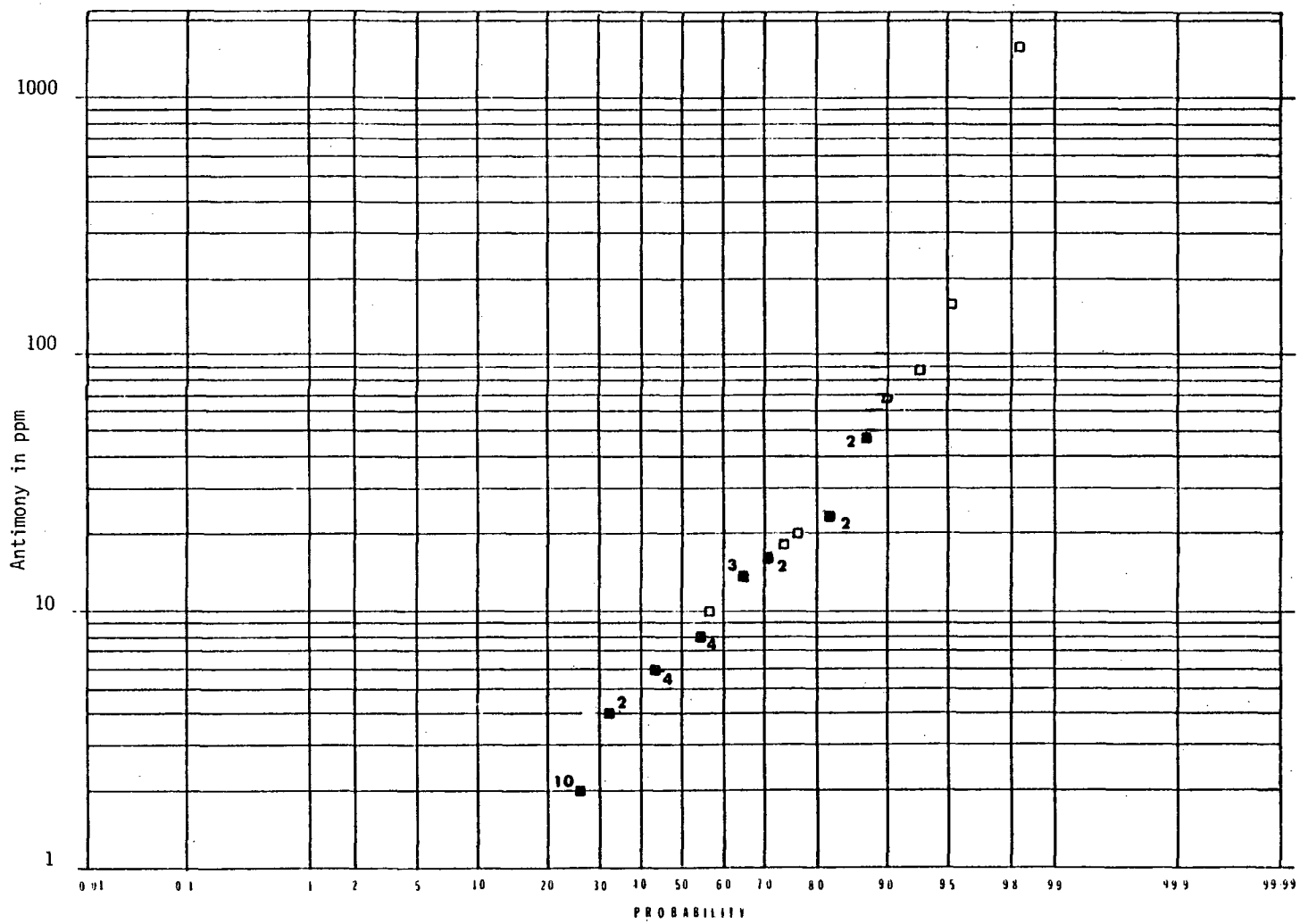

Figure 4-27. Log probability plot of antimony concentrations in heavy mineral fraction samples for DF 66-21. Open squares indicate single sample value; solid squares indicate multiple sample values.

Table 4-27

Mercury Distribution in DF 66-21 Heavy Mineral Fractions

Mercury (ppm)	Absolute Frequency	Plotting Percentage	Lithology*
0.105	1	1.8	A/B; T; FZ
0.225	1	4.5	A/c
0.260	1	7.1	A/B; T; FZ
0.285	1	9.8	A
0.305	1	12.5	M/M; G
0.315	1	15.1	A/c
0.375	1	17.9	A
0.400	1	20.5	A
0.435	2	25.9	A; A/c; G
0.660	1	28.6	G; QA
0.680	1	31.3	G
0.695	1	33.9	G
0.730	1	36.6	M/M
0.750	1	39.3	G; FZ
0.995	1	42.0	M/M; G; G/D; MZ; FZ
1.3	1	44.6	A
1.4	1	47.3	A
1.6	1	50.0	QA; FZ; MZ
1.8	2	55.4	A/c; G; QA
2.3	2	60.7	A; G; QA; MZ; FZ
2.5	1	63.4	A/B; T; A/c
3.5	1	66.1	G
5.5	1	68.8	A; A/c
7.2	1	71.4	M/M; G
8.6	1	74.1	M/M; G
10.3	1	76.8	A/B; T
13.0	1	79.5	A; A/c
13.4	1	82.1	QA; MZ; FZ
16.0	1	84.8	A/B; T; A/c
19.0	1	87.5	A/B; T; A/c; FZ
21.0	1	90.2	A/c; A/B; T
37.0	1	92.9	A/B; T; A/c
42.0	1	95.5	A/c
43.0	1	98.3	A/c

Mean 7.1 Std Err 1.9 Std Dev 11.6 Median 1.6

Kurtosis 4.1 Skewness 2.2

*Refer to Table 4-12 for explanation of symbols.

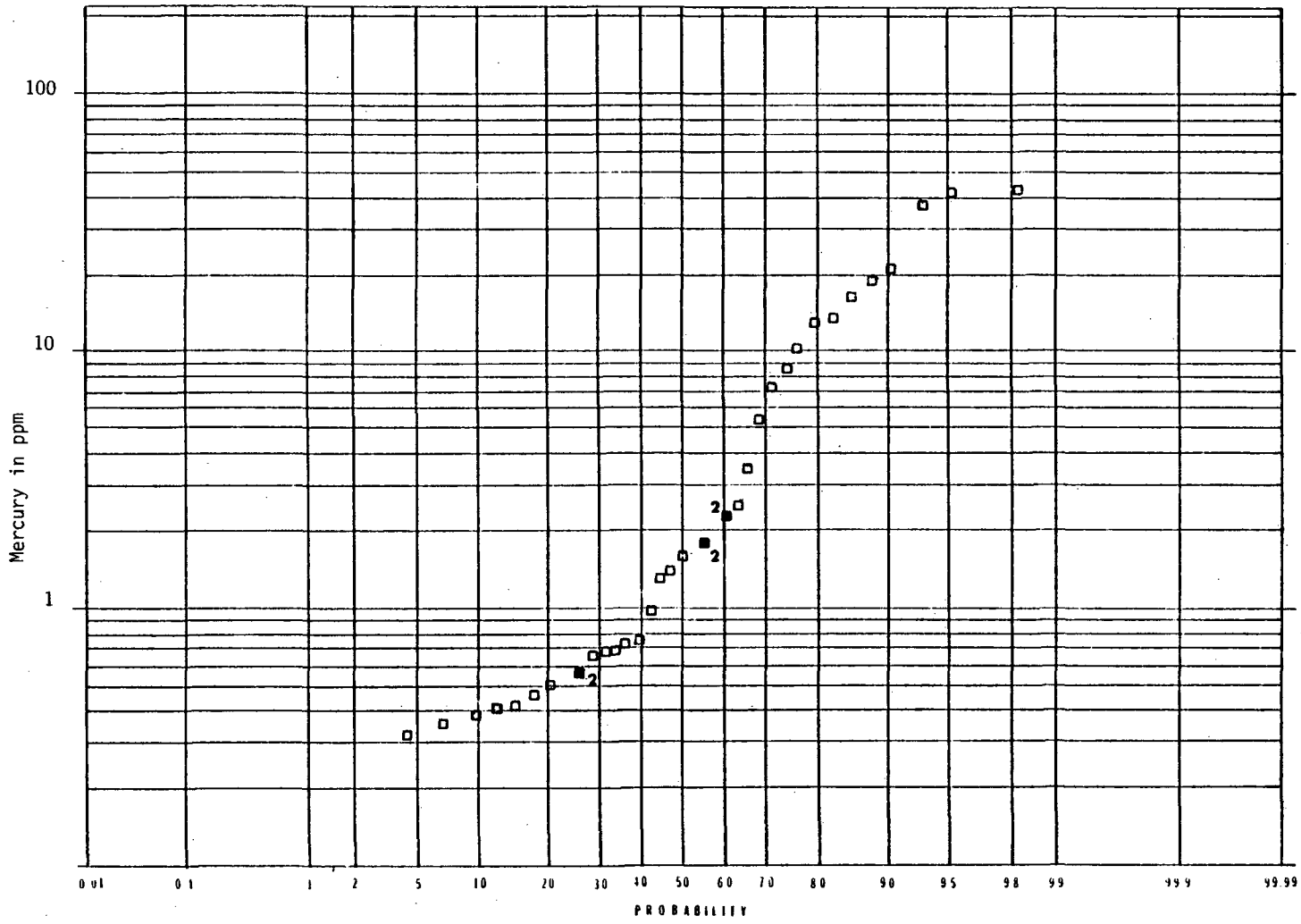

Figure 4-28. Log probability plot of mercury concentrations in heavy mineral fraction samples for DF 66-21. Open squares indicate single sample value; solid squares indicate multiple sample values.

Table 4-28

Lead Distribution in DF 66-21 Whole Rock Samples

Lead (ppm)	Absolute Frequency	Plotting Percentage	Lithology*
5	6	14.8	A; QA; G; MZ; FZ
10	11	43.5	A/c; A; A/B; T; G; QA
15	5	56.5	A/c;A;A/B;T;G;QA;FZ;MZ
20	10	82.6	G;A;QA;A/B;T;A/c;FZ;MZ
25	1	85.2	M/M; G
30	2	90.4	M/M; G
40	1	93.0	M/M
45	1	95.7	A/B; T; FZ
65	1	98.3	A; A/c

Mean 17.1 Std Err 2.0 Std Dev 12.2 Median 14.5
Kurtosis 5.8 Skewness 2.1

*Refer to Table 4-12 for explanation of symbols.

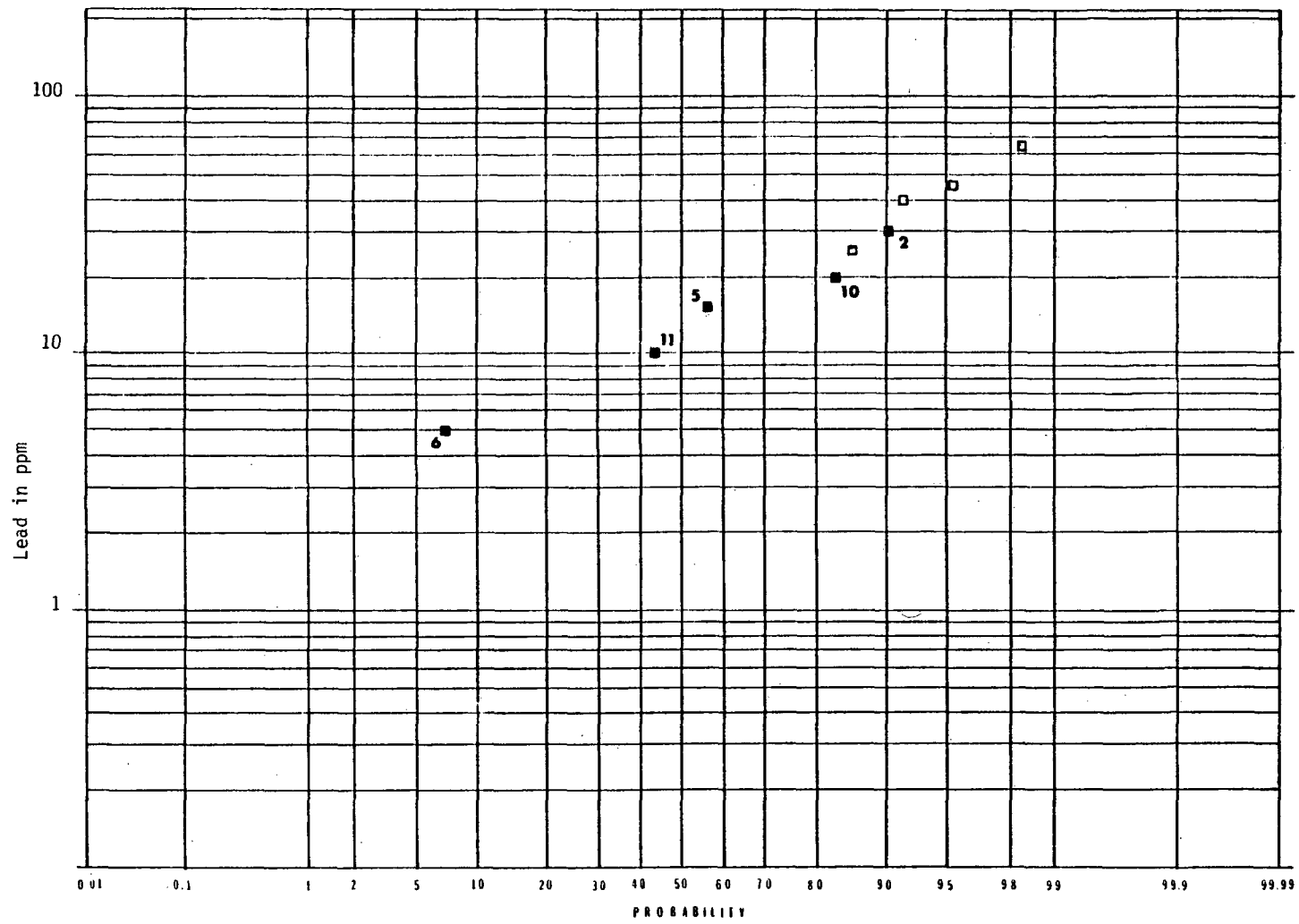

Figure 4-29. Log probability plot of lead concentrations in whole rock samples for DF 66-21. Open squares indicate single sample value; solid squares indicate multiple sample values.

Table 4-29

Zinc Distribution in DF 66-21 Whole Rock Samples

Zinc (ppm)	Absolute Frequency	Plotting Percentage	Lithology*
5	1	1.7	QA; MZ; FZ
10	5	14.8	G; QA; MZ; FZ
15	2	20.0	G; A/B; T; FZ
20	3	27.8	G; QA; A/B; T; FZ
25	2	33.0	G; QA; A/B; T
35	4	43.5	A; G; QA; A/B; T;MZ;FZ
40	2	48.7	A; A/c
45	2	53.9	A; A/c; A/B; T
50	4	64.3	A; A/c
55	3	72.2	A/c; A/B; T; FZ
60	3	80.0	A/c; M/M; G
65	3	87.8	M/M; G; A/c; A/B
70	1	90.4	M/M; G
75	2	95.6	M/M; A; A/c
80	1	98.3	M/M; G/D; G; MZ; FZ

Mean 40.7 Std Err 3.6 Std Dev 22.0 Median 42.5

Kurtosis -1.2 Skewness -0.04

*Refer to Table 4-12 for explanation of symbols.

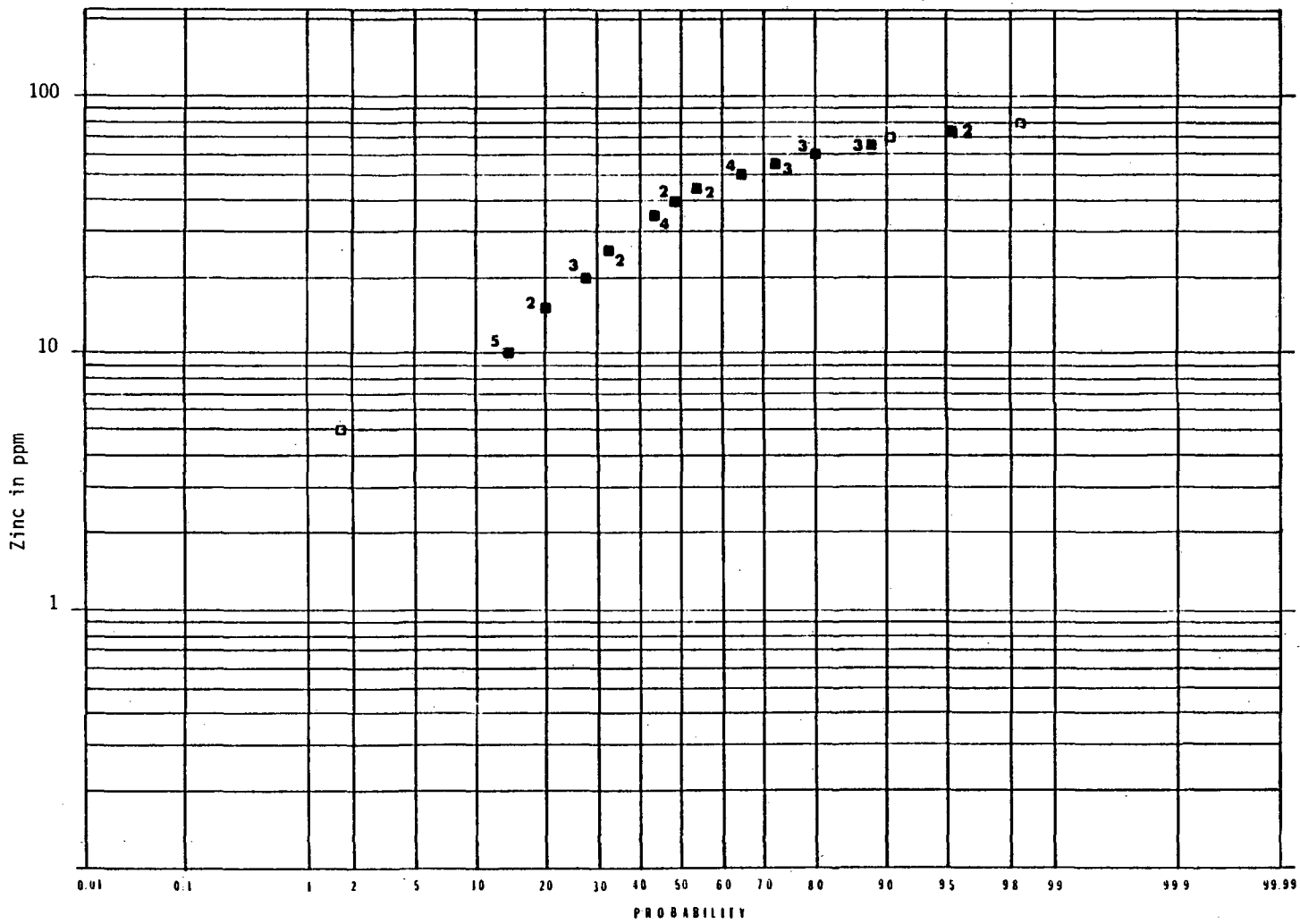

Figure 4-30. Log probability plot of zinc concentrations in whole rock samples for DF 66-21. Open squares indicate single sample value; solid squares indicate multiple sample values.

Table 4-30

Arsenic Distribution in DF 66-21 Whole Rock Samples

Arsenic (ppm)	Absolute Frequency	Plotting Percentage	Lithology*
5	24	61.7	G;M/M;A;A/c;A/B;T;QA;FZ;MZ
10	10	87.8	A;A/c;A/B;T;G;QA;FZ
15	1	90.4	A/c; A/B; T
20	1	93.0	A/B; A/c; T
30	1	95.6	M/M; G
50	1	98.3	G

Mean 8.8 Std Err 1.4 Std Dev 8.5 Median 6.5

Kurtosis 15.6 Skewness 3.7

*Refer to Table 4-12 for explanation of symbols.

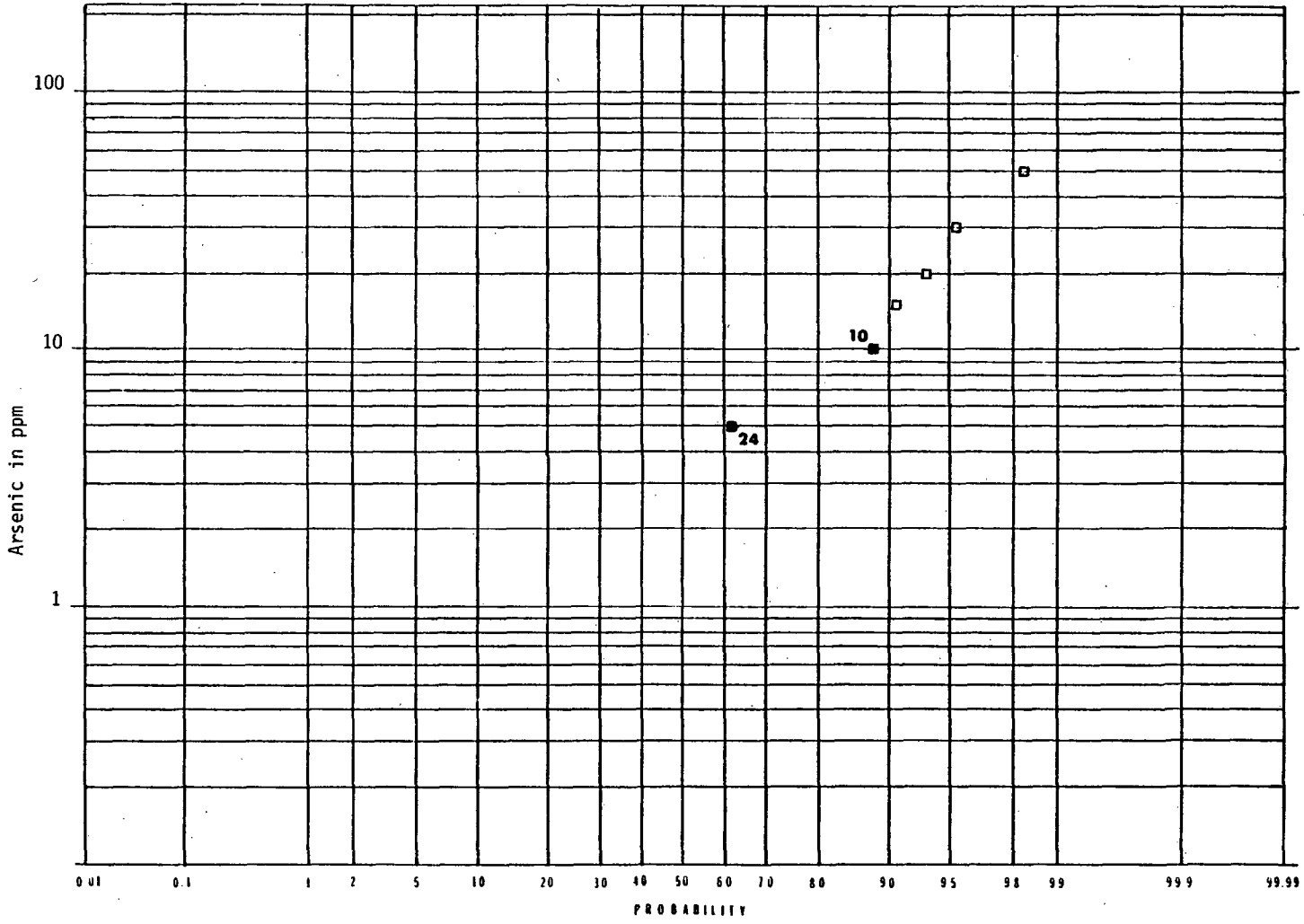

Figure 4-31. Log probability plot of arsenic concentrations in whole rock samples for DF 66-21. Open squares indicate single sample value; solid squares indicate multiple sample values.

Table 4-31

Antimony Distribution in DF 66-21 Whole Rock Samples

Antimony (ppm)	Absolute Frequency	Plotting Percentage	Lithology*
1	25	64.3	A;A/c;G;QA;M/M;G/D;MZ;FZ
2	7	82.6	A/B; T; M/M; G; FZ
3	2	87.8	A/c; A/B; T; G; QA
4	1	90.4	A/B; T; FZ
5	1	93.0	A/B; T; FZ
6	1	95.6	A/B; T
7	1	98.3	A/B; T

Mean 1.8 Std Err 0.2 Std Dev 1.5 Median 1.3

Kurtosis 5.3 Skewness 2.4

*Refer to Table 4-12 for explanation of symbols.

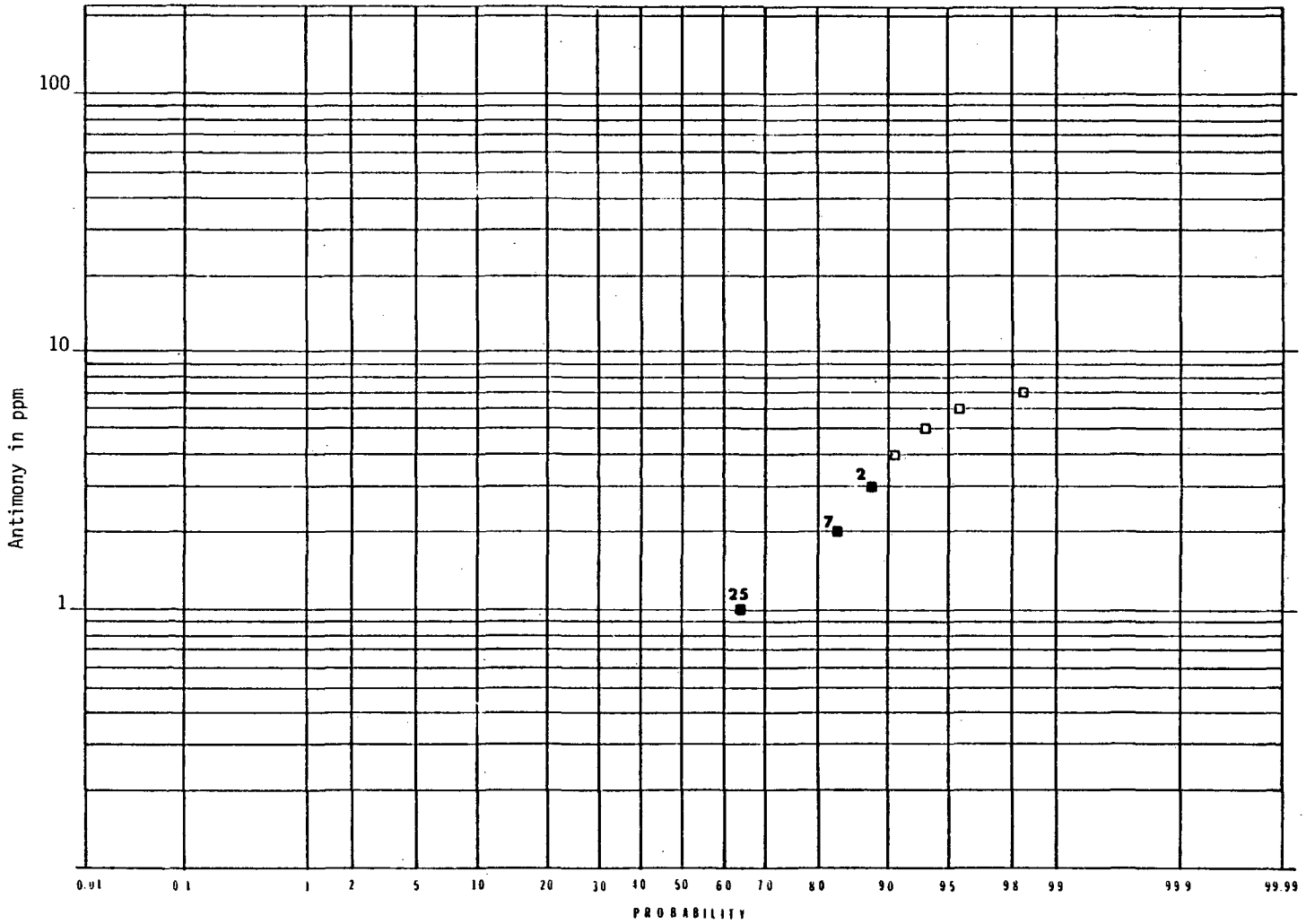

Figure 4-32. Log probability plot of antimony concentrations in whole rock samples for DF 66-21. Open squares indicate single sample value; solid squares indicate multiple sample values.

Table 4-32

Mercury Distribution in DF 66-21 Whole Rock Samples

Mercury (ppm)	Absolute Frequency	Plotting Percentage	Lithology*
0.085	1	1.7	G
0.095	1	4.3	A
0.105	2	9.5	M/M; G
0.115	1	12.2	M/M; G
0.120	2	17.4	A; A/c
0.125	2	22.6	G
0.130	4	33.0	A; A/c; G; QA; FZ
0.140	2	38.3	A; A/c
0.150	2	43.5	A/c; A
0.155	1	46.1	M/M; G
0.160	1	48.7	A; A/c
0.165	1	51.3	A
0.175	2	56.5	M/M; G; G/D; MZ; FZ
0.180	2	61.7	A; A/B; T; FZ
0.190	1	64.3	A/c; A/B; T
0.195	1	66.9	A/c; A
0.200	2	72.2	A; G; QA; FZ
0.235	1	74.8	A/B; T; FZ
0.255	1	77.4	G
0.260	1	80.0	G; QA
0.265	1	82.6	QA; MZ; FZ
0.280	1	85.2	A/B; T; A/c
0.300	1	87.8	A/B; T; A/c
0.330	1	90.4	G; QA
0.460	1	93.0	A/B; T
0.685	1	95.7	G; QA; MZ; FZ
0.720	1	98.3	A/B; T

Mean 0.2 Std Err 0.02 Std Dev 0.1 Median 0.2

Kurtosis 7.1 Skewness 2.6

*Refer to Table 4-12 for explanation of symbols.

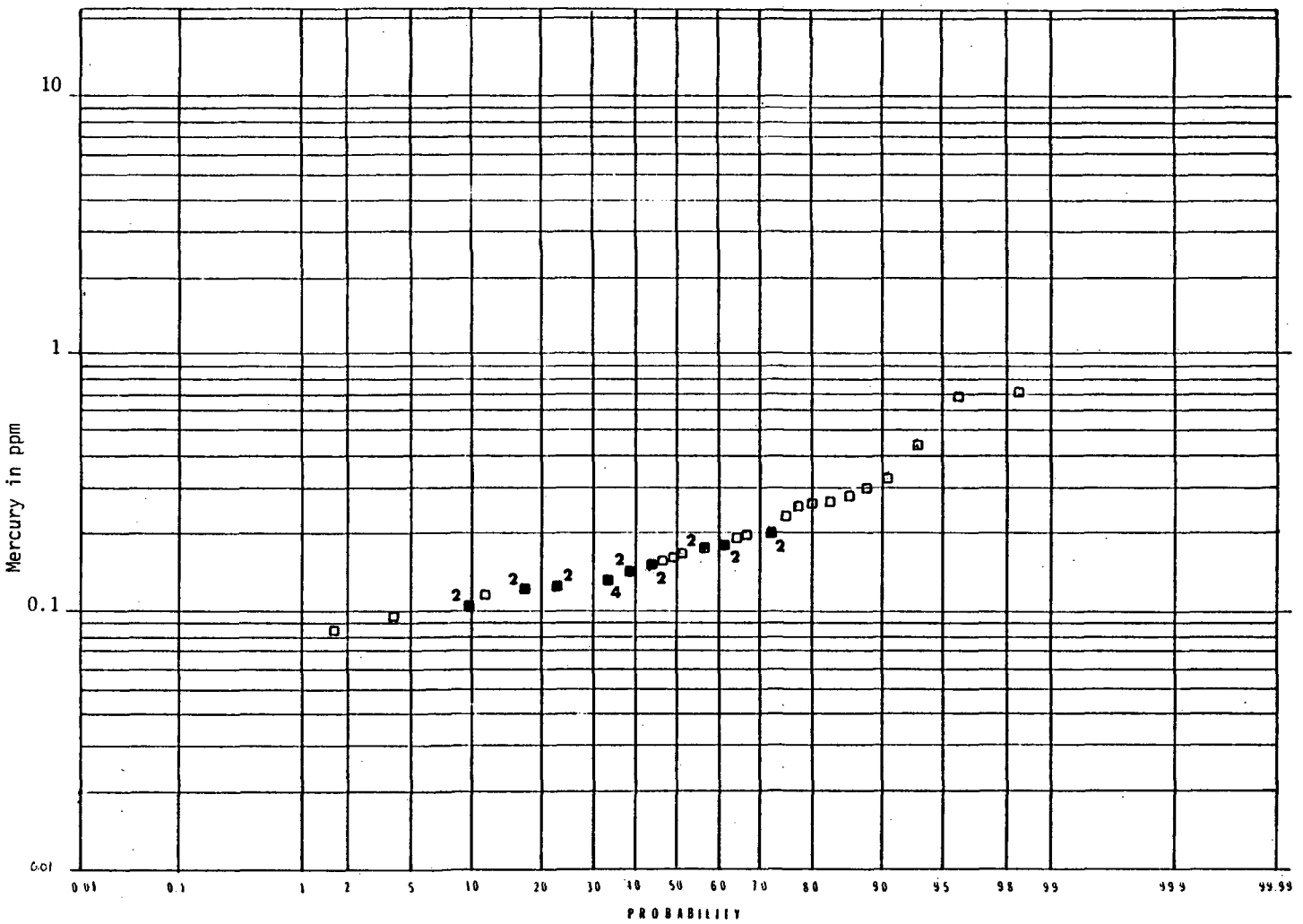

Figure 4-33. Log probability plot of mercury concentrations in whole rock samples for DF 66-21. Open squares indicate single sample value; solid squares indicate multiple sample values.